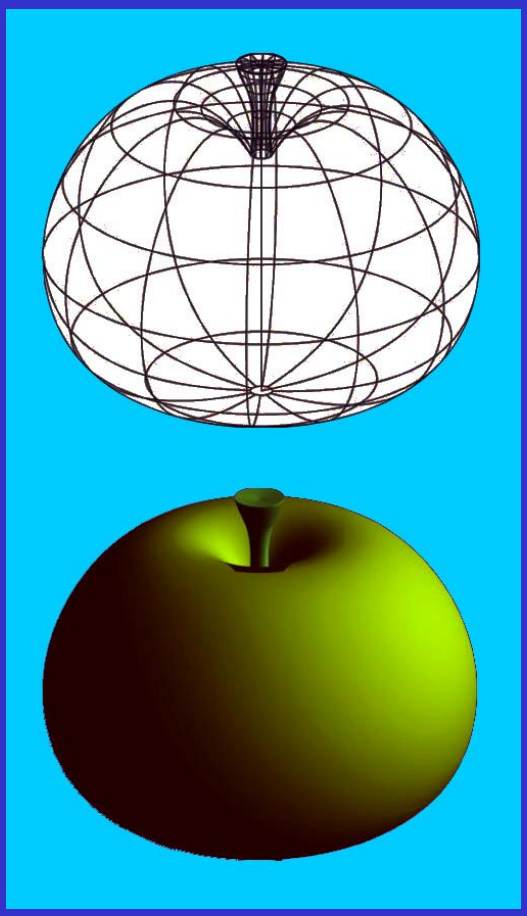

Bureau Gravimétrique International
International Geoid Service
Joint Bulletin

Newton's Bulletin

Issue n°1, December 2003

International Association of Geodesy
and
International Gravity Field Service

ISSN 1810-8555

FOREWORD

Dear friends and colleagues,

During the last 4 years the process of reviewing statutes and bylaws of IAG has deeply involved also the IAG Services and, among them, those Services which are related to the determination of the gravity field, like BGI, IGeS, ICeT, GFZ and NIMA with these already existing centers in mind and with the contribution of new Centers, namely the 2nd IGeS Center at NIMA (St. Louis) and the new International Centre of Global Earth Models (ICGEM) at GFZ we have created a new unified Service for the Gravity Field namely the International Gravity Field Service (IGFS).

Lately, from the Sapporo General Assembly, a new Center is being structured and is in the process of entering into IGFS; namely the DTM Centre (CeDiT) at the Montfort University (U.K.)

As part of this effort of unification and, continuing a period of good cooperation between BGI and IGeS, we have decided to start merging the two bulletins in one publication; the brand new "Newton's Bulletin" (N.B.).

Just to remind you of the preceding rules and to report the new ones, let us confirm that the N.B. will be essentially composed of two parts, one where we publish reviewed papers, in the spirit of IGeS Bulletin, namely the review concerns the correctness and uptodateness of the approach and not its novelty in theoretical matters, and one part where the "information" concerning new data set, the internal life of the centers and international events, gravity field related, is reported.

The mode of publication will be mixed; basically the N.B. will be put on-line and built as soon as the material arrives in an appropriate form.

In addition a certain number of CD will be published and distributed on the basis of a request covering the mail expenses; finally a small number of paper journal will be produced for libraries and agencies/individual scientists from areas of the world where internet connection is difficult.

As for the addresses where to send the material, the editorial board is done purposely half by BGI and half by IGeS and you can address whatever center you prefer exactly as you would have done before. The Editorial Board will then take care of unifying and homogeneizing the material, also concerning the reviewing process when applicable.

Finally let me recall that the N.B. in electronic form will be readable at the address "bgi.cnes.fr" or "www.iges.polimi.it" from which it can be downloaded too.

With that let me wish to all geodesists the best wishes for Happy New Year and good luck to the new born Newton's Bulletin.

Jean-Pierre Barriot (BGI Director) and Fernando Sansò (IgeS Director).

Newton's Bulletin N. 1

Summary

Foreword
(J.P. Barriot, F. Sansò) Page 1

SECTION I - "Reviewed Papers"
BGI Papers:

Ajustement des réseaux gravimétriques
(*J.P. Barriot, M. Sarrailh)* Page 2

Proposal for the precise definition of mean valuesof gravity field quantities
(*C.C. Tscherning*) Page 8

Abnormal temperature response of a Lacoste-Romberg gravimeter and procedures for tropical utilisation
(O.K. Nwofor and T.C. Chineke) Page 11

Preliminary results in the achievement of the new gravity system of Republic of Moldova
(*Besutiu L., Neaga V., Nicolescu A., Lorinczi J., Ilies I., Besutiu G.)* Page 28

IGeS Papers:

Surface modeling for GPS-levelling geoid determination
(M. Soycan, Msc. A. Soycan) Page 41

A Comparison of the classical and recent formulae of handling the effects of close and distant topographic masses in gravimetric geoid computations
(H. Nahavandchi) Page 52

Quasi-geoid BG03 computation in Belgium
(R. Barzaghi, A. Borghi, B. Ducarme, M. Everaerts) Page 75

II Section: "Communications and News"

Geoid and Ocean Circulation in the North Atlantic (GOCINA)
(P. Knudsen, R. Forsberg, O. Andersen, D. Solheim, R. Hipkin, K. Haines, J. Johannessen, and F. Hernandez)
Page 89

The New 'International Centre for Global Gravity Field Models (ICGG)' at GFZ Potsdam
(P. Schwintzer, F. Barthelmes, W. Köhler, H. Pflug) Page 94

SECTION I - "Reviewed Papers"

ADJUSTMENT OF GRAVIMETRIC NETWORKS*

Jean-Pierre Barriot and Michel Sarrailh

Bureau Gravimétrique International, Toulouse, France

* Lecture given by M. Sarrailh during the 3rd North African Workshop on the Unification of Geodetic Reference Systems – Rabat, October 16-17, 2003

Abstract: We summarize the current knowledge about the adjustment of gravimetric networks in terms of the pseudo-inverse theory of least-squares processes, and give the link with the so-called free adjustment often used in practice.

1 – INTRODUCTION

Let us consider the system

$$G \underset{\sim}{p} = \underset{\sim}{d} \tag{1}$$

where:

- the vector $\underset{\sim}{d}$ represents the data point values (number m),
- the vector $\underset{\sim}{p}$ represents the parameters (number n),
- the matrix G is the design matrix linking the parameters $\underset{\sim}{p}$ to the data $\underset{\sim}{d}$.

If G is of full rank (i.e. the problem is fully constrained), then, for the overdetermined case (more observation equations than unknowns), one and only one solution exists in the least squares sense, and is given by

$$\underset{\sim}{p}^{*} = \left(G^T G\right)^{-1} G^T \underset{\sim}{d} \tag{2}$$

If G is not of full rank, as it is always the case for networks, then $\left(G^T G\right)^{-1}$ does not exist. This signifies that there are several solutions $\underset{\sim}{p}$, each one verifying

$$\left(G^T G\right)\underset{\sim}{p} = G^T \underset{\sim}{d} \tag{3}$$

Then we have else:

- to pick up a particular solution, from an a priori rule,
- or to modify the system (1), in order to restore unicity

$$G \underset{\sim}{p} = \underset{\sim}{d} \rightarrow G' \underset{\sim}{p'} = \underset{\sim}{d'} \tag{4}$$

i.e. with a design matrix G' of full rank.

2 – CHOICE OF A PARTICULAR SOLUTION

If several solutions $\underset{\sim}{p}$ to Eq. (3) exist, a physically sound choice is to select the one that exhibits the lowest norm, (i.e. $\left\| \underset{\sim}{p} \right\|$ minimum). This solution is given by the generalized inverse of *G*, which is the unique matrix G^+ verifying

$$G\,G^+\,G = G$$
$$G^+\,G\,G^+ = G^+$$
$$\left(G\,G^+\right)^T = G\,G^+$$
$$\left(G^+\,G\right)^T = G^+\,G$$

On practical grounds, G^+ is computed through the so-called SVD (Singular Value Decomposition) algorithm, from the expansion

$$G = U\,\Lambda\,V^T$$

where $U\,U^T = U^T\,U = I_m$ $\quad U \quad m \times m$

$V\,V^T = V^T\,V = I_n$ $\quad V \quad n \times n$

$\Lambda \quad m \times n$

and

$$\Lambda = \left[\begin{array}{ccc|c} \lambda_1 & & & \\ & \lambda_2 & & \\ & & \circ & 0_{q,n-q} \\ & & \lambda_q & \\ \hline & 0_{m-q,q} & & 0_{m-q,n-q} \end{array}\right] \qquad \lambda_1 \geq \lambda_2 \geq \mathrm{K} \geq \lambda_q > 0 \tag{5}$$

There are *q* non-zero values λ_i. The number *q* is the rank of matrix *G*, and the rank defect of *G* is then $n - q$.

We have $G^+ = V\,\Lambda^+\,U^T$, with

$$\Lambda^+ = \left[\begin{array}{ccc|c} \lambda_1^{-1} & & & \\ & \lambda_2^{-1} & & \\ & & \circ & 0_{q,m-q} \\ & & \lambda_q^{-1} & \\ \hline & 0_{n-q,q} & & 0_{n-q,m-q} \end{array}\right] \qquad \Lambda^+ \quad n \times m \tag{6}$$

Furthermore, if $\underset{\sim}{d}$ is associated with the covariance matrix $C_d = \sigma_d^2\,I$, then

$$C_{\underset{\sim}{p^*}} = \left(G^+\right)\sigma_d^2\,I\left(G^+\right)^T = \sigma_d^2\left(G^T\,G\right)^+$$

and Trace $\left(\sigma_d^2\left(G^T\,G\right)^+\right)$ is minimal over the whole set of all possible solutions $\underset{\sim}{p}^*$ of Eq. (3). This is an another nice property.

In principle, the SVD algorithm permits to solve ALL least squares problems, and is part of all common least-squares software packages. But it is costly in terms of computer space and execution time, and sometimes its precision is not guaranteed for the determination of small singular values and corresponding eigenvectors. For overdetermined and underconstrained systems like the gravimetric or altimetric network

problem there is an alternative technique called “free network” which consists in writing Eq. (3) as (see annex)

$$\left(G^T\ G + \Phi\right) \underset{\sim}{p} = G^T\ \underset{\sim}{d}$$

with $\Phi\ \underset{\sim}{p} = 0$, in such a way that $\left(G^T\ G + \Phi\right)^{-1}$ exists, and that $\underset{\sim}{p}^* = G^+\ \underset{\sim}{d} = \left(G^T\ G + \Phi\right)^{-1} G^T\ \underset{\sim}{d}$ (7)

The immense advantage is that the use of a standard Cholesky algorithm to compute $\underset{\sim}{p}^*$ and its associated covariance is now allowed. Of course, the disadvantage is that we have to construct Φ.

A particular value of $\underset{\sim}{p}^*$ can be also computed through iterative processes, like

$$\underset{\sim}{p}^{(n+1)} = \left(G^T\ G + \lambda^2\ I\right)^{-1} \left(G^T\ \underset{\sim}{d} + \lambda^2\ \underset{\sim}{p}^{(n)}\right),$$

$$\text{with } \underset{\sim}{p}^{(1)} = \left(A^T\ A + \lambda^2\ I\right)^{-1} G^T\ \underset{\sim}{d}, \tag{8}$$

$$\text{and, in fine, } \underset{\sim}{p}^* = \underset{\sim}{p}^{(\infty)}.$$

But there is no longer a direct access to the covariance matrix…
If this covariance matrix is absolutely needed, G^+ can be iteratively built through

$$X^{(r+1)} = X^{(r)} \left(2I - G\ X^{(r)}\right) \tag{9}$$

with $X^{(o)} = \alpha\ G^T \qquad 0 < \alpha < 2 / \lambda_1,$

where λ_1 are the largest singular values of $G\ G^T$ (the convergence can be assessed by $\left\| G\ X^{(r)} G - G \right\| \rightarrow 0$).

A last possibility to pick up a particular solution of Eq. (3) is to split the normal matrix as

$G^T\ G = M - N$ with M^{-1} well defined.

This splitting allows us to write the iteration

$$\underset{\sim}{p}^{(n)} = M^{-1} N\ p^{(n-1)} + M^{-1}\ G^T\ \underset{\sim}{d} \tag{10}$$

starting from a given $\underset{\sim}{p}^{(o)}$.

This technique can be very cheap to implement, for example by selecting
$M = diag\left(G^T\ G\right)$.

The convergence of the method depends on the spectral properties of $M^{-1}\ N$ and on the particular value of the initial vector $\underset{\sim}{p}^{(o)}$.

The disadvantage is that, albeit if $\underset{\sim}{p}^{(\infty)}$ by construction strictly verifies Eq. (3), the non-unicity of the solution could be synonymous with long wavelength distortions in the network (otherwise perfectly adjusted).

3 – MODIFICATION OF THE INITIAL SYSTEM

There are two possibilities:

3.1. to complement the initial system $G\ \underset{\sim}{p} = \underset{\sim}{d}$ **with** $K\ \underset{\sim}{p} = \underset{\sim}{1}$**,**

in order to obtain the form $\left[\frac{G}{K}\right] \underset{\sim}{p} = \left[\begin{matrix} \underset{\sim}{d} \\ \underset{\sim}{1} \end{matrix}\right] = G'\ \underset{\sim}{p'} = \underset{\sim}{d'}$,

where G' is now of full rank.
The normal system has then a unique solution $\underset{\sim}{p}^{'*}$ given by

$$\underset{\sim}{p}'* = \left(G'^T\ G'\right)^{-1}\ G'^T\ \underset{\sim}{d}'$$

that can be rewritten as

$$\underset{\sim}{p}'* = \left(G^T\ G + K^T\ K\right)^{-1} \left(G^T\ \underset{\sim}{d} + K^T\ \underset{\sim}{1}\right)$$

If furthermore we assume that $\underset{\sim}{1} = \underset{\sim}{0}$, we obtain

$$\underset{\sim}{p}'* = \left(G^T\ G + K^T\ K\right)^{-1}\ G^T\ \underset{\sim}{d} \tag{11}$$

Let us note the formal analogy with Eq. (7), which corresponds to $\left\| \underset{\sim}{p}'* \right\| = \left\| \underset{\sim}{p}* \right\|_{\min}$

The additional assumption $K = \lambda\ I$ with $\lambda > 0$ is of courant use, and signifies that a solution $\underset{\sim}{p}'*$close to zero is sought. That corresponds to seek a value of $\underset{\sim}{p}'*$ close to zero, and that more especially as λ is large.

3.2. –to complement the normal system, the simplest form being

$$G^T\ G \ \rightarrow \left[\begin{array}{c|c} G^T\ G & u^T \\ \hline u & \underset{\sim}{0} \end{array}\right],$$

which is equivalent to solve the system

$$\left[\begin{array}{c|c} G^T\ G & u^T \\ \hline u & \underset{\sim}{0} \end{array}\right] \left[\begin{matrix} \underset{\sim}{p} \\ \underset{\sim}{\lambda} \end{matrix}\right] = \left[\begin{matrix} G^T\ \underset{\sim}{d} \\ \underset{\sim}{\mu} \end{matrix}\right] \tag{12}$$

or equivalently to minimize $G\ \underset{\sim}{p} - \underset{\sim}{d}$ under the constraint $u\ \underset{\sim}{p} - \underset{\sim}{\mu} = \underset{\sim}{0}$

This is the case when some data points on the network are frozen, i.e. if we suppose that the corresponding gravimetric values are perfectly known on these points.

References:

Lagios E., A Fortran IV Program for a Least-Squares Gravity Base Station Network Adjustment, Computers and Geosciences, Vol. 10, No 2-3, pp. 263-276, 1984.

Blaha G., Free Networks: Minimum Norm Solution as Obtained by the Inner Adjustment Constraint Method, Bulletin Géodésique, Vol 56, pp. 209-219, 1982.

Blaha G., Notes on Equivalent Forms of the General Least-Squares Solution, Bulletin Géodésique, Vol 56, pp. 220-230, 1982.

Blaha G., A Note on Adjustment of Free Networks, Bulletin Géodésique, Vol. 56, pp 281-299, 1982.
Sevilla M.J., Ajustes con Constrenimientos, Publication num. 198, Instituto de Astronomia y Geodesia, 2003.
Barriot J.P., Moindre Carrés et Problèmes Inverses : Théorie et Etude de cas en Géodésie et RadioSciences, Cours FYQU 3021, Université Catholique de Louvain, Mars 2003.
Vanicek P. and Krakiwsky E., Geodesy: The concepts, Elsevier, 1986.
Branham R.L. Jr., Scientific Data Analysis: An Introduction to Overdetermined Systems, Springer-Verlag, 1990.
Hwang C., Wang C. and Lee L., Adjustment of relative gravity measurements using weighted and datum free constraints, Computers and Geosciences, Vol 28, No 9, pp 1005-1015, 2002.

ANNEX – NOTION OF FREE NETWORK

From Eq. (5), one can see that

$$G^T G = V \begin{bmatrix} \lambda_1^2 & & & 0_{q,n-q} \\ & \circ & & \\ & & \lambda_q^2 & \\ \hline 0_{n-q,q} & & & 0_{n-q,n-q} \end{bmatrix} V^T \tag{13}$$

The idea is to complete $G^T G$ in such a way that

$$\left(G^T G\right)_{completed} = V \begin{bmatrix} \lambda_1^2 & & & & & 0 \\ & \circ & & & & \\ & & \lambda_q^2 & & & \\ & & & \lambda_{q+1}^2 & & \\ & & & & \circ & \\ 0 & & & & & \lambda_n^2 \end{bmatrix} V^T \tag{14}$$

Therefore, $(G^T G)_{\text{completed}}$ exists. This is equivalent to writing

$$\left(G^T G\right)_{completed} = G^T G + \Phi$$

where $\Phi = V \begin{bmatrix} 0 & & & 0_{q,n-q} \\ & \circ & & \\ & & 0 & \\ \hline & & b_{q+1}^2 & \\ 0_{n-q,q} & & & \circ \\ & & & \lambda_n^2 \end{bmatrix} V^T$ (15)

It is easy to see that $G\,\Phi = 0$ i.e. $G^T G\,\Phi = 0$. Eq. (15) suggest that Φ can be put on the form $\Phi = C^T C$,

where

$$C = \overline{U} \left[\begin{array}{c|c} \begin{matrix} 0 & & \\ & \circ & \\ & & 0 \end{matrix} & 0_{q,n-q} \\ \hline 0_{n-q,q} & \begin{matrix} b_{q+1}^2 & & \\ & \circ & \\ & & \lambda_n^2 \end{matrix} \end{array}\right] V^T \qquad (16)$$

with $\overline{U}$ verifying $\overline{U}\,\overline{U}^T = \overline{U}^T\,\overline{U} = I_m$

Then

$$\underset{\sim}{p}^{**} = \left(G^T G + \Phi\right)^{-1} G^T \underset{\sim}{d}$$

$$= V \begin{bmatrix} 1/\lambda_1^2 & & & & & \\ & \circ & & & & \\ & & 1/\lambda_q^2 & & & \\ & & & 1/\lambda_{q+1}^2 & & \\ & & & & \circ & \\ & & & & & 1/\lambda_n^2 \end{bmatrix} V^T\, V \left[\begin{array}{ccc|c} \lambda_1 & & & \\ & \circ & & 0_{q,m-q} \\ & & \lambda_q & \\ \hline \multicolumn{3}{c|}{0_{n-q,q}} & 0_{n-q,m-q} \end{array}\right] U^T \underset{\sim}{d}$$

$$= V \left[\begin{array}{ccc|c} 1/\lambda_1 & & & \\ & \circ & & 0_{q,m-q} \\ & & 1/\lambda_q & \\ \hline \multicolumn{3}{c|}{0_{n-q,q}} & 0_{n-q,m-q} \end{array}\right] U^T \underset{\sim}{d}$$

$= G^+ \underset{\sim}{d}$, the least norm solution.

We have also $\Phi\, p^{**} = \Phi\, p^* = 0$.

Proposal for the precise definition of mean values of gravity field quantities

by

C.C. Tscherning

Department of Geophysics,
University of Copenhagen.
Juliane Maries Vej 30,
DK-2100 Copenhagen Ø., Denmark
e-mail: cct@gfy.ku.dk

1. Introduction.

Some of the products of the GOCE mission are mean values of gravity anomalies and geoid heights. In order to avoid ambiguities a precise definition of these quantities is needed. First mean values are defined in a general manner, so it can be used for any gravity field related quantity, and finally the definition of specific GOCE mean values are proposed.

2. Mathematical definition of a mean value.

A mathematical definition of a mean value is the mean of values of a function or of a functional applied on a function,

$$f : \Omega \subseteq R^n \rightarrow R$$

The mean must be taken over a continous or discrete, bounded subset of Ω. The subset must have dimension less than or equal to n, which for the gravity field are 4 for time dependent quantities and otherwise 3. See for example Heiskanen and Moritz (1967, eq. (7-76)).

Examples are for

1D: discrete or contineous mean along a flight, ship or satellite track bounded in time or space.
2D: - discrete or contineous mean over a 2D surface bounded by parallels and meridians having a fixed ellipsoidal height (equi-angular or equal-area mean values).
- mean over an area bounded by a closed curve, such as over a lake.
3D: discrete or contineous mean over a volume defined by the coordinates of the corners of a convex area such as a sphere or a box.

DMA/NIMA 1º mean gravity anomalies are for example defined as the mean of 6x6 values in an equi-angular area (see DMAAC, 1973). The associated altitude is the mean topographic height.

3. Definition of a gravimetric quantity.

Let

- W be the gravity potential of the Earth,
- Φ the centrifugal potential
- U is the Somigliana-Pizetti normal potential of a specific reference system
- V_N a linear combination of N harmonic functions such as spherical or ellipsoidal harmonics to degree (and order) $\sqrt{(N+1)^2}$ without the centrifugal potential, and
- $T_N = V_N + \Phi - U$
- T=W-U

We do not require the zero and first order harmonics of T or T_N to be zero. V_N may also be a linear combination of potentials of point-masses or of covariance functions used in Least-Squares Collocation.

A gravimetric quantity is here

1) a functional applied on W, V_N , T or T_N , including or excluding effects of the atmosphere and the tides. Normal gravity γ in a point Q will be the magnitude of the gradient of U in the point.
2) an observed quantity like (a) the potential W(P) in a specific point P in a given datum, (b) g(P) the magnitude of the gravity vector in a point P, in a given reference system (one for P and one for g), (c) the second order radial derivative of W, W_{rr}(P) in a given point P. The altitude associated with P is always the ellipsoidal height.
3) an anomalous quantity, i.e. a functional applied on T or T_N .

For GOCE products anomalous quantities will be derived from $T_N = V_N + \Phi - U$.

A GOCE gravity anomaly Δg_N is then the difference between the norm of the gradient γ_N computed from $U_N = V_N + \Phi$ and normal gravity γ in a point Q on the same ellipsoidal normal, and where U_N (Q)= W(P). The linearized expression for the gravity anomaly will be for example,

$$\Delta g_N = -\frac{\partial T_N}{\partial n} - \frac{\partial \gamma_N}{\partial h} T_N / \gamma_N$$

The derivative must be computed in the direction of the vertical as defined by U_N . The height anomaly ζ_N is the distance along the ellipsoidal normal between the points P and Q. Note that P is on or outside the surface of the Earth, while Q may be inside.

The geoid height is obtained from the height anomaly at the surface of the Earth using a fixed conversion formula, such as the one which include the Bouger anomaly, see Heiskanen and Moritz, 1967, eq. (8.103).

A height anomaly may be computed from observed quantities at the surface of the Earth, e.g. from normal heights and ellipsoidal heights obtained using GPS. In contrast to geoid heights they do not include any hypothesis about the internal mass-distribution of the Earth. Such hypotheses are different from country to country, mainly due to different mass density values used to compute the Bouguer anomaly.

4. Computational considerations

Using the proper definitions of GOCE height anomalies and gravity anomalies it will not be difficult to evaluate these quantities at specific points, and subsequently compute a mean value. However in order to evaluate the quantities they must be compared with observed quantities. This is more problematic. Existing mean gravity anomalies have not been computed using procedures corresponding to the definitions above, see e.g. Wilcox(1974), Jones(1980).

First of all different procedures have been used to reduce the observed anomalies to a surface of constant height. Furthermore this height is generally taken as the mean topographic height, i.e. the anomalies are partly defined inside the masses. This should be avoided. But this means that mean gravity anomalies to be used for GOCE calibration must be recomputed. However, it is not the purpose of this note to discuss this aspect. But what is important is that the procedures must be rather easy to implement on a computer, and that the procedure adopted corresponds to the procedures to be used for the computation of GOCE height or gravity anomalies.

4. Conclusion. Proposed definitions of mean values

For computational use it is important that T_N (as determined by GOCE) is harmonic outside the surface of the Earth, i.e. it should not include any tidal or atmospheric effects.

Mean values of GOCE gravity anomalies and height anomalies should be defined as weighted sums of quantities associated with points which all are on or outside the surface of the Earth. However mean values in general may be computed from any of the 4 types of quantities discussed in section 2.

For 2D means, the mean values should be over surfaces with constant ellipsoidal heights. Area means are "equi-angular" means. A standard such as a 5x5 or 6x6 point set should be selected in accordance with NIMA definitions.

If geoid mean values have to be computed, the basis is height anomalies at the surface of the Earth. The corresponding geoid heights must then be computed using the conversion formula used by the country in which the block resides. For blocks overlapping two countries which use different hypothesis, they should not be computed. Note, that the conversion generally require that also the Bouguer anomaly is known for the points used to compute the mean value.

References:

DMAAC: Computational methods for determining 1 deg. x 1 deg. mean gravity anomalies and their accuracies. DMAAC Ref. Publ. 73-001, 1973.

Heiskanen, W.A. and H. Moritz: Physical Geodesy. W.H. Freeman & Co, San Francisco, 1967.

Jones, S.: A comparative study of the economy and accuracy of various methods of predicting 1 deg. x 1. deg. mean gravity anomalies. Thesis Washington University, Saint Louis, 1980.

Wilcox, L.: An analysis of gravity prediction methods for continental areas. DMAAC Ref. Publ., No. 74-001, 1974

Abnormal temperature response of a Lacoste-Romberg gravimeter and procedures for tropical utilisation

O.K. Nwofor and T.C. Chineke

Department of Physics
Imo State University
P.M.B 2000 Owerri
Nigeria

Abstract. A Lacoste-Romberg gravimeter was observed to exhibit abnormal drifts of varying character and magnitude when employed for field surveys under the Nigerian tropical heat. The gravimeter was therefore observed under specific instrumental and climatic conditions at a fixed location in Jos, Nigeria, in order to ascertain the nature of the abnormal drifts especially those influenced by temperature changes around the instrument. We found that temperature conditions affected both the drift and the sensitivity in such a manner that suggested that the temperature compensation of the instrument was inadequate possibly due to aging. The effect was the introduction of errors ranging between 10^{-3} mGals to 10^{-2} mGals. Given the cost of new instruments and the problems often associated with the repair of aging ones, we recommend that more compensation must be sought in addition to a measurement procedure that would enhance meter stability in order to improve the reliability of aging gravimeters in the tropics.

KEYWORDS-*Lacoste-Romberg, Gravimetric, Drift*

1 INTRODUCTION

Since the 1950's, two designs of portable gravity meters for use on land have dominated the field. The Worden gravimeter first developed in 1947 and the Lacoste-Romberg (LCR) gravimeter originally designed by Lacoste at about 1934, and in its present form with a metal sensor in 1945 (Huggil 1990, Torge 1989). In the 1960's and 70's, nearly all the major gravimetric surveys in Nigeria were accomplished with the aid of Worden gravimeters (Osazuwa and Ajakaiye (1982)).

Beginning from the 1980's however, the LCR gravimeters have gained popularity, accounting for over 80% of gravity surveys. The choice for the LCR instrument is largely due to its availability, portability, and cost-effectiveness in data acquisition. Although the instrument has been used primarily in Nigeria for monitoring groundwater resources and tectonic trends (Ojo, 1992), it has also been used severally for delineating basins prior to seismic search for petroleum. The continued use of this very versatile instrument especially in this seismic era will however depend on the reliability of its results. Technical improvements towards reducing environmental effects have been reported for the more recent instruments as can easily be seen from http://www.lacosteromberg.com

However, the problem of cost and availability of new instruments, and the maintenance of faulty ones in most tropical countries such as Nigeria, make the routine assessments of the performance of available ones, indispensable.

Although the LCR gravimeter has a data range of 7000 mGals and data resolution of 0.005 mGals, one often discovers that as a consequence of wrong usage, aging or mechanical faults, the instrument responds to several "error conditions", which in turn, result in abnormal drifts. The result is a reduction in accuracies. In the tropical environment as one finds in Nigeria, the error conditions are found to be mostly

associated with temperature changes. When the error input patterns and corresponding drift patterns can be foretold, the use can be twofold. First, it is possible to seek for more compensation for the effects (when the conditions cannot be avoided), and secondly one can construct a reproducible instrument-specific reactions for the basis of computational corrections.

Kangiessar (1982) has categorized errors in the use of the LCR gravimeter into systematic and random components. The systematic errors are "independent" of externally interfering factors. These include those from pointer reading and leveling. Using the optical reading method, the reading error is between 0.003 mGal and 0.005 mGal. Levelling errors depend on the calibration of the levels and on the precision in the process of centering the level bubbles, with a value below 0.002 mGal. Random components of the errors are caused by poor meter handling and atmospheric conditions of temperature, pressure, magnetic field variations, and others. Although ordinarily, enough insulation and compensations are provided for the atmospheric effects, especially in the more recent instruments, these are nonetheless inadequate, more so for an old meter. The buoyancy compensation and magnetic shielding for instance are easily lost due to shocks and vibrations, and the thermostat can be faulty.

Temperature gradients around the gravimeter, have been shown to affect meter performance considerably (Kangiessar, 1982; Nakagawa et al., 1983) and drastically, when there is fault as reported by Osazuwa and Ajakaiye (1982). Temperature gradients cause changes in the spring elasticity and the length. In the tropical climates, this phenomenon is more useful owing to observable higher temperatures (Chineke et al, 2000). Kiviniemi (1974) has established controlled condition laboratory experiments, yielding instrument specific reactions. The LCR scale reading was 16 mGa1/10^{o}C with a daily drift of 4.8 mGal/10^{o}C. Nakagawa et al. (1983), in precise calibration tests, reported high gravity values in cool environments and low values in cold environments. There is a renewed emphasis on increasing the chamber temperature for the more recent models, up to 50 ^{o} C as a way of reducing abnormal drifting. A major concern in countries like Nigeria with intense sunshine will be the problem of providing enough temperature shielding in order to maintain the chamber temperature.

2 THE GRAVIMETER RESPONSE

The LCR gravimeter, consists of a gravity response system and a thermostat. The gravity response is a weight borne on the end of a horizontal beam supported by a zero length spring. The horizontal beam carrying the mass is held at its' center of mass by an inclined counter spring. A lever arm principally to magnify the gravitational disturbance is connected to the meter housing by two symmetrically arranged horizontal springs. The measuring system can be controlled optically or electronically. In the former, the shadow of a tiny wire attached to the beam (the "crosshair") is projected on a divided scale and observed in an eyepiece. Electronically, a built-in galvanometer is used. The spring system is usually maintained at a position of optimum tilt, using a leveling mechanism, which is controlled, by two liquid bubble levels. The system is kept at an operating temperature of approximately 50^{o}C. The details of the instrument and other operational specifications are contained in the instruction manual (Lacoste&Romberg,, 2001).

Our observations have been based on the appreciation of the theory of the response (Fig. 1), of the spring system. The equation of motion is given by:

$$m\,g\,b\cos\theta = b\,k(X - X_o)\sin(\phi - \theta) = m\,b^2\,\ddot{\theta} \qquad (1)$$

where g is the magnitude of the gravitational field, k is the spring constant, and X_0 is the unstretched length of the spring. Using the sine law,

$$\frac{S}{\sin(\phi - \theta)} = \frac{X}{\sin(\pi/2 + \theta)} = \frac{X}{\cos\theta} \qquad (2)$$

We can set $\ddot{\theta} \to 0$ in equation (1). Then, combining equations (1) and (2),
we have,

$$m\,g = \frac{k\,S\,(X - X_0)}{X}$$

Simplifying then gives

$$m\,g = k\,S\left(1 - \frac{X_0}{X_e}\right) \tag{3}$$

where, $X \approx X_e$ is the equilibrium length of the spring (for y = 0)

For minute oscillations,

$$\frac{1}{x} \approx \left[\frac{1}{X_e}\right]\left[1 - \left(\frac{\Delta x}{X_e}\right)\right] \tag{4}$$

with $\Delta X \approx y \sin\phi_e$. The equation of motion now becomes

$$m\,\ddot{y} + \left[k\left(\frac{X_0}{X_e}\right)\sin^2\phi_e\right] y = 0 \tag{5}$$

This is of the usual form,

$$m\,y + \omega_0^2 \ddot{y} = 0 \tag{6}$$

$$\text{where } \omega_0 = \left[k\left(\frac{X_0}{X_e}\right)\sin^2\phi_e\right]^{1/2} \tag{7}$$

Since $\omega = 2\pi T, \quad T \propto \omega,$ then $\quad T \propto \sin\phi$.

Also since $\sin\phi_e = \frac{S}{X_e}$, the implication is that for equilibrium, T must be extended for $S \rightarrow 0$. The instrument is therefore essentially a long period vertical seismometer, and operationally unstable and bulky according to Peters (2001). The concept of zero length utilized to guard against this in the gravimeter presupposes that from equation (7), that T can also be lengthened by letting $X_0 \rightarrow 0$ for constant ϕ_e. This concept which leads to a pre-coiling mechanism, utilizing a helical configuration, only means that the first result, of tension as Melchior (1983) puts it, is to " uncoil the helix". This is a major constraint in the tropical use, as we discover that the normal linear drift of about 8 x 10^{-3} mGals /hour becomes abnormal as a result of temperature-induced tension coupled with the associated hysteresis in the spring.

3 OBSERVATION PROCEDURE

Our observations were made with a Lacoste-Romberg gravimeter model G (468), at a fixed location in Jos, Nigeria (longitude 8° 53' E, latitude 9° 57' N and elevated at 1159 meters above sea level). Since conditions could not be simulated, we found the area is particularly suitable for the study, given its peculiar geology and temperature. In addition, it has low seismicity, and records temperature extremes (the lowest in Nigeria) of about 4-9° C to moderately high values approximately 23-35° C. Preliminary investigations to determine gravimeter specifications i.e. reading line, sensitivity, and normal drift, were carried out and compared with the manufacturer's specifications. The systematic components of associated errors namely reading error, and leveling were found. The effect of fluctuations in chamber temperature and the relationships with variations in system voltage was assessed. Since the external temperature effects were of prime interest in this study, we monitored the drifts and sensitivity on a daily basis, recording the temperature, atmospheric pressure, and the relative humidity (R.H) for a 30-day period. We have only selected the temperature extremes for those times when the pressures and the R.H were the same for the basis of comparison. Also since each reading recorded was an average of three observations which were then corrected for earth tides, our assessment is quite representative of the true picture of the temperature phenomenon, other meter conditions being constant.

4 RESULTS AND DISCUSSION

We present here the deviations of the gravimeter drift and sensitivity from some predetermined "optimum" values. The optimum values were obtained at a chosen tropical temperature of 23° C. The normal drift at this temperature derived from the linear trend of a 72-hour tidal response is shown in Figure 2 to be 0.0079 mGals/hour. It should be noted that 1mGal = 10^{-5} m s^{-2}. The value of the R-squared was almost 85 percent. The gravimeter sensitivity defined as the number of cross hair divisions corresponding to one complete turn of the measuring dial, has a value of almost unity (Fig. 3) which is in line with the manufacturer's specification. At a temperature of 10° C, there were not any noticeable changes in the drift, but the correlation of the sensitivity has dropped by roughly 0.02 (Fig. 4). The drift pattern for sudden changes in the external temperature is however phenomenal and is plotted in figure 5. Beginning from the point of the temperature jump, the initial creeping response associated with hysteresis is evident, and the response is repeated on reverting to the initial temperature.

Generally, it was revealed that a positive drift yielded when the meter was brought from a cooler environment to a warmer one and a negative drift when it was moved the opposite direction. The "creep" arising from spring contraction and relaxation has been explained by Torge (1983), as initiating a temporary variation in the spring constant. Considering the fact that the meter spring is enclosed in an insulating shield and maintained at an operating temperature of 49.5° C well above most tropical temperatures, we suppose that either the heat shield was no longer sufficient or that the thermostat must have been faulty. Both possibilities would pose very serious constraints on meter function. The change in temperature within the chamber in both directions exhibits long period non-linearity, as we show from the heating and cooling curves in figure 6. The two curves form truncated hysteresis loops like observed earlier by Osazuwa and Ajakaiye (1982). A closed loop formed from the two truncated ones will have a period of about 96 minutes. A gravimeter that has just been turned on heat from an idle period requires 100-120 minutes waiting time for readings to be obtained with normal drift (Fig. 7). This, we feel, translates to the time for closing up the hysteresis loop initiated by temperature "tension", similar to the time that must be observed for the unclamped spring to stabilize.

For the analysis of the drift above to be better understood, we here evoke the usual theory of the long period vertical seismograph. The period T of the system is given by

$$T^2 = \frac{4\pi^2}{\Delta g}\left(X - X_0\right) \tag{8}$$

where the extension of the meter from equilibrium $X - X_0$, corresponds to a gravity change Δg. The Taylor series expansion of the meter reading with respect to time t is given by Torge (1989) as

$$g(t) = g(t_0) + \left(\frac{\partial g}{\partial t}\right)_0 (t - t_0) + \frac{1}{2}\left(\frac{\partial^2 g}{\partial t^2}\right)_0 (t - t_0)^2 + \frac{1}{6}\left(\frac{\partial^3 g}{\partial t^3}\right)_0 (t - t_0)^3 + \mathrm{K} \tag{9}$$

with t_0 being the reference time of the respective measurement period. The first two terms of equation (9) yields the drift i.e.

$$\frac{dg(t)}{dt} = \frac{4\pi^2}{T^2}\left(X - X_0\right) \tag{10}$$

For a gravimeter initially unclamped from equilibrium position, short periodic movements give rise to abnormal non-linear drifts. Temperature changes have similar quasi-static elastic effects. For measurements made immediately after unclamping, Nwofor (1994) has recorded errors of about 6 x 10^{-1} mGals/minute in the normal drift. This reduced to about 10^{-3} mGals /minute when 5 minutes was allowed after unclamping and before measurements were taken. For similar reasons, it is recommended that the gravimeter be allowed at least 1 hour for stability in a new temperature environment, or whenever temperatures change suddenly near the meter, that is in case the internal temperature provisions are not effective.

In the case of the sensitivity-temperature anomalies observed, we refer to the normal positions of the spring system at the time of gravity measurements (Fig. 8). We can set the force laws of the system to be

$$m\,g\,b\cos\gamma = b\,k\,X\sin\phi \tag{11}$$

and from Sine law $X\sin\phi = s\sin\beta$ (12)

From analysis similar to that by Melchior (1983), we can show that the sensitivity of the instrument is

$$dg = \frac{g\,b\sin\beta\,d\beta}{X^2(X-1)} \tag{13}$$

The angles α and β can be modified to obtain optimum operational sensitivity by using the long level and measuring spring respectively. Melchior (1983) had shown that

$$dg = g\cot g\,(\alpha+\beta)\,\Delta\alpha \tag{14}$$

where $\Delta\alpha$ is the setting or leveling error, given by

$$\Delta\alpha = \alpha_s - \alpha_0 \tag{15}$$

α_s is the setting angle and α_0 is any optimum setting angle. When $\alpha_s = \alpha_0$, there is no error in leveling. When $\gamma = 0, (\alpha+\beta) = \frac{\pi}{2}$ and we can write equation (14) as

$$dg = c\,g\,\Delta\alpha \tag{16}$$

where c is a constant.

Hence, the sensitivity is uniquely determined by the setting error and as such by the long level. As we have shown from equation (16), errors in the long level will be perceived in the form of gravity change.

We obtained for a 13° C decrease in temperature, a drop in sensitivity of about 0.02 counter divisions/dial unit. Since 1 complete dial turn is equivalent to 1 mGals, and 1 unit of the measuring dial is 0.1mGal, then about 0.002 mGals error would have resulted due to the temperature difference. Temperature changes can affect the sensitivity by affecting either the measuring spring or by imposing some setting errors. Temperature-induced bubble drifts of the liquid level mechanism that now reduces their precision for meter leveling, we understand, could cause the later. Although we could not assess completely, the bubble drift–sensitivity relationship, when we tilted the meter by one scale division, in the long level (Fig. 9), the observed sensitivity did go up by about 0.001 counter divisions / dial unit, becoming exactly unity. The result was the limiting of crosshair motion to units above the reading line (2.2). Again like the problem of gravimeter spring drifting, the requirement for arresting temperature induced sensitivity problem would be to observe some time for bubble stability, since the liquid bubble type, LCR gravimeters are still the most common in countries like Nigeria.

5 CONCLUSIONS

In the tropics where erratic and high magnitude temperature variations are common, there seem to be severe limitations in the use of aging Lacoste-Romberg gravimeters for gravity surveys as its temperature compensation may be inadequate. This is because the active components of the instrument are largely temperature–dependent. A temperature variation in the environment where the LCR is located, affects the sensitivity of the instrument. This it does by realigning the measuring spring and the liquid bubbles thereby causing leveling errors. This in turn affects the meter drifts by initiating elastic hysteresis in the spring. These cause errors in gravity measurements that are often very difficult to account for in field work, and equally difficult to model. The implication is that certain field procedures for achieving optimum results must be adopted in the utilization of the LCR gravimeters. We have summarized these in Table 1. This is in addition to the error buggets provided ealier by Torge (1983, 89), Kangiessar (1986) and others.

An essential part of the present procedure would require long periods of waiting for meter stability. In the study of certain short period geodynamic phenomena, such time observance for stability may be unrealistic. The best option will then be to correct for these effects from prior instrument-specific responses,

aided by knowledge of associated periodicities (Mishra and Rao, 1997). It may also be necessary for accurate temperature forecasts to accompany the deployment of gravimeters for fieldwork.

ACKNOWLEDGMENT

This work was concluded during the authors' research visit at the Abdus Salam International Centre for Theoretical Physics (ICTP), Trieste, Italy. The authors are grateful to Professor D.E. Ajakaiye, formally of the University of Jos, Nigeria, whose LCR gravimeter was used for this study.

REFERENCES

Ajakaiye D.E. (1976) A gravity survey of the Nigerian younger granite province. In: Kogbe C.A (ed) Geology of Nigeria. Elizabeth Publishing Company Lagos, pp 225–233.

Chineke T.C, Nwofor O.K, Ezike F.M (2000) Patterns of daily maximum and minimum temperature data in Nigeria. Meteorology & Atmospheric Physics 75: 61-67.

Huggil A (1990) The Santrex CG-3 automated gravity meter description and field results. (unpublished monograph), University of Delft.

Kangiessar E (1986) The gravimeter calibration system Hanover. (unpublished monograph)

Kiviniemi A (1974) High precision measurements for studying the secular variation in Finland Publications of the Finish Geodetic Institute, Helsinki

Macleod W.N, Turner D.C & Wright E.P (1971) The geology of the Jos plateau. Geological Survey of Nigeria, 1(32): 2 –6

Melchior P (1983) The tides of the planet earth. Pergamon, New York pp 268 -270

Mishra D.C & Rao M.B.S. (1997) Temporal variations in gravity field during solar eclipse on 24th October 1995. Current science 72(11): 783

Nakagawa I et al (1983) Precise calibration of scale constants of Lacoste–Romberg gravimeters and international gravimetric connection along the circum pacific zone. Final report on the Reform of International Gravity Standardization Network (IGSN) 1971

Nwofor O.K (1994) An experimental study of some factors affecting precision gravimetry using the Lacoste-Romberg gravimeter. MSc Thesis, University of Jos

Ojo S.B (1992) The application of gravity method in groundwater, mineral exploration and the study of crustal deformation, tectonics and geodynamics. Proceedings of an international research workshop on Physics of the Solid Earth with special reference to gravimeter. Jos, Nigeria May 1992

Osazuwa I.B, Ajakaiye D.E (1982) The effect of chamber temperature variations on the Lacoste-Romberg gravimeter. Nigeria Journal of Mining and Geology. 19(1): 267 – 277

Peters R.D (2000) Physics of the zero length spring of Geoscience. (unpublished mimeograph) Mercer University

Torge W (1983) Gravimetry, new developments. IGC report 1978-1982, presented to the 10th IGC commission Tokyo

Torge W (1989) Gravimetry. Walter deGruyter, Berlin. pp 200 –235

Table 1: Summary of error reduction of the temperature effects by the optimum procedure with the errors represented by root-mean-square (Δg) values in microgals

Error Source	Associated Error in the normal procedure	Additional measures in the optimum procedure	Possible Errors after additional measures
1) Spring hysteresis	~ 10 depending on magnitude and period of the change	At least 30 minutes waiting time in new temperature environment for spring stability	< 1
2) Leveling Errors	- do –	a) at least 30 minutes waiting time in new temperature environment for bubble stability b) sensitivity check by temperature parallax	<1
3) Chamber temperature variations	- do-	a) at least 2 hours waiting time from the time gravimeter is operated from idle periods b) additional aluminum casing c) modelling of thermostatic errors	

LIST OF FIGURES

Figure 1 : The Lacoste–Romberg gravimeter principle
Figure 2 : Gravimeter drift, measured at a temperature of 23ºC
Figure 3 : Gravimeter sensitivity, measured at a temperature of 23ºC
Figure 4 : Gravimeter sensitivity, measured at a temperature of 10ºC
Figure 5 : Gravimeter drifts for sudden changes in the external temperature
Figure 6 : Cooling (shaded squares) and heating (solid diamonds) curves of the gravimeter plotted on same axis
Figure 7 : Gravimeter drift response from an idle period
Figure 8 : Schematic representation of the spring system along the long level at any setting position in gravity measurements (adapted from Nakagawa et al, 1983)
Figure 9 : Effects of leveling on the sensitivity of the gravimeter.

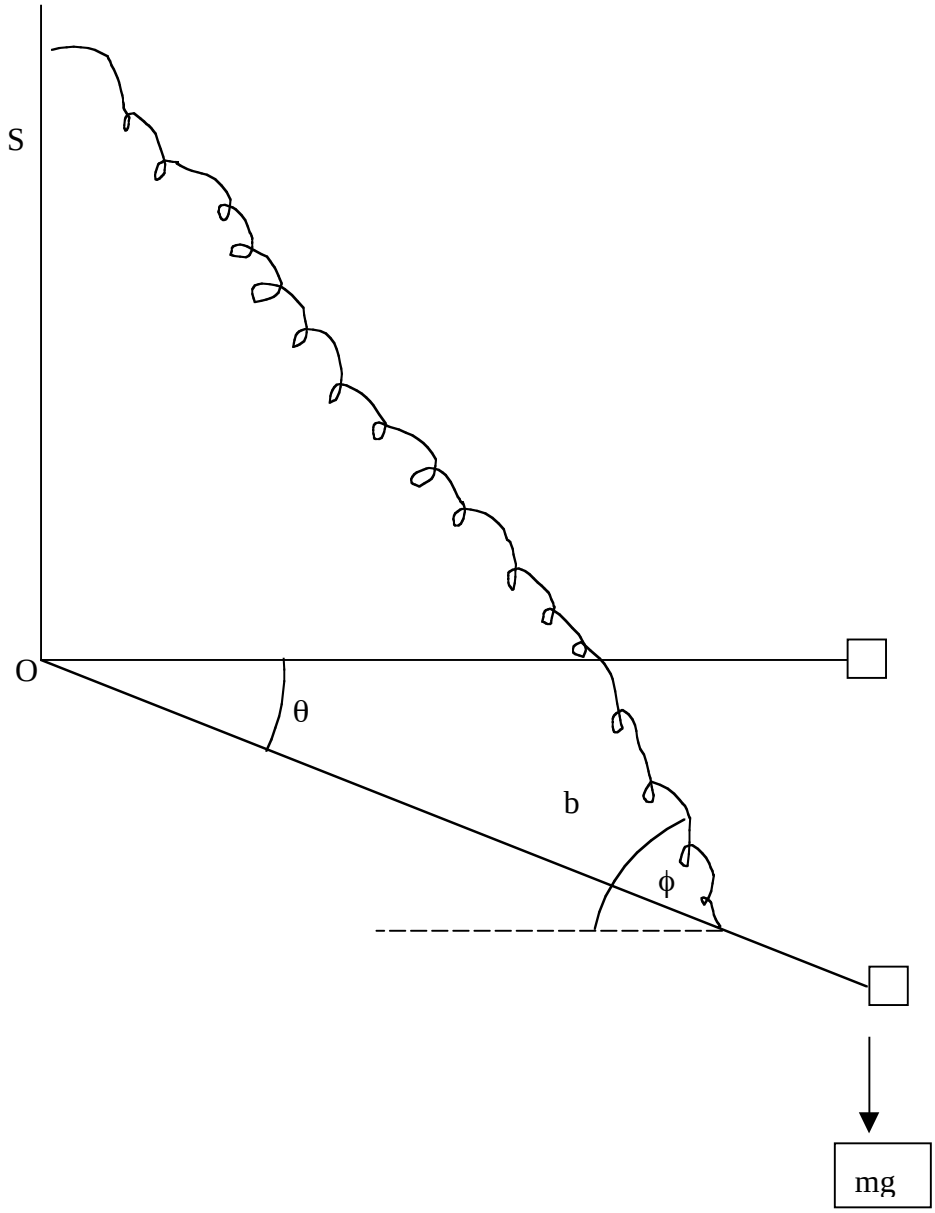

Figure 1

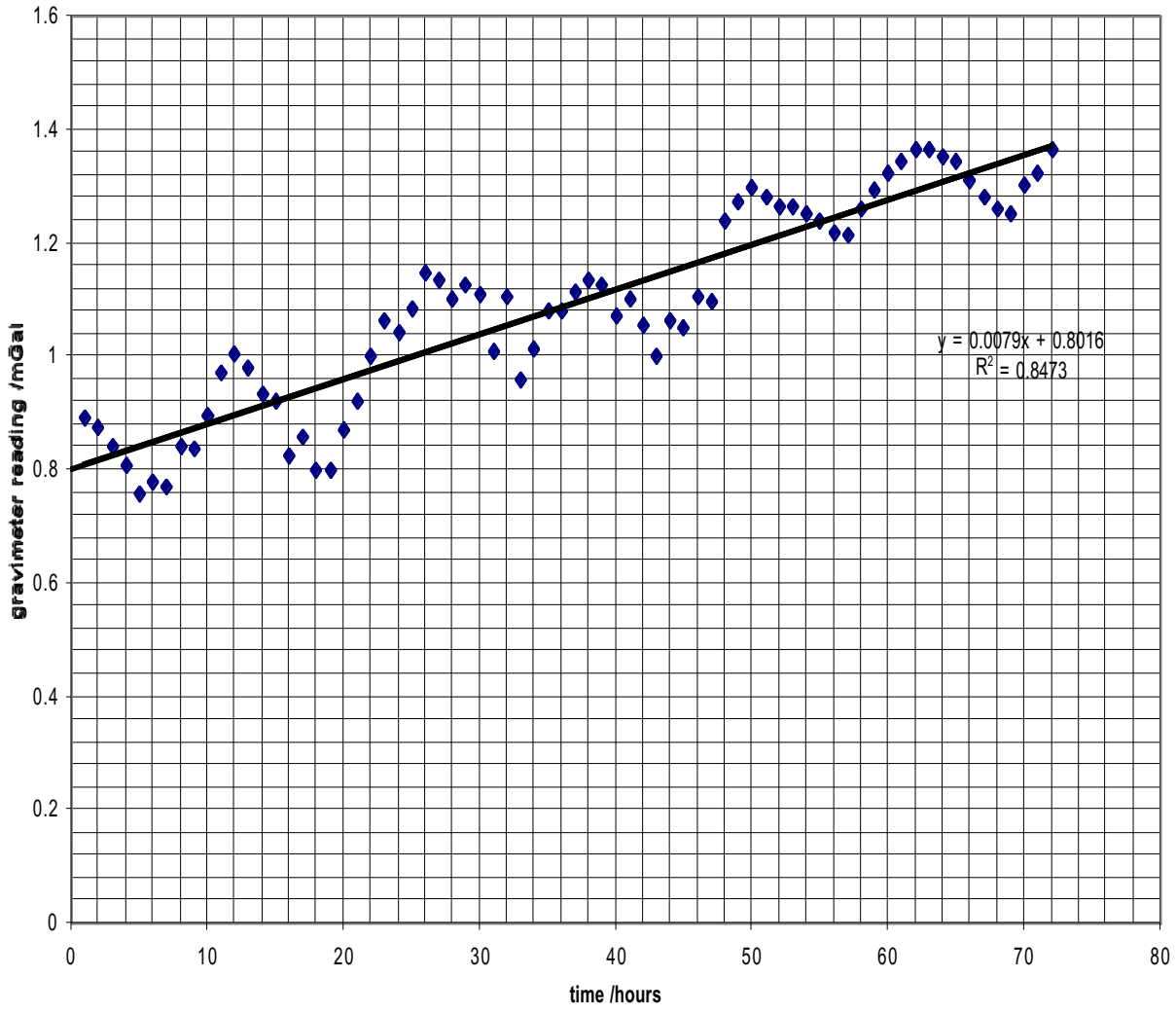
gravimeter reading /mGal
time /hours
y = 0.0079x + 0.8016
R2 = 0.8473
0
0.2
0.4
0.6
0.8
1
1.2
1.4
1.6
0
10
20
30
40
50
60
70
80

Figure 2

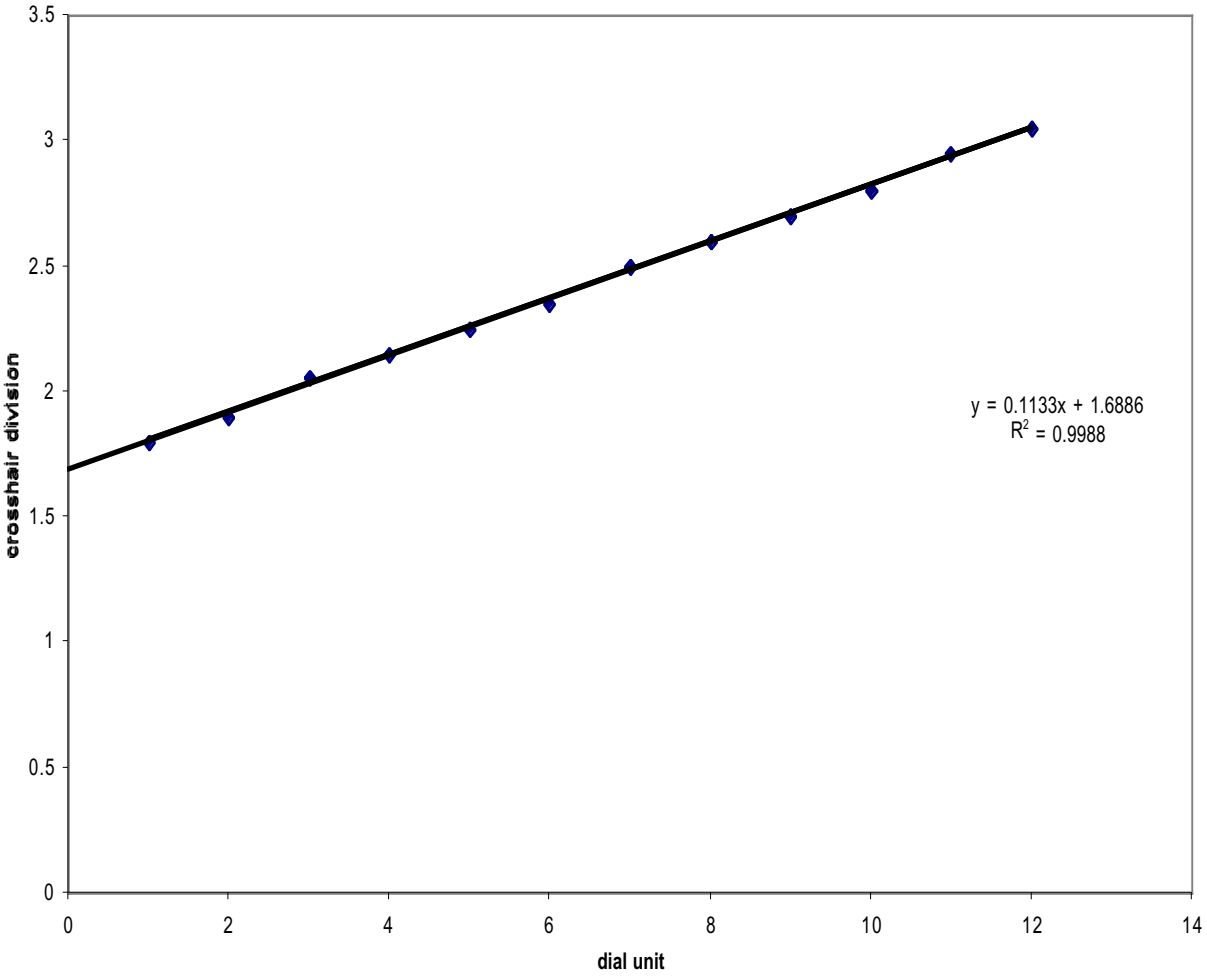
3.5
3
2.5
2
1.5
1
0.5
0
crosshair division
0
2
4
6
8
10
12
14
dial unit
y = 0.1133x + 1.6886
R2 = 0.9988

Figure 3

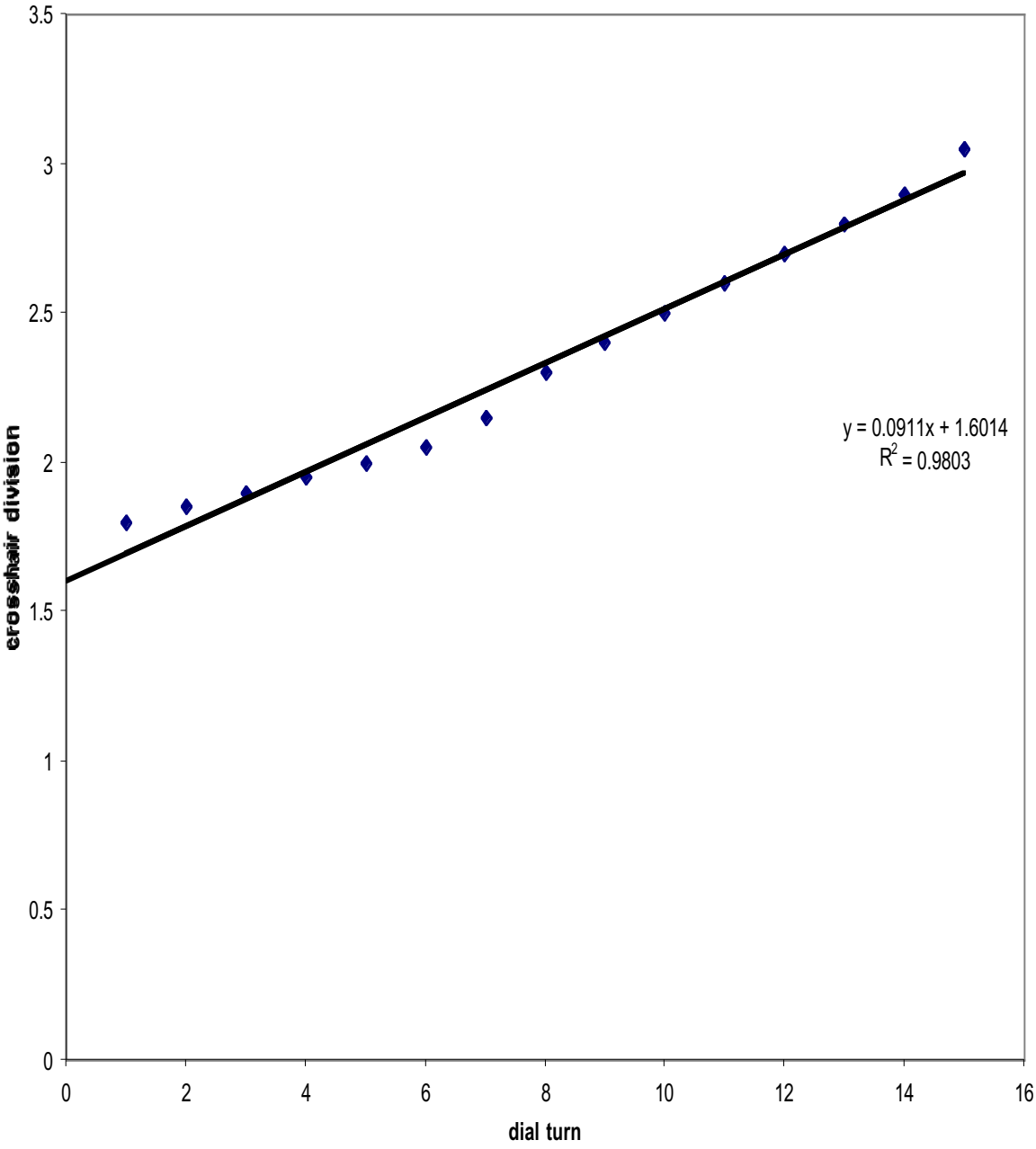
3.5
3
2.5
2
1.5
1
0.5
0
crosshair division
0
2
4
6
8
10
12
14
16
dial turn
y = 0.0911x + 1.6014
R2 = 0.9803

Figure 4

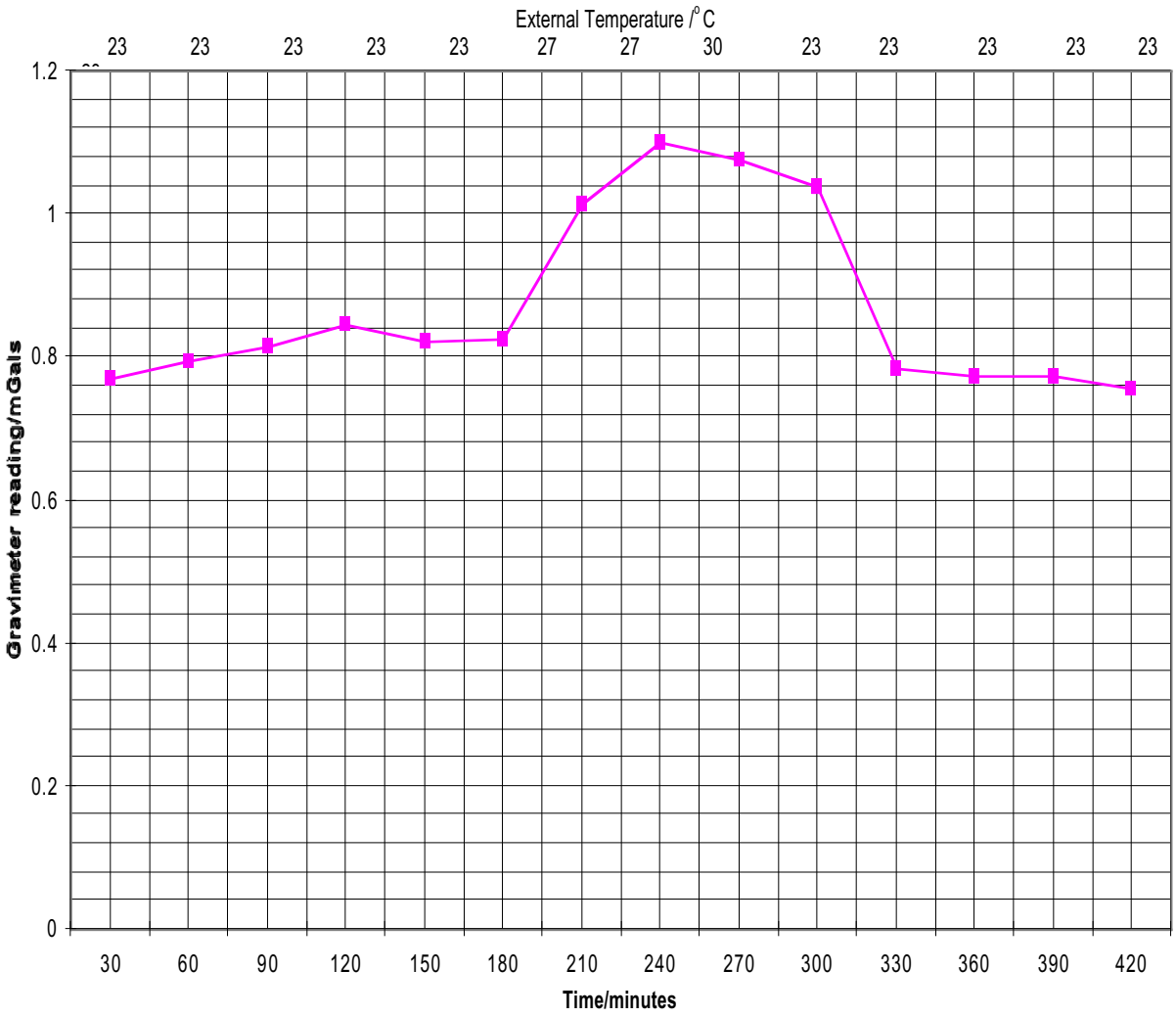
External Temperature /° C
23 23 23 23 23 27 27 30 23 23 23 23 23
1.2
1
0.8
0.6
0.4
0.2
0
Gravimeter reading/mGals
30 60 90 120 150 180 210 240 270 300 330 360 390 420
Time/minutes

Figure 5

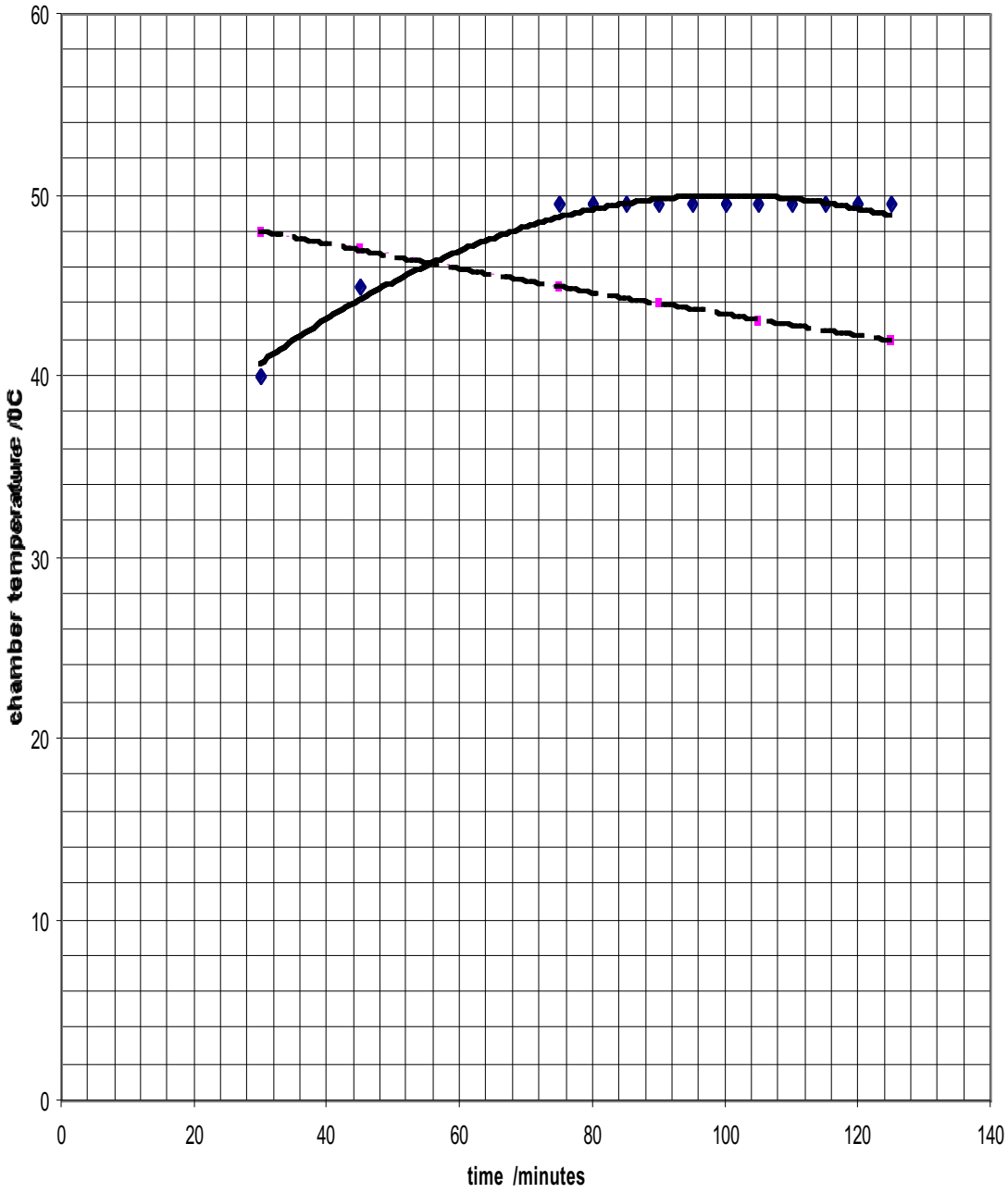
60
50
40
30
20
10
0
chamber temperature /0C
0
20
40
60
80
100
120
140
time /minutes

Figure 6

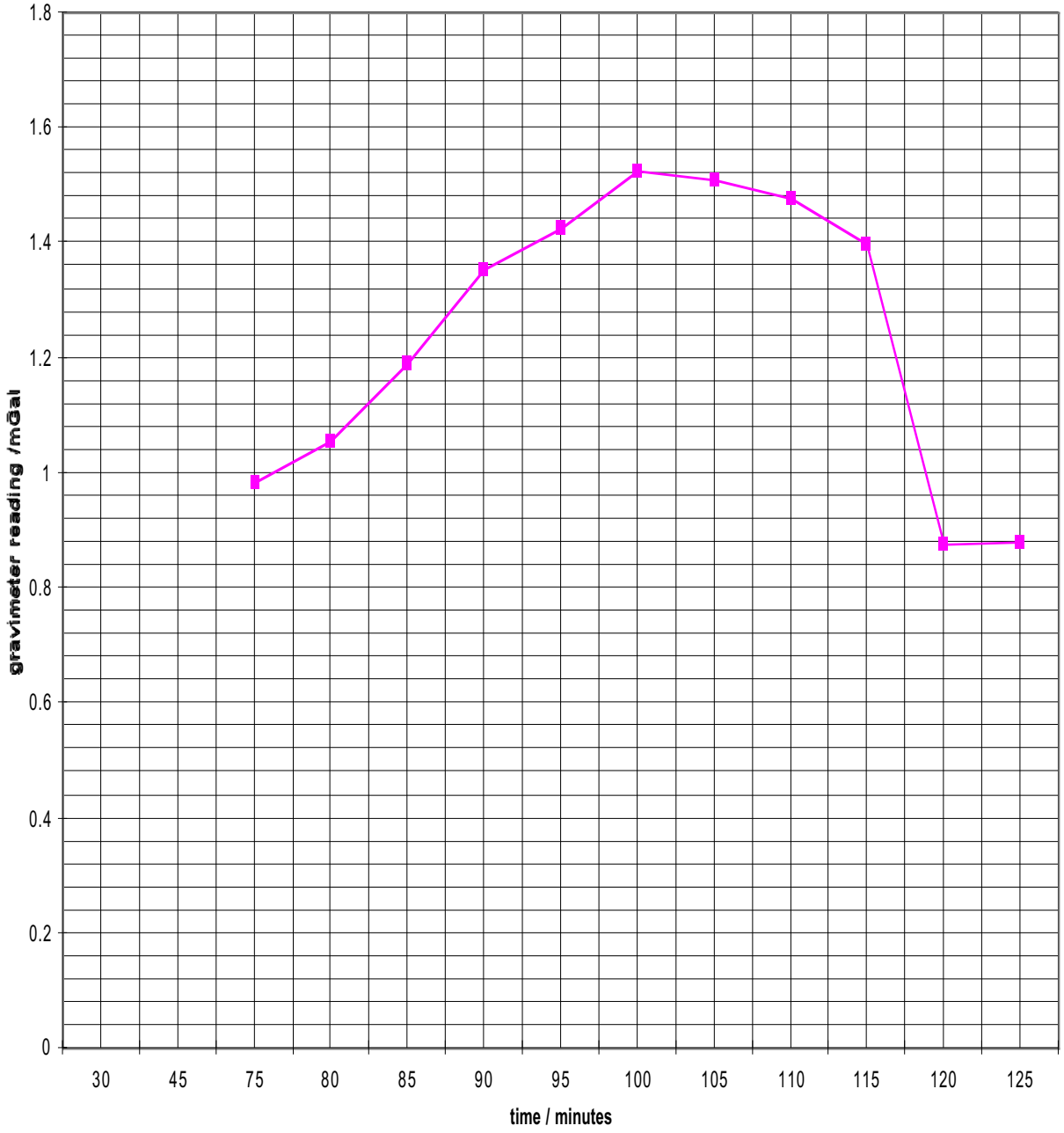
1.8
1.6
1.4
1.2
1
0.8
0.6
0.4
0.2
0
gravimeter reading /mGal
30
45
75
80
85
90
95
100
105
110
115
120
125
time / minutes

Figure 7

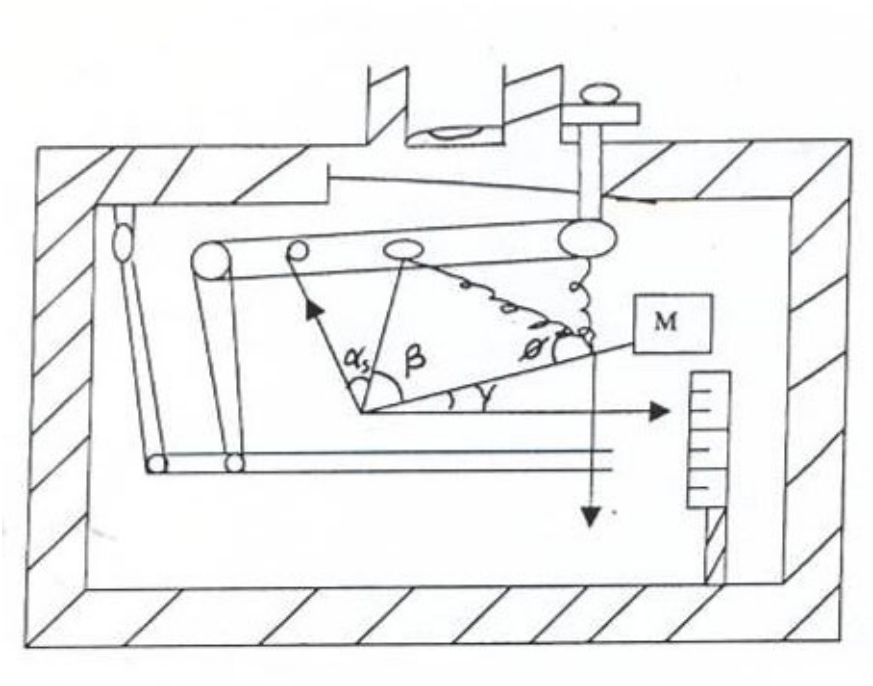

$$\alpha_s + \beta + \gamma = \pi/2 \; ; \; \beta + 2\phi = \pi$$

Figure 8

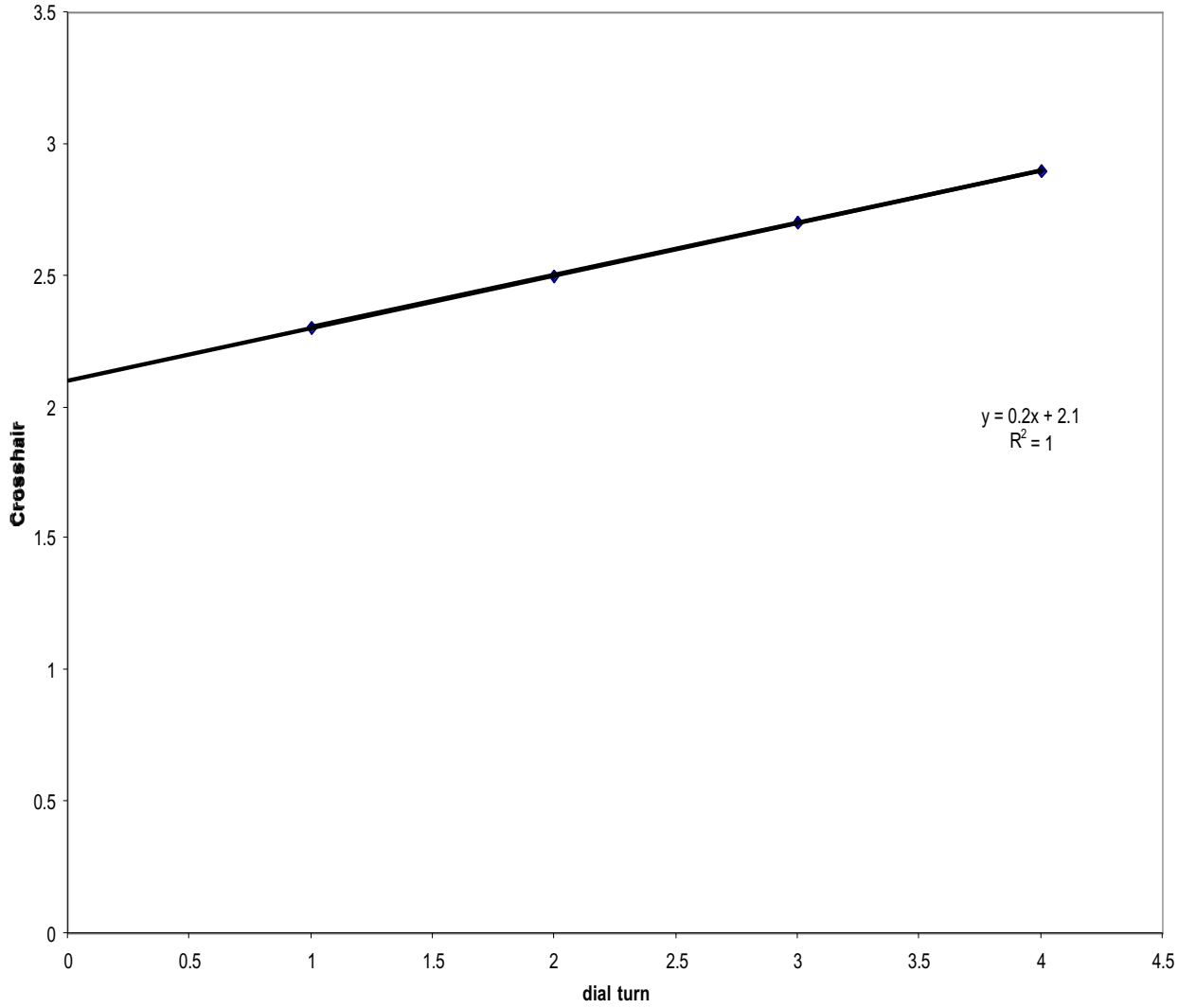
3.5
3
2.5
2
1.5
1
0.5
0
Crosshair
0
0.5
1
1.5
2
2.5
3
3.5
4
4.5
dial turn
y = 0.2x + 2.1
R2 = 1

Figure 9

Preliminary results in the achievement of the new gravity system of Republic of Moldova

Besutiu, L.[1], Neaga, V.[2], Nicolescu, A.[3], Lorinczi, J.[1], Ilies, I.[2], Besutiu, G.[3]

[1]Institute of Geodynamics of the Romanian Academy, 70201 Bucharest 37, 19-21, Jean-Louis Calderon St., e-mail: **besutiu@geodin.ro**

[2] Institute of Geophysics and Geology of the National Academy of Sciences of Moldova, 277028 Chisinau, 3, Academiei St., Republic of Moldova

[3]Geological Institute of Romania, 78344 Bucharest 32, sector 1, str. Caransebes 1, Romania

ABSTRACT

The achievement of the national gravity reference network of Republic of Moldova (**NGRNM**) represents the first step in merging gravity networks of Romania and Republic of Moldova. The project started as a joint venture of the Institute for Geophysics and Geology of the Academy of Sciences of Republic of Moldova and the Geological Institute of Romania. It is part of a larger program, GRANAT (**G**ravity **N**etworks **A**dvanced **T**ies), aimed to join gravity images over the state borders of Romania, Ukraine and Republic of Moldova, in an area where several major geotectonic units met each other along the SW margin of the East European Plate.

The paper mainly deals with problems connected to gravity determinations along the **NGRNM** ties and their adjustment. The **NGRNM** consists of seven first order gravity stations regularly spaced over the Moldavian territory. They have been tied within a triangle network with central base station (Chisinau) by using a LaCoste & Romberg model D gravity meter. Gravity vertical gradient determinations in every base station have been also performed by repeated measurements at every site at two different levels: 0.30 meters, and 0.80 meters above the ground.

The **NGRNM** has been adjusted by least square method as a free network, using four stochastic models based on various weighting systems.

Provisional absolute gravity values within the **NGRNM** have been obtained by connecting the new network to the national reference networks of Romania.

Key words: gravity, reference network, Republic of Moldova, GRANAT project

GENERAL CONSIDERATIONS

Located in the eastern part of the Central Europe (Fig. 1), Republic of Moldova was one of the components of the former Soviet Union. After getting the independence, the new state faced a lot of problems connected to its new status, and, among them, the necessity for a national gravity system, as close as possible to the EU gravity standard.

Taking the advantage of the fact that one of the neighboring countries, Romania, had been actively taking part to the UNIGRACE project (Rosca, 1999; Rosca and Besutiu, 2000), aimed to the integration of the gravity systems of the former European socialist countries into the EU system, a joint venture of the Institute of Geophysics and Geology of the Moldovan Academy of Sciences, and the Geological Institute of Romania started in the year 2000 in order to accomplish this task. Actually, this work represents, in a way, an extent of the above mentioned EU funded project, and is part of a larger project, GRANAT (**G**ravity **N**etworks

Advanced **T**ies), which was aimed to join gravity images over the state borders of Romania, Ukraine and Republic of Moldova, in an area where several major geotectonic units met each other: East European Plate, Alpine Carpathian Orogene, North Dobrogea folded belt, Moesian Plate and Scythian Plate.

NETWORK DESIGN

The design and field activities for the achievement of the national gravity reference network of Moldova (**NGRNM**) were thoroughly presented in a previous paper (Besutiu et al, 2001b). However, for a better understanding of the stochastic models used in the adjustment, in the followings the main aspects of its achievement will be summarized.

The gravity reference network was designed as a triangle network with central station, in a similar manner to the former 1st order gravity reference network of Romania (Botezatu, 1961). Location of the gravity stations were mainly planned on the concrete pillars of the seismological stations of the National Seismic Monitoring Network of Republic of Moldova (Chisinau, Soroca, Cahul, Leova).

As this configuration proved to be too scarce for gravity purposes, several base stations were added to appropriately cover the territory: Balti (located at the orthodox cathedral "St. Nicolae", in the central part of the city), Ungheni (at the orthodox church "St. Alexander Nevski"), and Causeni (at the memorial dedicated to Alexei Mateevici, located in the central square of the town). Table no. 1 shows the geographical coordinates of the NGRNM base stations.

Table no. 1 - Location of the NGRNM base stations

Station code	latitude	longitude
CHISINAU*	46º59' 52.0"	28º 40' 05.0"
SOROCA*	48º 07' 53.5"	28º 20' 31.0"
BALTI	47º 45' 40.0"	27º 56' 00.0"
UNGHENI	47º 12' 00.0"	27º 48' 00.0"
LEOVA*	46º 28' 24.6"	28º 14' 53.3"
CAHUL*	45º 54' 18.8"	28º 12' 02.4"
CAUSENI	46º 38' 15.0"	29º 24' 30.0"

Asterisks mark common location with seismic monitoring network stations.

Special forms including map sketches and photos have been also provided for a complete description of every base station.

DATA ACQUISITION

Instruments

Gravity determinations along the **NGRNM** ties were performed by using the LaCoste & Romberg D-214 meter owned by the Geological Institute of Romania.

During the works, factory scale factor has been used to turn direct readings into gravity units. However, the meter has been checked up before, and after the end of the field campaign, by measuring along the UNIGRACE calibration line Cluj-Napoca – Belis (Besutiu et al, 2001a). Figures provided by factory were fully confirmed by gravity range determined along this calibration line (172.118 mgals).

Although the meter is fully thermostatic, due to the extremely low external temperatures experienced during the works, small variations of the temperature inside the instrument occurred during the measurements.

Consequently, the measuring temperature was carefully read every time, and took into consideration as a weighting constraint when adjusting the results.

Methodology

As previously mentioned, the **NGRNM** was designed as a triangle network with central station. Each gravity tie was measured at least twice, within independent measuring loops performed in different days. At least three dial readings were taken each time at every location.
Drift and tidal corrections have been applied to every measurement. Average values of the distinct determinations were taken into consideration as representative values for each gravity tie. The quality of the obtained results was carefully examined and evaluated (Besutiu et al, 2001b). Table no. 2 summarizes the results.

Table 2 - Mean gravity and associated measuring parameters along the NGRNM ties

Network tie	Tie code	Δg (mgal)	rms (mgal)	e (mgal)	Δt (^{0}C)	ΔT (minutes)
Chisinau-Soroca	1	120.217	0.018	0.008	0.10	375
Chisinau-Balti	2	79.518	0.018	0.007	0.06	366
Balti-Soroca	3	40.701	0.002	0.002	0.01	223
Ungheni-Balti	4	45.272	0.002	0.002	0.02	156
Chisinau-Ungheni	5	34.236	0.010	0.006	0.08	320
Chisinau-Albita	6	13.969	0.006	0.005	0.08	290
Leova-Albita	7	30.037	0.005	0.005	0.01	200
Leova-Chisinau	8	16.068	0.014	0.004	0.09	314
Cahul-Chisinau	9	96.858	0.012	0.004	0.15	598
Cahul-Leova	10	80.795	0.002	0.002	0.05	268
Causeni - Cahul	11	91.430	0.020	0.020	0.02	600
Causeni-Chisinau	12	5.442	0.010	0.004	0.13	278

where Δg = mean gravity value along the network tie
rms = mean standard deviation of a measurement
e = standard deviation of the mean gravity
Δt = maximum temperature deviation during the measuring loop
ΔT = mean duration of the measuring loop

Fig. 2 presents the network design and triangle closures.

NETWORK ADJUSTMENT

Network adjustment has been performed under the hypothesis that measurements along the ties have been affected by random errors only. Systematic effects (such as the influence of the scale factor for instance) have been not taken into account at this research stage.
Mean gravity value observed along the network ties was the entity to be adjusted according to the adopted model

$$\Delta G_i = \Delta g_i + v_i \qquad (i = 1,2, \ldots ,12) \qquad (1)$$

where ΔG_i represents an estimate of the gravity after the adjustment
Δg_i represents the observed gravity (before the adjustment)
v_i represents the correction to remove the observation error

Least square method in the variant of conditioned direct observations within a free network has been considered. As random errors affecting the observations have been considered to represent a normal repartition, the adjustment was made under the well–known constraint of minimization (2)

$$[pvv] = \sum_{i=1}^{12} p_i v_i^2 = V * PV \quad (2)$$

where p_i represents the weight of the observation *i* (i = 1,2, … , 12)
P is the weight diagonal matrix ($P = [p_{ii}]$)
V is the corrections (v_i) vector ($V = [v_i]$)
V* represents its transposed matrix.

According to Wolf (1975) and Detrekoi (1991) the weights can be inferred from a simple equation

$$p_i = \frac{c^2}{m_{l_i}^2} \quad (i=1, 2, \ldots,12) \quad (3)$$

where c is the unit weight error, and m_{l_i} is the RMS error of the mean value of the observations along the tie **i**.

It has been previously demonstrated (Detrekoi, 1991) that **c** value can be estimated from

$$\bar{c}^2 = V^* PV/f \quad (4)$$

where f is the number of conditional equations, and P is the weights diagonal matrix.

Four functional-stochastic models have been used during the network adjustment, based on different weighting systems:

a) equal accuracy observations, meaning

$$p_i = 1 \quad (5)$$

b) weights related to the temperature variations during the measuring cycle,

$$Y_i = 0.06/\Delta t_i \quad (6)$$

c) weights related to the eventual drift nonlinearities, depending on the length of the measuring loop

$$Z_i = 314/ d_i \quad (7)$$

and, finally,

d) weight as a function of the RMS error of the observations on each tie, meaning

$$X_i = (0.004)^2/ m_{l_i}^2 \quad (8)$$

The weight systems used for the network adjustment are shown in Table no.3.

Table 3 - Weighting systems used in the adjusting

weighting factor	RMS error of the gravity mean value (mgal)		temperature variations		duration of the measuring cycle	
gravity tie i	m_{l_i}	weight X_i	Δt_i (^{0}C)	weight Y_i	d_i (minutes)	weight Z_i
1	0.008	1/4	0.10	3/5	375	314/375
2	0.007	16/49	0.06	1	366	157/183
3	0.002	4	0.01	6	223	314/223
4	0.002	4	0.02	3	156	157/78
5	0.006	4/9	0.08	3/4	320	157/160
6	0.005	16/25	0.08	3/4	290	157/145
7	0.005	16/25	0.01	6	200	157/100
8	0.004	1	0.09	2/3	314	1
9	0.004	1	0.15	2/5	598	157/299
10	0.002	4	0.05	6/5	268	157/134
11	0.020	1/25	0.02	3	600	157/300
12	0.004	1	0.13	6/13	278	157/139
unit weight before the adjustment	0.004	1	0.06	1	314	1

Table no. 4 illustrates the conditional equations as inferred from the triangle closures.

Table no. 4 Conditional equations within the network adjustment

Network triangle	network tie	tie code i	observed gravity l_i (mgal)	RMS error $\pm m_{l_i}$ (mgal)	**Conditional equation**	**Tolerance threshold** (mgal)
I	Chisinau → Soroca	1	120.217	0.008	$-v_1+v_2+v_3+$ **0.002**$=0$	**0.0108**
	Chisinau → Balti	2	79.518	0.007		
	Balti → Soroca	3	40.701	0.002		
II	Chisinau → Balti	2	79.518	0.007	$-v_2+v_4+v_5-$ **0.0100**$=0$	**0.0094**
	Chisinau → Ungheni	5	34.236	0.006		
	Ungheni → Balti	4	45.272	0.002		
III	Chisinau → Leova	8	-16.068	0.004	$v_6+v_7-v_8+$ **0.0000** $=0$	**0.0081**
	Chisinau → Albita	6	13.969	0.005		
	Albita → Leova	7	-30.037	0.005		
IV	Chisinau → Cahul	9	-96.858	0.004	$-v_8+v_9+v_{10}+$ **0.0050**$=0$	**0.0060**
	Cahul → Leova	10	80.795	0.002		
	Chisinau → Leova	8	-16.068	0.004		
V	Chisinau → Cahul	9	-96.858	0.004	$-v_9+v_{11}+v_{12}-$ **0.0140**$=0$	**0.0208**
	Cahul → Causeni	11	-91.430	0.020		
	Chisinau → Causeni	12	-5.442	0.004		

The last column in Table 4 shows the tolerance threshold (Detrekoi, 1991). The appropriate quality of the gravity observations is emphasized by the fact that no closure is above the computed tolerance. The slight disagreement noticed in the case of triangle II is insignificant, and much below the instrument accuracy.
The matrix of the coefficients of the normal equations (N) will be

$$N = A^{*}P^{-1}A \tag{9}$$

where P^{-1} represents the inverse of the weight matrix.
The corrections vector has been obtained through the inverse matrix of the coefficients of the normal equations system (N^{-1})

$$V = - P^{-1}AN^{-1}T \tag{10}$$

where T is the closures vector.
The covariance matrix is defined by

$$Q = [q_{ij}] = P^{-1} – (P^{-1}A)\, N^{-1}(A^{*}P^{-1}) \qquad i, j = 1, 2 \ldots 12 \tag{11}$$

and unit weight after the adjustment

$$\bar{c} = (V^{*}PV /f)^{1/2} \tag{12}$$

where f is the number of equations used.

RMS error of the adjusted gravity on each tie was computed from the coefficients of the covariance matrix and the related unit weight

$$m_i = \bar{c}\ (q_{ii})^{1/2} \tag{13}$$

The coefficients of the equations and the results of the network adjustment for various stochastic models using different weighting systems are shown in Table 5.

Table 5 Conditional equations and adjustment variants for various weighting systems

Gravity tie	Conditional equations coefficients (equal weight)					adjustment values for various weighting systems			
i	I	II	III	IV	V	a	b	c	**d**
1	-1					-0.0005	-0.0011	-0.0012	**-0.0025**
2	1	-1				-0.0030	-0.0037	-0.0033	**-0.0046**
3	1					0.0005	0.0007	0.0001	**0.0002**
4		1				0.0035	0.0021	0.0013	**0.0005**
5		1				0.0035	0.0042	0.0054	**0.0048**
6			1			0.0000	-0.0001	-0.0005	**0.0009**
7			1			0.0000	-0.0001	-0.0001	**0.0009**
8			-1	-1		0.0001	-0.0002	-0.0005	**0.0017**
9				1	-1	-0.0048	-0.0054	-0.0061	**-0.0027**
10				1		-0.0001	0.0002	0.0006	**-0.0006**
11					1	0.0046	0.0059	0.0011	**0.0109**
12					1	0.0046	0.0027	0.0068	**0.0004**
t^*	0.002	-0.010	0	0.005	-0.014				
[pvv]						$9.9381.10^{-5}$	$8.1311.10^{-5}$	$7.9358.10^{-5}$	**$0.7613.10^{-5}$**
unit weight error			before adjustment			1.0000	314.0000	0.0600	**0.0040**
			after adjustment			0.0045	0.0040	0.0040	**0.0027**
| deviation |						0.9955	313.9960	0.0560	**0.0013**

where

a, equal weights

b, weighting according to the length of the measuring cycle

c, weighting according to the temperature deviation inside the meter

d, weighting according to the RMS error of the observations mean value

Among the four solutions of the network adjustment the best fit to the constraint

$$[pvv] = \min \qquad (14)$$

is reached for the variant "**d"** (weighting related to the RMS error of the mean gravity along the tie), which was somehow expected, as in this case the used weight cumulates the action of all error factors.

On the other hand, the worse fit was obtained in the case of the weight based on the length of the measuring cycle (variant "**b"**). This shows that LaCoste & Romberg gravity meter accuracy was practically not dependent on the drift factor.

Gravity ties considered after the network adjustment are presented in Table no. 6.

Table 6 Observed and adjusted gravity along the network ties

i	gravity tie	Δg_i (mgal)	v_i (mgal)	ΔG_i (mgal)	m_i (mgal)
1	Chisinau → Soroca	120.217	-0.0025	120.2145	± 0.0029
2	Chisinau → Balti	79.518	-0.0046	79.5134	± 0.0028
3	Balti → Soroca	40.701	0.0002	40.7012	± 0.0013
4	Ungheni → Balti	45.272	0.0005	45.2725	± 0.0013
5	Chisinau → Ungheni	34.236	0.0048	34.2408	± 0.0028
6	Chisinau → Albita	13.969	0.0009	13.9699	± 0.0026
7	Albita → Leova	-30.037	0.0009	-30.0361	± 0.0026
8	Chisinau → Leova	-16.068	0.0017	-16.0663	± 0.0018
9	Chisinau → Cahul	-96.858	-0.0027	-96.8607	± 0.0019
10	Cahul → Leova	80.795	-0.0006	80.7944	± 0.0013
11	Cahul → Causeni	-91.430	0.0109	-91.4191	± 0.0032
12	Chisinau → Causeni	-5.442	0.0004	-5.4416	± 0.0026

where
Δg_i represents the observed gravity along the tie *i*
v_i is the correction along the tie *i*
ΔG_i represents the adjusted gravity along the tie *i*
m_i is the RMS error after the adjustment

NETWORK DATUM

As previously mentioned, NGRNM datum was provided by connecting the Moldovan network to the national gravity reference networks of Romania (Besutiu et al, 1994). To avoid long measuring cycles when crossing the state border checking points, the transfer operation was planned and executed in two steps.
During **the first step**, the transfer station Albita, located in the cross-border area, was tied to the national gravity reference network of Romania. To monitor the quality of the determinations a triangle system was used (Fig. 3). Two base stations (conventionally called station N and station S) were used to transfer the absolute gravity value into the cross-border area. Table no. 7 summarizes the results of these determinations.

Table no. 7 Gravity ties between Albita and the Romanian gravity reference networks

Base station code	Absolute gravity (mgals)	Gravity tie to Albita (mgals)	Gravity transferred (mgals)
Station N	980735.45 ± 0.046	46.050 ± 0.030	980781.500 ± 0.060
Station S	980749.83 ± 0.050	31.669 ± 0.030	980781.499 ± 0.060

Triangle closure (0.001 mgals) was far below the instrumental accuracy, advocating for the high quality of the gravity transfer.
Thereafter, the average absolute gravity value transferred to the Albita station was considered 980780.500 ± 0.060 mgals.

The second step in the datum transfer consisted in gravity ties between the base station Albita and the central base station of the NGRNM, Chisinau. A similar triangle system was used on purpose, by linking the Romanian Albita transfer station to both Chisinau and Leova NGRNM base stations (see Fig. 2). This

absolute gravity transfer triangle was then integrated into the stochastic model for NGRNM adjustment, and observed values accordingly corrected. Finally, the absolute gravity assigned to the central station of the NGRNM, Chisinau, was equal to 980767.530 mgals.
Following this operation, absolute gravity values were transferred to each base station of the NGRNM through the adjusted gravity ties connecting them to the central station. The results are summarized in table no. 8.

Table no. 8 Absolute gravity values and the vertical gradient of the gravity within the base stations of NGRNM

Station code	Geographical co-ordinates		Absolute gravity (mgals)		Vertical gradient (mgals/m)	
	latitude	longitude	Mean value	rms	Mean value	rms
CHISINAU*	46º 59’ 52.0”	28º 40’ 05.0”	980767.530	±0.067	-0.279	±0.007
BALTI	47º 45’ 40.0”	27º 56’ 00.0”	980847.043	±0.067	-0.282	±0.003
CAHUL*	45º 54’ 18.8”	28º 12’ 02.4”	980670.669	±0.067	-0.295	±0.006
CAUSENI	46º 38’ 15.0”	29º 24’ 30.0”	980762.088	±0.067	-0.294	±0.007
LEOVA*	46º 28’ 24.6”	28º 14’ 53.3”	980751.467	±0.067	-0.323	±0.006
SOROCA*	48º 07’ 53.5”	28º 20’ 31.0”	980887.745	±0.067	-0.284	±0.008
UNGHENI	47º 12’ 00.0”	27º 48’ 00.0”	980801.771	±0.067	-0.309	±0.005

***** located on the pillars of the National Seismic Monitoring Network

It should be mentioned that absolute gravity values in the table refer to the relative height of 0.30 meters above the ground. Vertical gradient values, valid between 0.30 m and 0.80 m (Besutiu et al, 2001b), are also added to allow eventual gravity transfers from NGRNM to other locations according to the height of the tripod of the meter used.

FINAL REMARKS

The new national gravity reference network of Republic of Moldova was achieved as a triangle network with central base station located in the capital of the country. Gravity measurements along its ties were performed by using the high accuracy LaCoste and Romberg D-214 meter owned by the Geological Institute of Romania. The obtained accuracy was fully within the instrumental range. Starting from the triangle closures, the network was adjusted by using least square method for several weighting systems. Among them, the best result was obtained when referring to the standard deviation of the mean gravity values along the ties.
NGRNM datum was provided by transferring absolute gravity from the Romanian gravity reference network to its central base station.
It is expected that provisional absolute gravity values, as provided in the table no. 8, would be slightly altered after re-adjusting the Romanian national gravity reference networks by constraining them on the UNIGRACE absolute base stations. However, mention should be made to the fact that comparisons between the actual Romanian gravity system, and the gravity standard of the Central and Western Europe, showed an excellent scale factor and small differences only in the network datum (Besutiu et al, 2001a). Therefore, it is likely that the gravity system of Republic of Moldova would be easily integrated into the EU gravity standard.

Acknowledgements. The research was funded by the Romanian Ministry for Education and Research through the grant no. 6176GR/2000.

The authors wish to thank the managements of the Geological Institute of Romania, and the Institute of Geophysics and Geology of the National Academy of Sciences of Moldova for their efforts and permanent support.
Thanks are also due to the technical staff that assisted field activities: Marin Stancu, and Dumitru Popescu.

REFERENCES

Besutiu, L., Rosca, Vl., Gulie, N., 1994. *On the reference gravity networks of Romania*: Bur. Grav. Int., Bull. Inf. No. 73, p. 35-41, Toulouse

Besutiu, L., Nicolescu, A., Zorilescu, Vl., 2001. *Considerations on the gravity system of Romania*: Bur. Grav. Int., Bull. Inf. No. 89, p. 35-47, Toulouse

Besutiu, L., Neaga, V., Nicolescu, A., Besutiu, G., Ilies, I., 2001. *Consideratii preliminare asupra integrarii retelelor gravimetrice ale României si Republicii Moldova (Preliminary considerations on the integration of the gravity networks of Romania and Republic of Moldova)*. St. cerc. geofizica, 39, in press, Bucharest (*in Romanian)*

Botezatu R., 1961. *Reteaua gravimetrica a R. P. Române. Triangulatia statiilor gravimetrice de ordinul I a R. P. Române (The gravity network of Popular Republic of Romania. Triangulation of the 1st order gravity base stations)*: Probleme de geofizica, vol. II, p. 7-18, Bucharest (*in Romanian)*

Detrekoi, Á., 1991. *Kiegyenlítoszámítás (Adjusting calculations*): Tankönyvkiadó, 685 pp., Budapest, (*in Hungarian*)

Rosca Vl., 1999. Romanian Annual Progress Report, Contract no. ERBIC15CT970805, *Reports on Geodesy, 2(43), p. 69-73, Warszaw*

Rosca, Vl., Besutiu, *L., 2000.* Romanian Annual Progress Report for the UNIGRACE Project*: Reports on Geodesy, No. 5 (51), 71-76, Warszaw*

Wolf, H., 1975. *Ausgleichungsrechnung I. Formeln zur praktischen Anwendung* Dümmler's Verlag, 324 pp., Bonn

Wolf, H., 1979. *Ausgleichungsrechnung II Aufgaben und Beispiele zur praktischen Anwendung.* Dümmler's Verlag, 354 pp., Bonn

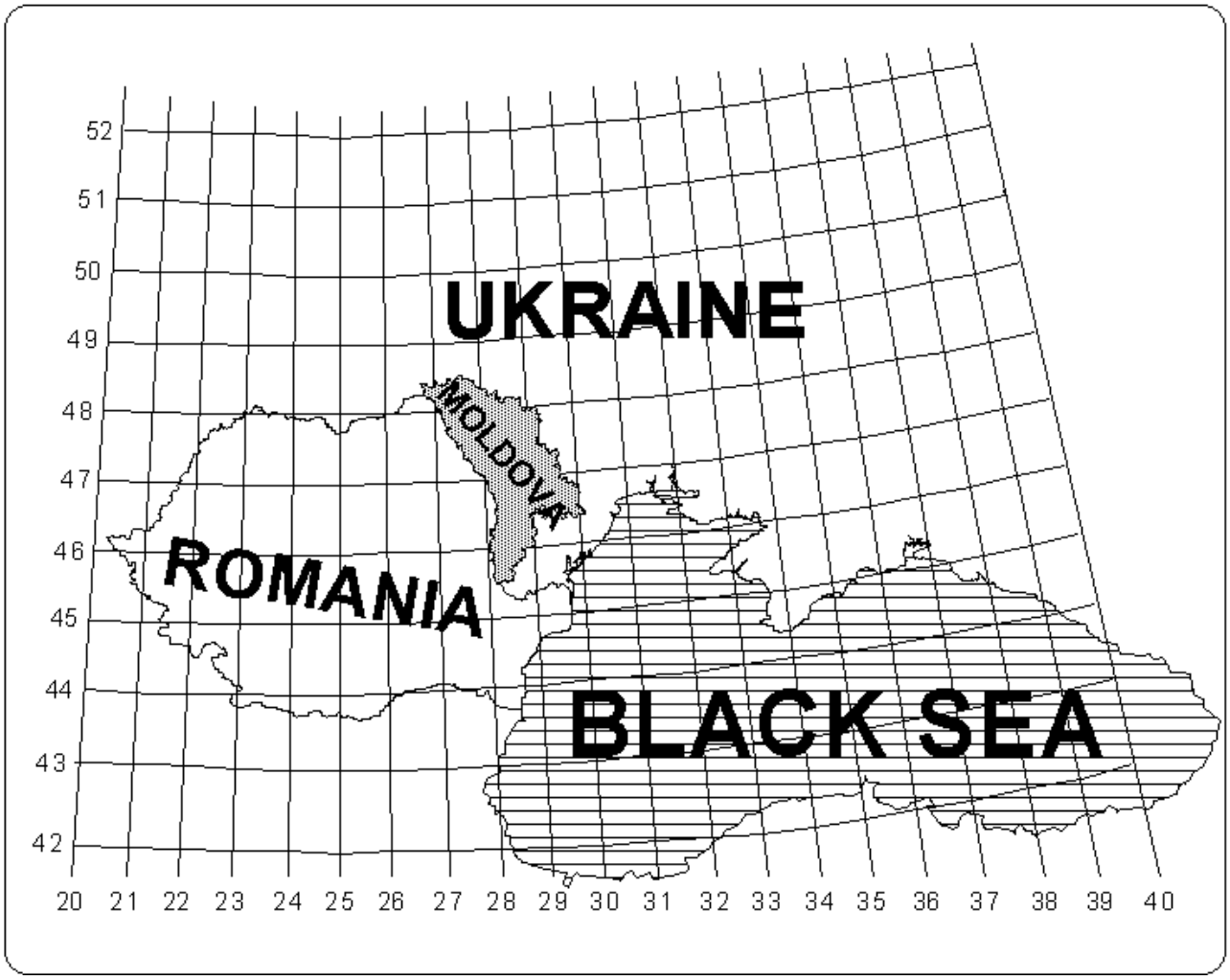

Fig. 1 Location of the study area

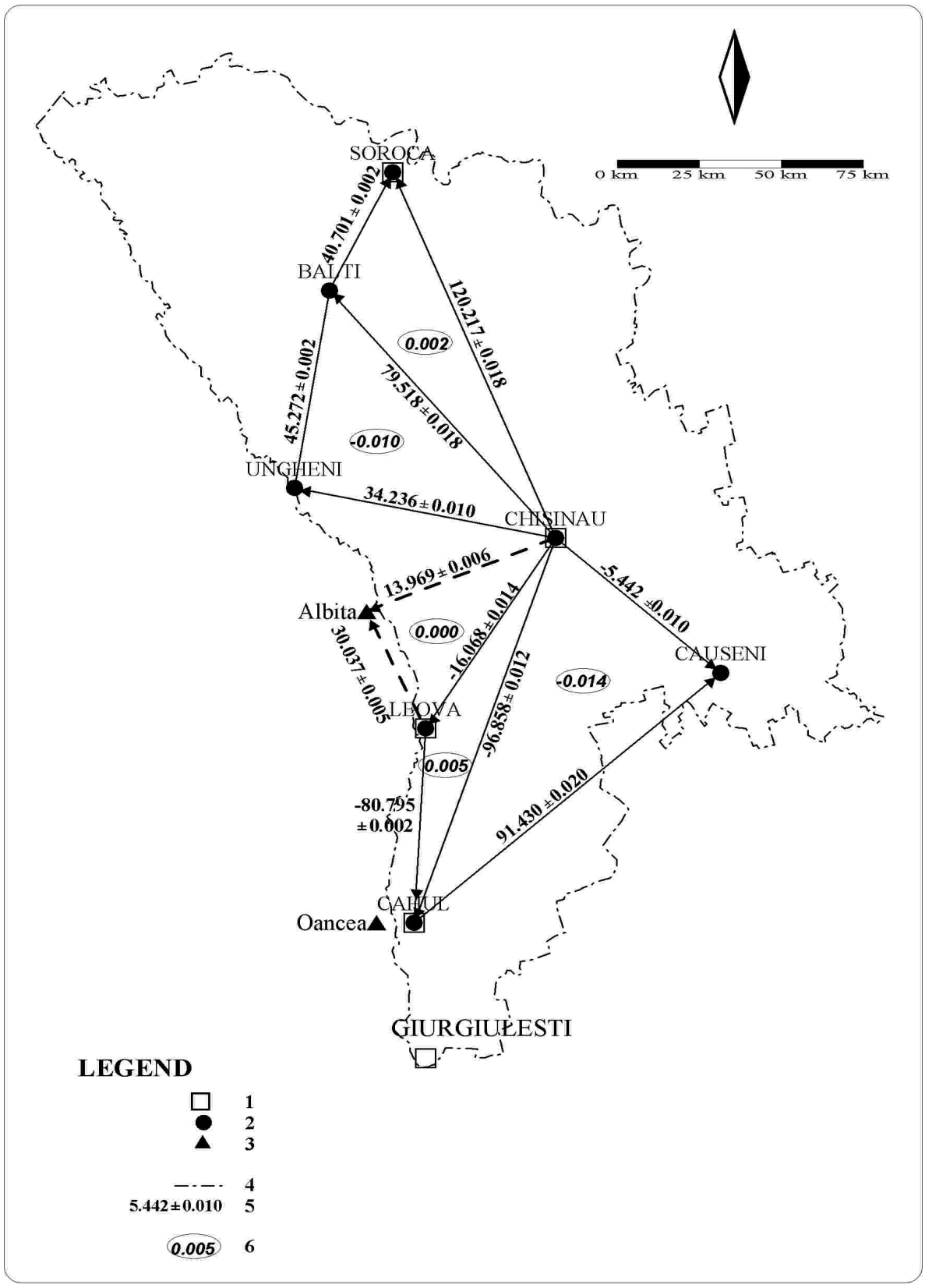

Fig. 2 Gravity variations along the ties of the Moldovan gravity reference network and triangle closures
1, seismic monitoring base stations; 2, gravity reference network base stations; 3, Romanian base station for the gravity datum transfer; 4, state border; 5, gravity range (in mgals); 6, triangle closure (in mgals)

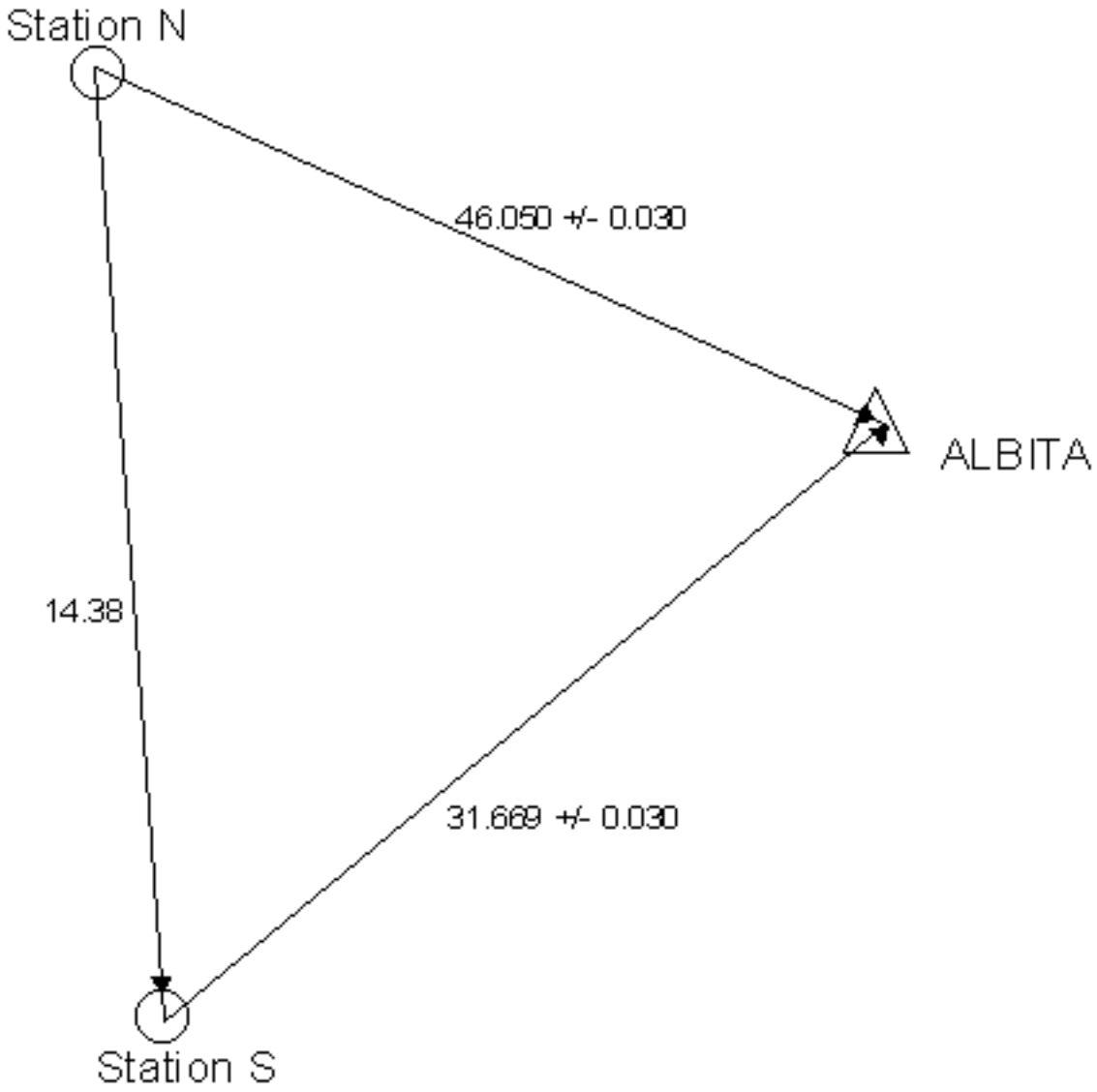

Fig. 3 The design of the network for the gravity datum transfer from the Romanian gravity reference networks to border area

Surface modeling for GPS-levelling geoid determination

DR.METIN SOYCAN, MSC.ARZU SOYCAN
Yıldız Technical University Civil Engineering Faculty Geodesy and Photogrametry Engineering Division
Main Campus,80750 Beşiktaş/İSTANBUL
TEL:+902122597070/2833-2712
FAX:+902122610767
e_mail: soycan@yildiz.edu.tr ; metinsoycan@yahoo.com ; topbas@yildiz.edu.tr

Abstract: Many surface modeling techniques can be used for local geoid determination. These can be listed as; Inverse distance to a power, kriging, minimum curvature, nearest neighbor, polynomial regression, radial basis function, Shepard's Method's, Triangulation/Linear Interpolation, collocation etc. Each technique has different calculation methods and used for different type of land. At the same time, each of them has some advantage and disadvantage.
In this paper, theoretical and mathematical principles of some surface modeling techniques for geoid determination have been examined. In this concept, a test area has been selected and geoid models of this area have been created by some selected modeling techniques.
Here it is searched that accuracy, practicability and serviceability of surface modeling techniques. All techniques have been compared to each other and known geoidal heights values from GPS and geometric levelling for 26 selected points.

1 Introduction

Heights, obtained from GPS are ellipsoidal heights and this kind of heights has theoretical meaning. In practice, ortometric heights are used commonly.
Ellipsoidal height of point P on the earth is distance between points P and ellipsoid surface at ellipsoidal center direction. Ortometric height of points P is distance between point P and geoid surface at gravity vector direction.

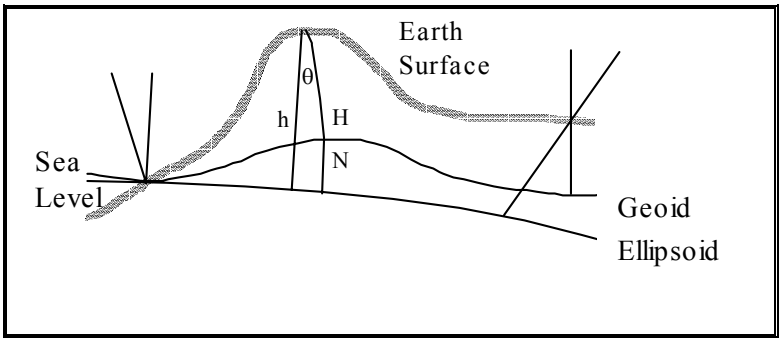

Fig (1) Relationship between ellipsoidal and ortometric heights

After GPS observation and processing it can be obtained (XYZ) cartesian or (φλh) geographic coordinates of point P. Determination of ortometric height H of point P from ellipsoidal height h depends on determination of geoidal height N.

In practice, for determination of geoidal heights especially for local application, require control points which both ellipsoidal and ortometric heights are known. Thus geoidal heights of control points N can be calculated from difference between ellipsoidal and ortometric heights. For calculation of geoidal height of a point with (φλ) geographic or (x,y) plan coordinates is required determination of geoid surface model of application area by using control points geoidal heights (Akçın 1998;IGNA 1999;Ollikainen 1997; Soycan 2002; Zhang 2000).

There are a lot of techniques for determination of surface models of geoid. Some of these techniques are used direct observation values and the others can be used after adjustment and filtering. Models using determination of geoid surface must be realistic and well adjusted with structure of surface. However surface models must be suitable for structure of surface and filtering and susceptible for extrapolation and interpolation.

Several techniques are used for determination of geoid surface and it can be listed as;

- Interpolation
- Finite Elements
- Collocation
- Numerical differential solution
- One dimensional datum transformation

In this paper it has been examined some interpolation techniques. For this purposes, geoid models of Istanbul have been calculated, processed and compared. The digital elevation model of the test area has been reported in fig (2).

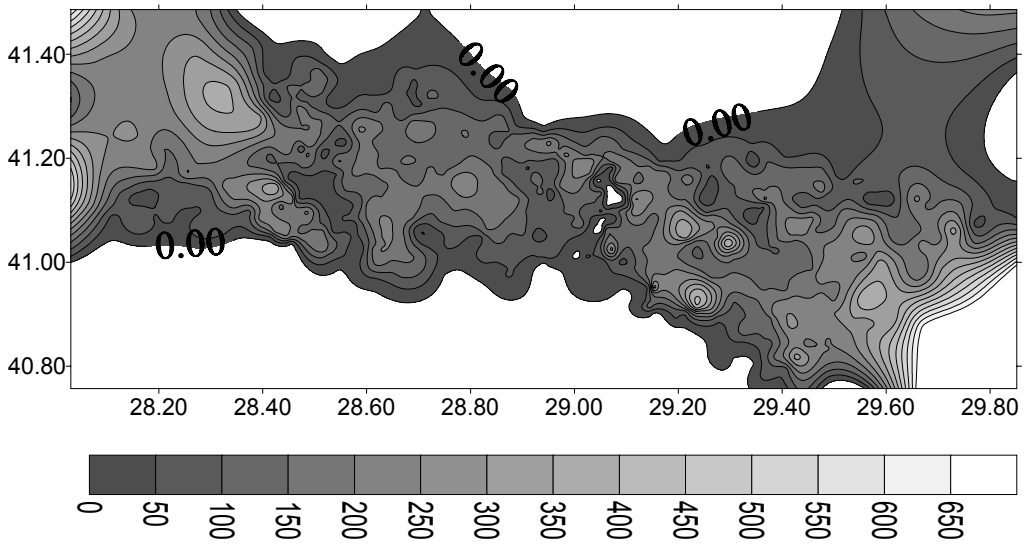

Fig (2) Digital elevation model of test area

In calculation, it has been used Surfer (Win32) software. It is very powerful for the 3D-Visualization, it is fast, without consuming much disk space and uncomplicated with object manager. All processes (gridding, mapping) can be automated with writing programs in Visual Basic. Help menus content is very useful and describes also background information (Golden Software).

2 Some surface models for determination of GPS local geoid

2.1 Polynomial regression methods

Polynomial regression is the most common method for geoid surface modeling and this is described as;

$$N = (\varphi, \lambda) = \sum_{i=0}^{n} \sum_{j=0}^{m} a_{ij} \varphi^i \lambda^j \tag{1}$$

This method is used to define large-scale trends and patterns in data, there are several options to define the type of trend surface and this can be listed in below. Polynomial regression is not really an interpolator but it can be used for determination of trend surface (Golden Software).

- Simple Planar Surface

$$N_0 = a_0 + a_1\varphi + a_2\lambda \tag{2}$$

- Bi-Linear Saddle

$$N_0 = a_0 + a_1\varphi + a_2\lambda + a_3\varphi\lambda \tag{3}$$

- Quadratic Surface

$$N_0 = a_0 + a_1\varphi + a_2\lambda + a_3\varphi^2 + a_4\lambda^2 + a_5\varphi\lambda \tag{4}$$

- Qubic Surface

$$N_0 = a_0 + a_1\varphi + a_2\lambda + a_3\varphi^2 + a_4\lambda^2 + a_5\varphi\lambda + a_6\varphi^3 + a_7\lambda^3 + a_8\varphi^2\lambda + a_9\varphi\lambda^2 \tag{5}$$

For higher degree polynomial it can be used equation (1). In practice, for surfacing with polynomial regression, selection of polynomial degree is very important. The surface can be lost its reality and suitability due to wrong selection of coefficient and polynomial degree. In surfacing with polynomial regression methods, degree of polynomial is depending on number of points and degree of freedom. As possible as it must be started with the highest degree and the most suitable coefficient must be determined by using statistical tests (Kraus 1972; Miller 1958; Schut 1976;Yanalak 1991). In this research, polynomial degree has been selected 5,6,7,9 respectively for 25,50,100,214 control points. Contour plot of the geoidal heights for 25,50,100,214 control points has been reported fig (3).

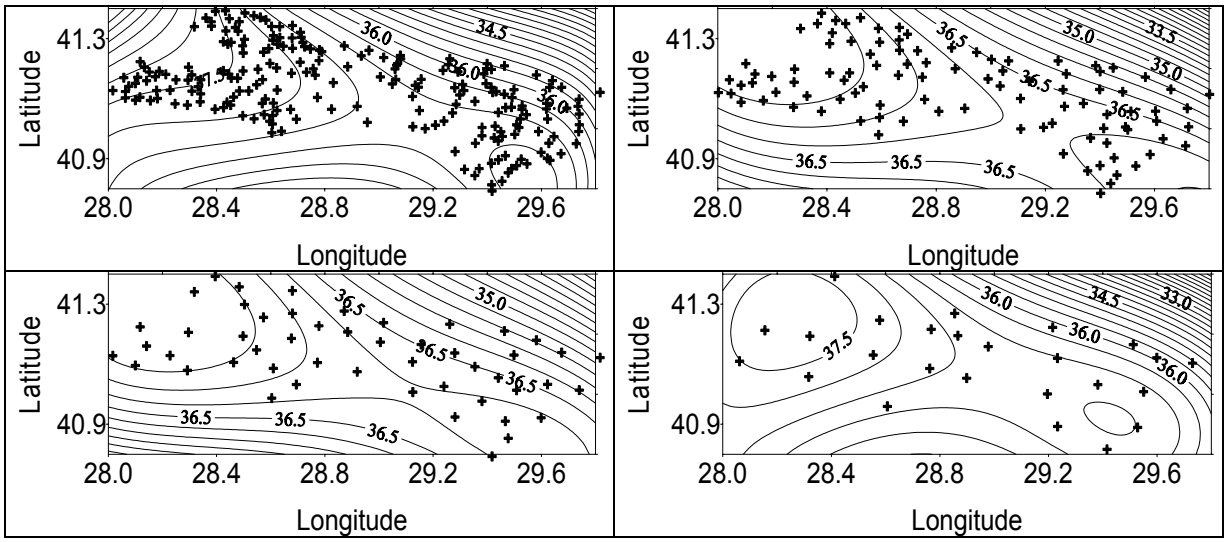

Fig (3) Counter maps of geoid obtained from polynomial regression

2.2 Multi-quadratic surface models

In this method, depending on known control points, a trend surface is determined by using simple planar or quadratic surface. After this operation, residuals in control points are used for surfacing and all surface coefficients are calculated (Golden Software). All surface area is described with only one function. Parameters of function are determined from all control points. For multi-quadratic surface model;

$$\Delta N = \sum_{j=1}^{n} C_i Q(x_i, y_i, x, y) + f \tag{6}$$

$$Q(x_i, y_i, x, y) = \left[(x_i - x)^2 + (y_i - y)^2 \right]^{1/2} \tag{7}$$

f: correction value(it can be selected 0.1 or $0.6Q^2_{min}$). For determination of surface coefficient eq.(6)is re-written as below;

$$\Delta N_1 = c_1 Q_{11} + c_2 Q_{12} + c_3 Q_{13} + \ldots\ldots\ldots\ldots + c_n Q_{1n}$$
$$\Delta N_2 = c_1 Q_{11} + c_2 Q_{12} + c_3 Q_{13} + \ldots\ldots\ldots\ldots + c_n Q_{1n}$$
.
. (8)
.
$$\Delta N_n = c_1 Q_{n1} + c_2 Q_{n2} + c_3 Q_{n3} + \ldots\ldots\ldots\ldots + c_n Q_{nn}$$

This equation set can be solved by least squares method and coefficients are obtained. Geoidal heights of new P(x,y) point can be calculated as below;

$$N_P = t(x,y) + \sum_{j=1}^{n} c_j \sqrt{(x_j - x)^2 + (y_j - y)^2} \quad (9)$$

Here t(x,y) is trend value obtained from simple planar or quadratic surface polynomial regression. After Multi-quadratic surfacing, there are any residuals in control points and distribution of control points does not affect results (Kraus 1972; Miller 1958; Schut 1976;Yanalak 1991). Contour plot of the geoidal heights for 25,50,100,214 control points has been reported fig (4).

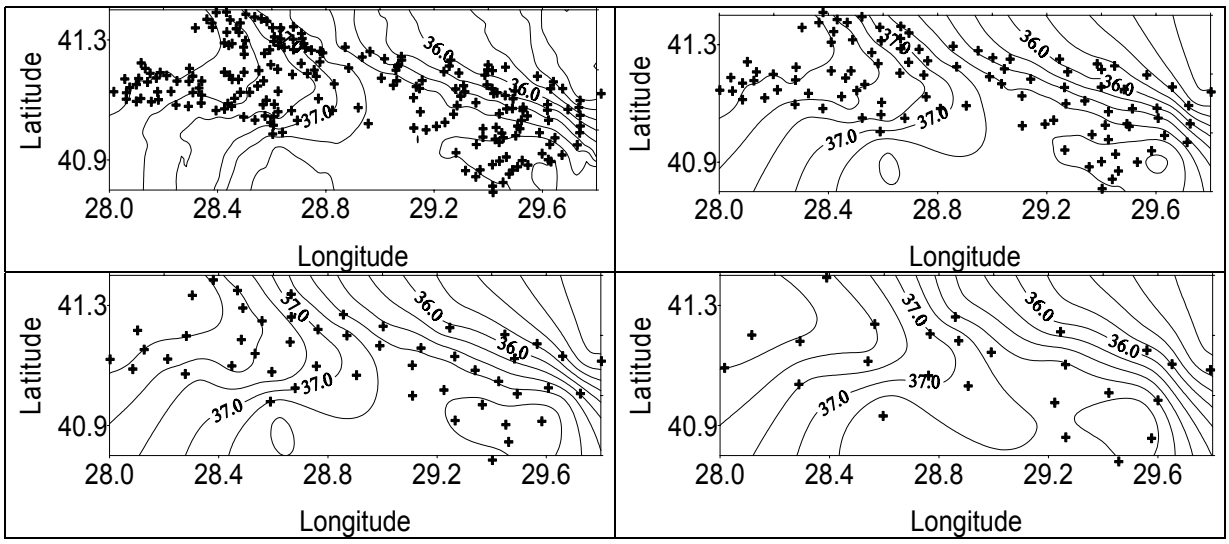

Fig (4) Counter maps of geoid obtained from multi-quadratic surface models

2.3 Triangulation- Linear interpolation

The Triangulation interpolator is an exact interpolator. Linear surface is a planar and it can be described as $N_0 = a_0 + a_1\varphi + a_2\lambda$ simple planar surface. In fig (5) the planar surface for points 1,2,3 is shown.

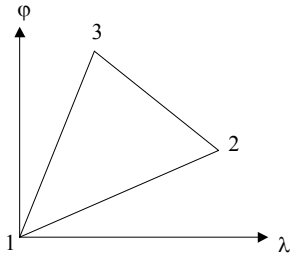

Fig (5) Planar Surface

$$N_1 = a_0 + a_1\varphi_1 + a_2\lambda_1$$
$$N_2 = a_0 + a_1\varphi_2 + a_2\lambda_2 \ , \ \varphi_1,\lambda_1=0 \ , \quad \underline{N} = \begin{vmatrix} N_1 \\ N_2 \\ N_3 \end{vmatrix} = \begin{vmatrix} 1 & 0 & 0 \\ 1 & \varphi_2 & \lambda_2 \\ 1 & \varphi_3 & \lambda_3 \end{vmatrix} \begin{vmatrix} a_0 \\ a_1 \\ a_2 \end{vmatrix} \tag{10}$$
$$N_3 = a_0 + a_1\varphi_3 + a_2\lambda_3$$

Where; a_0, a_1, a_2 coefficients are calculated from these equations;

$$a_0 = N_1$$

$$a_1 = \frac{\left[(\lambda_2 - \lambda_3)N_1 + \lambda_3 N_2 - \lambda_2 N_3\right]}{\left(\varphi_2\lambda_3 - \varphi_3\lambda_2\right)} \tag{11}$$

$$a_2 = \frac{\left[(\varphi_3 - \varphi_2)N_1 + \varphi_3 N_2 - \varphi_2 N_3\right]}{\left(\varphi_2\lambda_3 - \varphi_3\lambda_2\right)}$$

Triangulation works best when data points are evenly distributed over the grid area (Golden Software). Data sets that contain sparse areas result in distinct triangular facets on a surface plot or contour map. Triangulation is very effective at preserving break lines (Kraus 1972; Miller 1958; Schut 1976;Yanalak 1991). Contour plot of the geoidal heights for 25,50,100,214 control points has been reported fig (6).

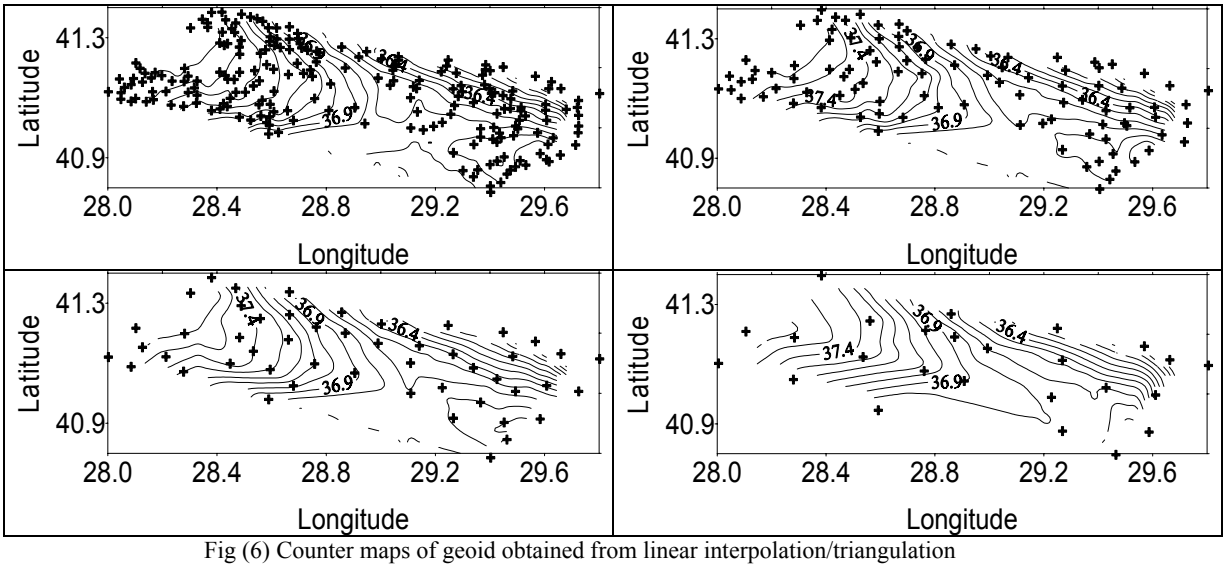

Fig (6) Counter maps of geoid obtained from linear interpolation/triangulation

2.4 Nearest neighborhood surface models

In this approach, geoid surface is divided small parts and each part is described with a different function. To calculated geoidal height of a new P point; it is used surface obtained from nearest control points. In selection of control points, it is used user defined search circle or ellipse. As a function of this surface it can be used lower degree polynomial. Using different function is caused splits; break lines and discontinuity along the boundaries (Golden Software).

If the surface is not homogenous, this method can be used. To pretend splits, break lines and discontinuity, conjunction function must be used and these problems are solved by only one function for this surface. Thus, this method cannot be suitable in every respect (Kraus 1972; Miller 1958; Schut 1976;Yanalak 1991). Contour plot of the geoidal heights for 25,50,100,214 control points has been reported fig (7).

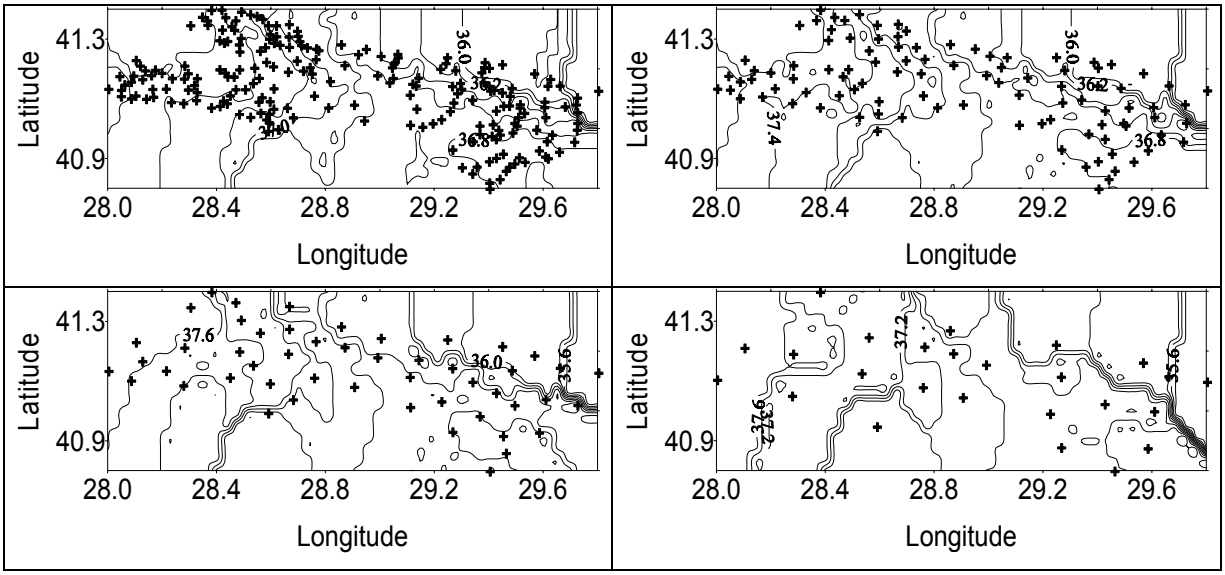

Fig (7) Counter maps of geoid obtained from nearest neighborhood surface models

2.5 Inverse distance to a power surface models

The inverse distance to a power method is a weighted average interpolator. The power parameter controls how the weighting factors drop off a distance from a new unknown point. For a larger power, closer data points are given a higher fraction and the overall weight. For a smaller power, the weights are more evenly distributed among the data points (Golden Software).

Surfacing with these methods, firstly a trend surface from polynomial regression and residuals in control points are used for determination surface (Kraus 1972; Miller 1958; Schut 1976;Yanalak 1991).

$$N(\varphi,\lambda)=t(\varphi,\lambda)+\frac{\sum_{i=1}^{n}P_i N_i}{\sum_{i=1}^{n}P_i},\ P_i=\frac{1}{D_i^n} \tag{12}$$

The most important property of method is generation of "bull's-eye" surrounding the position of observation within the gridded area. These effects can be reduced by using smoothing parameters. Contour plot of the geoidal heights for 25,50,100,214 control points has been reported fig (8).

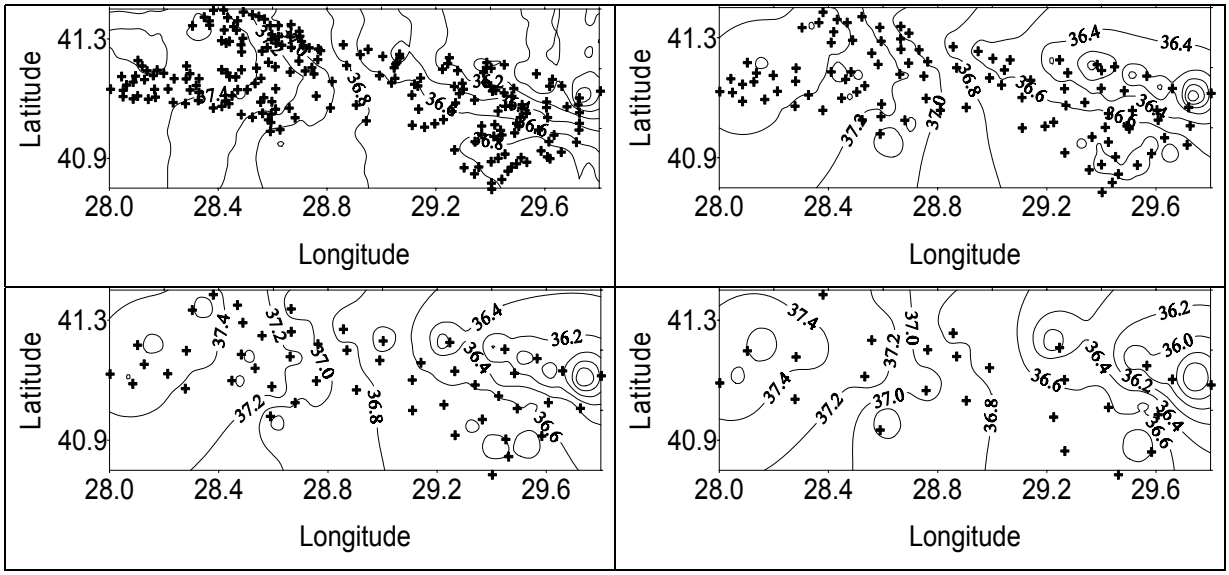

Fig (8) Counter maps of geoid obtained from inverse distance to a power surface models

3 Comparison of surface and evaluations

For comparison and defining optimum surface models, surfacing is made by different number of control points. In addition, 26 new points (distributed homogenous) have been selected in application area and geoidal heights of new points calculated from GPS-Geometric leveling measurement. 26 new points geoidal heights have been calculated from each model by using 214,100,50 and 25 control points, and these have been compared with geoidal heights which have been calculated from GPS-Geometric levelling, differences and rms values have been evaluated.

Table (1) Comparison of methods by using geoid obtained from 214 control points

214 Control Points				
Methods	Max. Difference (mm)	Min. Difference (mm)	Average of Absolute Differences (mm)	RMS of Differences (mm)
Polynomial Regression	93.9	2.5	29.6	39.86
Multi-Quadratic	80.3	0.4	20.9	31.96
Triangulation-Linear İnterpolation	70.0	1.1	17.1	24.90
Nearest Neighborhood	143.0	2.0	66.6	86.92
Inverse Distance to a Power	80.6	0.4	35.21	46.51

Table (2) Comparison of methods by using geoid obtained from 100 control points

100 Control Points				
Methods	Max. Difference (mm)	Min. Difference (mm)	Average of Absolute Differences (mm)	RMS of Differences (mm)
Polynomial Regression	98.8	3.0	30.58	39.94
Multi-Quadratic	84.8	1.0	28.12	37.59
Triangulation-Linear İnterpolation	80.7	1.3	32.05	39.69
Nearest Neighborhood	177.9	0.0	90.54	108.52
Inverse Distance to a Power	135.4	0.0	56.48	66.72

Table (3) Comparison of methods by using geoid obtained from 50 control points

50 Control Points				
Methods	Max. Difference (mm)	Min. Difference (mm)	Average of Absolute Differences (mm)	RMS of Differences (mm)
Polynomial Regression	123.2	0.7	34.42	50.27
Multi-Quadratic	94.6	4.9	30.20	42.70
Triangulation-Linear İnterpolation	81.8	5.6	40.44	49.06
Nearest Neighborhood	208.0	0.0	94.87	109.43
Inverse Distance to a Power	174.2	0.2	48.04	67.09

Table (4) Comparison of methods by using geoid obtained from 25 control points

25 Control Points				
Methods	Max. Difference (mm)	Min. Difference (mm)	Average of Absolute Differences (mm)	RMS of Differences (mm)
Polynomial Regression	209.2	2.8	56.42	86.18
Multi-Quadratic	127.2	5.2	43.34	57.03
Triangulation-Linear İnterpolation	135.4	0.6	44.79	55.81
Nearest Neighborhood	254.3	0.0	82.68	111.93
Inverse Distance to a Power	136.2	0.4	59.3	71.78

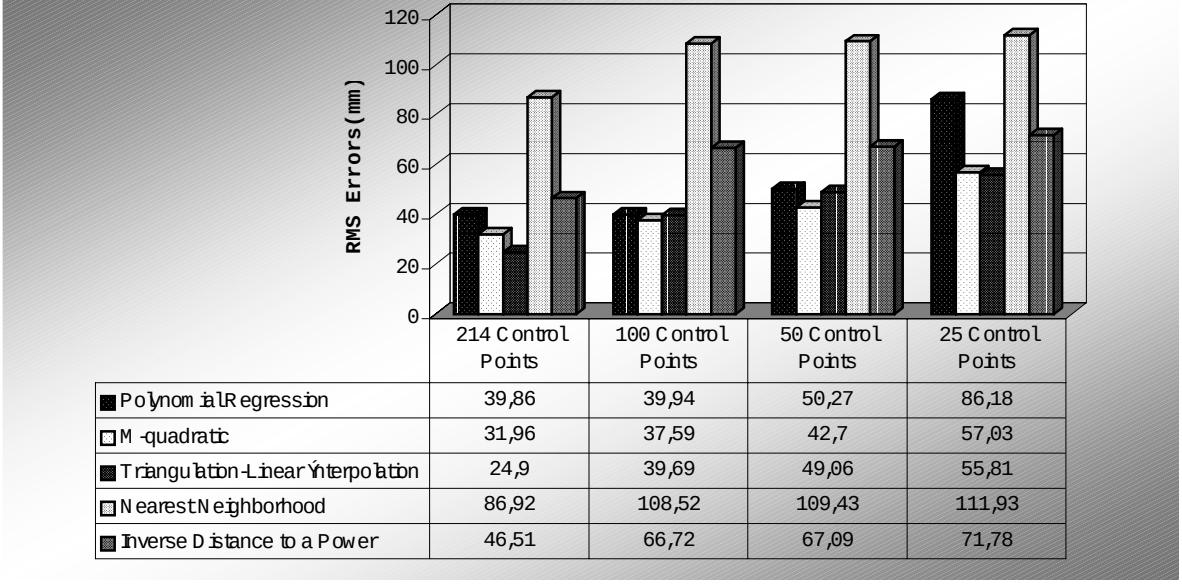

Fig (9) RMS error of each methods obtained from 26 known geoidal heights.

4 Results

Polynomial regression is easy and practical methods and offer smooth surface, when surfacing with polynomial regression; all coefficient must be tested and optimum coefficient must be selected. Generally, this model is used for determination trend surface. Multi-quadratic models use residuals in control points; residuals can be calculated from trend value obtained from simple planar or quadratic surface polynomial regression. After Multi-quadratic surfacing there are any residuals in control points and distribution of control points does not affect results. It is very important property for surfacing. Triangulation works best when data points are evenly distributed over the grid area. Data sets that contain sparse areas result in distinct triangular facets on a surface plot or contour map. Triangulation is very effective at preserving break lines. Nearest neighborhood method uses different function for each part. Using different function is caused splits; break lines and discontinuity along the boundaries. In application it can be seen easily that rms error of this methods are very high. Surfacing with inverse distance to a power method, firstly a trend surface from polynomial regression and residuals in control points are used for determination surface. The most important property of method is generation of "bull's-eye" surrounding the position of observation within the gridded area. It can be seen in figure 8. Rms of these methods is higher than polynomial regression, multi-quadratic and triangulation-interpolation methods. As a result of all evaluation polynomial regression, multi-quadratic and triangulation-interpolation methods can be used for geoid surface; these models supply enough accuracy for determination of ortometric heights from GPS.

5 References

AKÇIN H. ‘A study on the obtaining practice heights from GPS measurement’ Phd Thesis, Istanbul, 1998

GOLDEN SOFTWARE SURFER Win-32 Software ‘Help menus’

IGNA (Istanbul GPS benchmark Network) Technical Report November 1999 (Supervisor AYAN T.)

KRAUS K. And MIKHAIL E.M ‘Linear Least-Squares Interpolation’ 12. Congress of the International Society of Photogrammetry, Ottawa, Canada, July 23-August 5,1972

MILLER C.L. and LAFLAMME R.A., ‘The Digital Terrain Model Theory and Application’ Presented at the Society’s 24. Annual Meeting, Hotel Shoreham, Washington, D.C March 27, 1958

OLLIKAINEN MATTI ‘Determination Of Orthometric Heights Using GPS Levelling’ Publications of the Finnish Geodetic Institute’ KIRKKONUMMI, 1997

SCHUT G.H., ‘Review of Interpolation Methods for Digital Terrain Models’ The Canadian Surveyor, Vol.30.No.5, December 1976

SOYCAN M, “Determination of Geoid Heights by GPS and precise trigonometric levelling” ,Phd. Thesis ,ISTANBUL, 2002

YANALAK M., ‘Digital Terrain Models and Interpolation Methods’ Master Thesis ITU-1991-Istanbul

ZHANG, S. “Interpolation of Geoidal/Quasigeoidal Surfaces for Height Determination with GPS, Phd Thesis, Hannover, 2000

A comparison of different procedures of handling the effects of close and distant topographic masses in gravimetric geoid computations with the classical and recent formulae

Hossein Nahavandchi

Norwegian University of Science and Technology,
Department of Geomatics, N-7491 Trondheim
E-mail: hossein.nahavandchi@ntnu.no

Abstract

Different procedures for considering the effects of topographic masses in Stokes-Helmert scheme of geoid determination are reviewed. Classical integral formulae use a planar approximation of the geoid and a limited area of integration, and thus account only for the local contributions of topographic effects. In the other hand, the spherical harmonic representation of the topographic effects normally only includes the long-wavelength information. Another description of the effects of topographic masses given by Martinec and Vaníček (1994a, b) uses near and far-zone integration areas and a spherical approximation of the geoid. Finally, two formulae, that combine short and long-wavelength contributions, are presented for topographical effects. These recent formulae imply that the integral formulae for determining the topographic effects may have some numerical problems in representing global information (for truncated integration domain). On the other hand, a representation of the effects by a set of spherical harmonic coefficients of the topography to, say, degree and order 360 leads to omission of significant short-wavelength information. All above-mentioned procedures were used for computation and comparisons in a test area in Iran with the maximum elevation of 3053 m. The results of these comparisons show that the Martinec and Vaníček (1994a, b) integral formulae and the recent combined formulae presented by Sjöberg and Nahavandchi (1999) and Nahavandchi (2000) are in good agreement with each other. These formulae use a spherical approximation of the geoid, contrary to the classical formulae which use a planar approximation. Only the combined formulae include, however, all wavelength constituents and are recommended for precise geoid determination. Further, the gravimetric geoidal heights were computed applying these different procedures of handling the topographic effects. The results were then compared at Global Positioning System (GPS)-leveling stations in Iran. The standard deviation of the fit with the combined formulae is the best among the other methods and is equal to ± 10.1 cm.

Newton's Bulletin - n°1, Dec. 2003 - ISSN 1810-8555

Key words: Direct topographic effect, Indirect topographic effect, Geoidal height, Helmert condensation

1 Introduction

The geoid is frequently determined from ground gravity data by the well-known Stokes formula. This integral formula is the solution of an exterior type boundary value problem, which implies that masses exterior to the geoid are not permitted in the formulation of this problem. This is achieved mathematically by removing the effect of external masses and replace them by the effect of additional masses below the geoid [direct topographic effect (DTE) on gravity]. However, it should be noted that the DTE on gravity anomaly equals the sum of the DTE on gravity and the so-called indirect effect of the topography on gravity or the secondary indirect topographic effect (SITE) on the geoidal height. Thereafter, as Helmert's reduction is used, the corrected ground gravity anomaly (Helmert anomaly) must be continued downward to the geoid (downward continuation) prior to perform Stokes's integration. The effect of removed masses is then restored after applying Stokes's integral [primary indirect topographic effect (PITE) on the geoidal height]. These procedure follows the principals described in Vaníček and Martinec (1994), Martinec (1998) or Nahavandchi and Sjöberg (1998).

Recognizing that a valid solution to geoid determination would occur only if there were no masses outside the geoid, Helmert suggested that the masses outside the geoid could be condensed as a surface layer directly at the the reference sphere in a spherical approximation of the geoid. In this study, Helmert's second condensation method is used that preserves the Earth mass, for which the Helmert model of the Earth has the same mass as the real Earth. A discussion of some attributes of Helmert's second method of condensation may be found in Heiskanen and Moritz (1967), Wichiencharoen (1982), Heck (1992), Martinec et al. (1993), Vaníček et al. (1995) and Nahavandchi and Sjöberg (1998).

Two different formulae for the remove-restore problem were presented by Moritz (1980) and Vaníček and Kleusberg (1987). Moritz (1968, 1980) examined the role of the topography to show a relationship between Helmert's condensation reduction and the approximate solution of the Molodenskij boundary value problem. He derived the DTE referred to the geoid. Vaníček and Kleusberg (1987) derived the DTE referred to Earth's surface, which means that the ground gravity anomalies corrected with their formula still need a downward continuation correction to be used in Stokes's integral. These two classical formulae are limited to the second power of elevation H and suffer from the planar approximation of the geoid.

Sjöberg (1994) suggested a spherical harmonic representation of the topographic effects. This approach was implemented by Sjöberg (1995, 1996) to the second power of

elevation H and by Nahavandchi and Sjöberg (1998) to the third power of elevation H, where the DTE was derived at the surface of the Earth, respectively.

Another description of the Stokes-Helmert method for geoid determination was given by Vaníček and Martinec (1994). The specific problem of determining the DTE and the PITE were treated by Martinec and Vaníček (1994a, b), who pointed out that the classical formulae may severely be biased because of the planar approximation of the geoid in the derivations.

Later, Nahavandchi (1998a, b), Sjöberg and Nahavandchi (1999), Sjöberg (2000) and Nahavandchi (2000) argued that the DTE and the PITE were composed of both short (local effects) and long-wavelength (global effects) contributions. This implies that the integral formulae for determining the topographic effects (using a limited spherical cap around computation points) may have some problems in representing the long-wavelength contributions. On the other hand, a representation by the set of spherical harmonic coefficients of the topography omits significant short-wavelength information, as in the practice it is limited to a maximum degree of 360 in this study. They derived two formulae for handling the DTE and the PITE with a combination of the integral formulae and the set of spherical harmonic coefficients of Earth's topography.

In this paper, all above-mentioned formulae for topographic effects will be computed in the test area with maximum elevation of 3053 m. The differences will be compared and discussed. Finally, the results of gravimetric geoid heights computed with different topographic effects will be compared to the geoidal heights derived at GPS-leveling stations.

2 Topographic effects in gravimetric geoid determination

The formulae used for topographic effects here are based on a constant topographic density. These formulae can also be generalized to a laterally variable density simply by putting it inside the surface integrals of the DTE and the PITE (see also Martinec 1998) . In addition to topographic effects, geoid determination by Stokes's formula also requires that the gravity anomalies, Δg, must refer to the geoid. For satisfying this condition, the gravity anomalies available on Earth's surface have to be reduced to the geoid. This reduction is called a downward continuation.

The Stokes integration with the Helmert anomaly and considering the PITE on geoid is realized by the formula (Heiskanen and Moritz 1967, p. 324)

$$N = \frac{R}{4\pi\gamma} \iint_{\sigma} S(\psi) \Delta g^{\mathrm{H}^*} d\sigma + \delta N_{\mathrm{I}}^* \tag{1}$$

where N is the geoid height, Δg^{H^*} is the ground free-air gravity anomaly (Δg) corrected for the DTE (resulting in Helmert's anomaly Δg^H at the Earth's surface) and then reduced to the geoid (i.e., downward-continued to the geoid), γ is normal gravity, $S(\psi)$ is Stokes's

function, ψ is the spherical distance between the computation and running points, σ is the unit sphere, R is the mean radius of the Earth, and $\delta N_{\mathrm{I}}^{*}$ is the PITE on the geoid. In this study, the Helmert second condensation method was used to remove the effect of external masses and replace them by the effect of additional masses below the geoid. The Helmert anomaly Δg^{H} at Earth's surface can therefore be expressed via

$$\Delta g^{\mathrm{H}} = \Delta g + \delta\Delta g_{\mathrm{dir}} \tag{2}$$

where Δg is the ground free-air gravity anomaly and $\delta\Delta g_{\mathrm{dir}}$ is the DTE on gravity anomaly determined at Earth's surface. In this section, different formulae for correcting the effects of topographic masses in gravimetric geoid computations within the Stokes-Helmert scheme are presented, and the downward continuation problem will be discussed in Sect. 3.

The SITE on the geoidal height is usually two orders of magnitude smaller than the DTE. Nahavandchi (1998b) computed this effect at 23 GPS-leveling stations in Sweden with the mean value of less than 0.7 cm. This term is neglected in this study. Also, the geoid atmospheric effect (Sjöberg and Nahavandchi 2000) and other corrections to Helmert's anomalies on the Earth's surface (see e.g. Vaníček et al. 1999), are not studied here.

2.1 DTE to gravity anomaly

2.1.1 DTE with the classical integral formulae

Moritz (1980) derived a formula for the removing of the effect of topographic masses. This correction should be added to the ground free-air gravity anomalies in Stokes's formula. This formula which uses the planar approximation of the geoid, is expressed as (Moritz 1980)

$$\delta\Delta g_{\mathrm{dir}}^{\mathrm{M}^{*}}(H_P) = \frac{\mu R^2}{2}\int\int_{\sigma}\frac{(H-H_P)^2}{\ell_0^3}d\sigma \tag{3}$$

where μ=$G\rho$, G is the universal gravitational constant, ρ is the constant density of topography, H and H_P are the orthometric heights of the running and computation points, respectively, and the spatial distance $\ell_0 = R\sqrt{2(1-\cos\psi)} = 2R\sin\frac{\psi}{2}$.
The topographic effect $\delta\Delta g_{\mathrm{dir}}^{\mathrm{M}^{*}}$ is related to the points on the geoid. This formula assumes that the gravity anomalies in a downward continuation integral are linearly proportional to the topographical heights according to the so-called Pellinen assumption (Moritz 1968, 1980). Hence, the resulting Moritz topographic effect also involves the effect of the downward continuation of gravity anomalies. This effect is, however, described only approximately since the linear relationship between gravity anomalies and topographical heights coresponds to the reality only roughly (see e.g. Heiskanen and Moritz 1967).

Vaníček and Kleusberg (1987) approximated the geoid by a horizontal plane and the constant topographic density ρ was also used in their derivations. Their formula for DTE determination at the point P, at Earth's surface, can be approximated as follows (Vaníček and Kleusberg 1987)

$$\delta\Delta g_{\rm dir}^{\rm VK}(H_P) = \frac{\mu R^2}{2}\int\int_{\sigma}\frac{H^2 - H_P^2}{\ell_0^3}d\sigma \tag{4}$$

In a strict sense, Eqs. (3) and (4) can only be used for the far-zone integration area, where $\ell_0 \gg H$, and the effect of the near zone and the Bouguer shell (which cannot be derived in the planar model) are completely missing (Martinec and Vaníček 1994a; Nahavandchi 2000). It should be mentioned that the power series of height H used in the integration is limited to the second order. In addition, Eqs. (3) and (4) also suffer from other approximations. The most important one is that the slope of the topography must be within 45°. This limitation was pointed out by, e.g., Heck (1992), Martinec and Vaníček (1994a) and Sjöberg and Nahavandchi (1999).

The DTE used by Moritz (1980), and Vaníček and Kleusberg (1987) may significantly be different. One notes that Eq. (3) is always a positive quantity while Eq. (4) may be both positive and negative. Wang and Rapp (1990) and Nahavandchi (1998a) compared these two methods. They obtained large differences in the DTE on gravity and geoid. These differences are larger with complexity of the topography. They proposed that Vaníček and Kleusberg's free-air gravity anomaly should not be used in the Stokes formula. The difference was also explained by Martinec et al. (1993) as being due to the fact that while Vaníček and Kleusberg's results refer to the Earth surface, Moritz's results refer to the geoid.

2.1.2 DTE represented by the spherical harmonic expansion

Sjöberg (1994, 1995) developed the DTE in spherical harmonics to power H^2, and Nahavandchi and Sjöberg (1998) extended this approach to power H^3. The DTE on gravity with the spherical harmonic representation is (Nahavandchi and Sjöberg 1998)

$$\begin{aligned}
\delta\Delta g_{\rm dir}^{\rm NS}(H_P) &\doteq \frac{\pi\mu}{2R}\Big[5H_P^2 + 3\overline{H_p^2} + 2\sum_{n,m}^{M'} n(H^2)_{nm}Y_{nm}(P)\Big] \\
&+ \frac{\pi\mu}{2R^2}\Big[\frac{28}{3}H_P^3 + \frac{9}{2}\overline{H_P^2}H_P - \frac{1}{2}\overline{H_P^3} \\
&+ H_P\sum_{n,m}^{M'} n(2n+9)(H^2)_{nm}Y_{nm}(P) \\
&- \frac{1}{3}\sum_{n,m}^{M'} n(2n+7)(H^3)_{nm}Y_{nm}(P)\Big]
\end{aligned} \tag{5}$$

where Y_{nm} are fully normalized spherical harmonics obeying the following rule

$$\frac{1}{4\pi}\iint_{\sigma} Y_{nm}Y_{n'm'}d\sigma = \begin{cases} 1 & \text{if } n=n' \text{ and } m=m' \\ 0 & \text{otherwise} \end{cases} \tag{6}$$

and

$$(H^v)_{nm} = \frac{1}{4\pi}\iint_{\sigma} H_P^v Y_{nm}d\sigma \ ; \ v=2,3, \tag{7}$$

$$H_P^v = \sum_{n,m}^{M'} (H^v)_{nm}Y_{nm}(P), \tag{8}$$

$$\overline{H_P^v} = \sum_{n,m}^{M'} \frac{1}{2n+1}(H^v)_{nm}Y_{nm}(P). \tag{9}$$

In Eq. (5), M' is the maximum degree and order of height coefficients in a spherical harmonic expansion. Rewriting the formula in Eq. (5) for the point P at Earth's surface to the second power of elevation H, one obtains (Nahavandchi 2000)

$$\delta\Delta g_{\rm dir}^{\rm NS}(H_P) \ \doteq \ \frac{-2\pi\mu}{R}\sum_{n,m}^{M'}\left(\frac{R}{r}\right)^{n+1}\frac{(n+2)(n+1)}{2n+1}(H^2)_{nm}Y_{nm}(P). \tag{10}$$

These spherical harmonic representations [Eqs. (5) or (10)] of the DTE are simple for practical computations. They are also free from the problems encountered in the integral formulae, such as the singularity at the computation point. However, the harmonic expansion series of H^2 (and H^3) will only include the long-wavelength constitutents for M' =360. To incorporate all significant contributions of both short and long-wavelength constitutents, an expansion in spherical harmonics of H^2 (and H^3) to very high degrees should be required, which is practically difficult and ruins the simplicity of this method. Nahavandchi and Sjöberg (1998) showed that the dominant part of the power series in Eq. (5) is the second power of elevation H. For example, the contribution from the harmonic expansion series H^3 on the geoid is within 9 cm in the Himalayas. Later, Nahavandchi (1999) showed that the contribution from the harmonic expansion series H^4 and H^5 can safely be neglected for M'=360 (also see Sun and Sjöberg 2001).

2.1.3 DTE presented by the integral formula of Martinec and Vaníček (1994a)

The specific problem on determining the DTE was also treated by Martinec and Vaníček (1994a), who pointed out that the classical formulae may severely be biased because of the planar model of the geoid used in their derivations. To solve this problem, the spherical approximation of the geoid was used, but the effect was still considered only locally as a

result of a limited integration area. Martinec and Vaníček (1994a) divided the integration area(full spatial angle) (σ) into a near zone (σ_1) and a far zone (σ_2) resulting in:

$$\begin{aligned}\delta\Delta g^{\mathrm{MV}}_{\mathrm{dir}}(H_P) &= -\frac{4\pi\mu}{R}H_p^2+\frac{\mu R^2}{2}\iint_{\sigma_1}\frac{H_P^2-H^2}{\ell^3}\Big(1-\frac{3H_P^2}{\ell^2}\Big)d\sigma \\ &\quad+\frac{\mu R^2}{2}\iint_{\sigma_2}\frac{H_P^2-H^2}{\ell^3}\Big(1-3\sin^2\frac{\psi}{2}\Big)d\sigma \qquad (11)\end{aligned}$$

where the spatial distance $\ell=\sqrt{r^2+R^2-2rR\cos\psi)}$.

The above formula produces a relative error of 3×10^{-3} for the spherical approximation of the geoid, which in turn causes an error in geoidal heights of 6 mm at most. Also, a planar approximation of distances (not to be confused with the planar approximation of the geoid) is used in this formula which produces another error which is of the same order of magnitude as the error of the spherical approximation of the geoid. This error is acceptable for the precise determination of the regional geoid. Note that in Eq. (11) ℓ is used instead of ℓ_0 that is used in the classical integral formulae (3) and (4). Contrary to Eqs. (3) and (4), the near-zone effect and the Bouguer shell are also included in this formula. It is obvious that both of these effects are significant and must be considered in precise geoid determination.

2.1.4 DTE with combination of an integral formula and the spherical harmonic expansion

The spherical harmonic representations of the DTE [Eqs. (5) or (10)] are simple for practical computations. However, the harmonic expansion series of H^2 (and H^3) will include only the long-wavelength constitutents for M'=360. On the other hand, integral formulae are computed locally and include the short and in the most cases also the medium-wavelength constitutents (depending on the cap size).

A combination of local contributions and long-wavelength information was firstly proposed by Nahavandchi (1998a). Later, Nahavandchi (1998b), Sjöberg (2000) and Nahavandchi (2000) derived the direct gravitational effect of the topography at a topographic surface point P to the second power of H with a combination of the integral formula and the spherical harmonic expansion as (Nahavandchi 2000)

$$\begin{aligned}\delta\Delta g^{\mathrm{new}}_{\mathrm{dir}}(H_P) &= -\frac{4\pi\mu}{R}H_p^2-\frac{3\mu}{8}\iint_{\sigma}\frac{H^2-H_P^2}{\ell_0}d\sigma \\ &+ \frac{\mu R^2}{2}\iint_{\sigma}\frac{H_P^2-H^2}{\ell^3}\Big(1-\frac{3H_P^2}{\ell^2}\Big)d\sigma \qquad (12)\end{aligned}$$

or

$$\delta\Delta g^{\mathrm{new}}_{\mathrm{dir}}(H_P)=-\frac{5\pi\mu}{2R}H_p^2-\frac{3\pi\mu}{2R}\overline{H_P^2}+\frac{\mu R^2}{2}\iint_{\sigma}\frac{H_P^2-H^2}{\ell^3}\Big(1-\frac{3H_P^2}{\ell^2}\Big)d\sigma \qquad (13)$$

Equation (13) uses the spherical model of the geoid and contrary to Eq. (11) can include long-wavelength constituents (if Eq. (11) uses a limited integration area). The effect of the Bouguer shell is also included. It is also free from the singularity problems and topography limitations (Sect. 2.1.1) in classical integral formulae as it uses ℓ instead of ℓ_0. The same relative errors as in Eq. (11) are produced in Eq. (13).

2.2 Primary indirect topographic effect

2.2.1 PITE with the classical integral formula

The classical formula for determining the PITE on the geoid for Helmert's second condensation method with mass preservation is (Wichiencharoen 1982)

$$\delta N_{\mathrm{I}}^{\mathrm{classic}^*}(P') = \frac{-\pi\mu H_{P'}^2}{\gamma} - \frac{\mu R^2}{6\gamma}\iint_\sigma \frac{H^3 - H_{P'}^3}{\ell_0^3} d\sigma \tag{14}$$

with the same notations as before. This formula uses the planar approximation of the geoid and assumes the constant topographic density. Martinec and Vaníček (1994b) and Sjöberg and Nahavandchi (1999) showed that the PITE determined on the basis of the planar approximation of the geoid differs significantly from that resulting from the spherical model of the geoid. They obtained differences up to a 0.5 m.

2.2.2 PITE represented by the spherical harmonic expansion

The spherical harmonic representation of the PITE can be shown to the third power of topographic height in the point P' on the geoid as (Nahavandchi and Sjöberg 1998)

$$\delta N_{\mathrm{I}}^{\mathrm{NS}^*}(P') = -\frac{2\pi\mu}{\gamma}\sum_{n=0}^{\infty}\frac{n-1}{2n+1}H_n^2(P') + \frac{2\pi\mu}{3R\gamma}\sum_{n=0}^{\infty}\frac{n(n-1)}{2n+1}H_n^3(P') \tag{15}$$

where

$$H_n^\nu(P') = \frac{2n+1}{4\pi}\iint_\sigma H^\nu P_n(\cos\psi)d\sigma;\ \nu = 2,3 \tag{16}$$

where $P_n(\cos\psi)$ is the Legendre polynomial. Again, this formula is very simple for practical computations but with the global height information available in this study, it represents only the long-wavelength constitutents.

2.2.3 PITE represented by the integral formula of Martinec and Vaníček (1994b)

The PITE derived by Martinec and Vaníček (1994b) is based on the spherical approximation of the geoid. However, they considered this effect only locally as a result of a limited

integration area (spherical cap). The PITE in the point P' on the geoid is (Martinec and Vaníček 1994b)

$$\begin{aligned}\delta N_{\mathrm{I}}^{\mathrm{MV}^*}(P') &= -\frac{2\pi\mu}{\gamma}H_{P'}^2+\frac{\mu R^2}{\gamma}\iint_\sigma\Big[2\frac{(\ell_0^2+H^2)^{0.5}-(\ell_0^2+H_{P'}^2)^{0.5}}{R}\\ &+ \ln\frac{\frac{\ell_0}{2R}+H+(\ell_0^2+H^2)^{0.5}}{\frac{\ell_0}{2R}+H_{P'}+(\ell_0^2+H_{P'}^2)^{0.5}}-\frac{H-H_{P'}}{\ell_0}\Big]d\sigma \qquad (17)\end{aligned}$$

The spherical approximation of the geoid in this formula produces again an relative error of 3×10^{-3} in the geoidal heights. On the other hand, a planar approximation of distances is used in this formula which produces an error of the same order of magnitude as the error due to the spherical approximation of the geoid.

2.2.4 PITE with combination of the integral formula and the spherical harmonic expansion

The classical formula [Eq. (14)] is not practical for numerical evaluations, as it requires an integration over surface of the whole Earth to include long-wavelength contributions. It also suffers from the planar approximation of the geoid (Martinec and Vaníček 1994b, Sjöberg and Nahavandchi 1999). On the other hand, the spherical harmonic representation of the PITE [Eq. (15)] needs a very high maximum degree of expansion, to consider all short-wavelength information. A suitable compromise may therefore be of the form (Sjöberg and Nahavandchi 1999)

$$\begin{aligned}\Delta\delta N_{\mathrm{I}}(P') &= \delta N_{\mathrm{I}}^{\mathrm{classic}^*}-\delta N_{\mathrm{I}}^{\mathrm{new}^*}=-\frac{3\pi\mu}{\gamma}H_{P'}^2-\frac{3R\mu}{4\gamma}\\ &\times\iint_\sigma\frac{H^2-H_{P'}^2}{\ell_0}d\sigma-\frac{\mu}{8\gamma}\iint_\sigma\frac{H^3-H_{P'}^3}{\ell_0}d\sigma \qquad (18)\end{aligned}$$

or

$$\delta N_{\mathrm{I}}^{\mathrm{new}^*}=\delta N_{\mathrm{I}}^{\mathrm{classic}^*}-\Delta\delta N_{\mathrm{I}} \qquad (19)$$

where $\Delta\delta N_{\mathrm{I}}$ in spectral form is approximated as

$$\Delta\delta N_{\mathrm{I}}(P')=-\frac{3\pi\mu}{\gamma}\overline{H_{P'}^2}+\frac{\pi\mu}{2R\gamma}(H_{P'}^3-\overline{H_{P'}^3}) \qquad (20)$$

Equation (19) includes the integral part for short-wavelength constituents and the spherical harmonic representation to consider the long-wavelength information. It produces the same relative errors as Eq. (17).

3 Numerical investigations

3.1 Data sources

A test area of size $2^\circ\times2^\circ$ in Iran is chosen. It is limited by latitudes 31° N and 33° N and longitudes 54° E and 56° E. The topography in this area varies from 785 to 3053

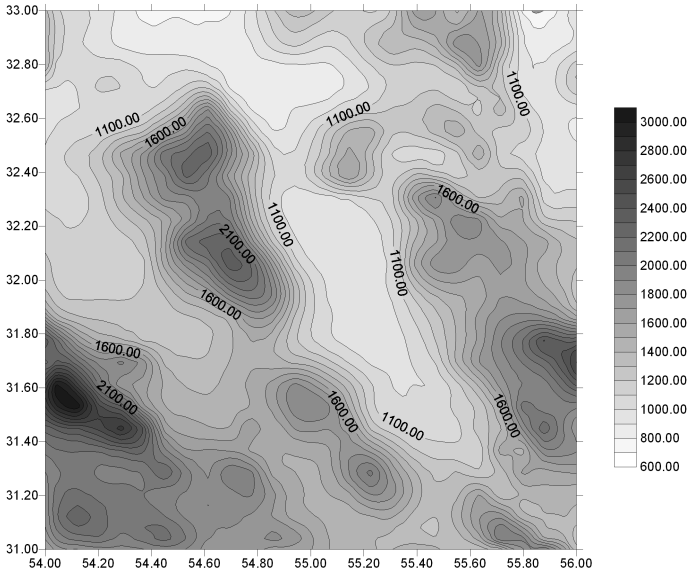

Figure 1: Presentation of topography in the test area. Contour interval =100 m

metres, shown in Fig. 1. The height spherical harmonic coefficients $(H^2)_{nm}$ and $(H^3)_{nm}$ are determined from Eqs. (7) and (8) using global topography. For this, a $30' \times 30'$ Digital Terrain Model (DTM) is generated by averaging the Geophysical Exploration Technology (GETECH) $5' \times 5'$ DTM (GETECH 1995a), using area weighting. Since the interest is in continental elevation coefficients and one aims to evaluate the effect of the masses above the geoid, the heights below sea level are all set to zero. The spherical harmonic coefficients are computed to degree and order 360. The parametr $\mu = G\rho$ is computed using $G = 6.673 \times 10^{-11} m^3\ kg^{-1}\ s^{-2}$ and $\rho = 2670\ kg/m^3$. The values of R=6371 km, and $\gamma = 9.81\ m/s^2$. are also used in computations. In all the integral equations in this study a $2' \times 2'$ DTM produced in National Cartographic Center of Iran is used. It should be mentioned that this DTM is not adequate for computing the local contributions of topographic effects in practice and only give an insight in the medium-wavelength constituents. A denser DTM is in preparation. Height data in all integral equations are extended to 6° from the computation point.

3.2 Computations of the DTE with different formulae

The DTE is computed in the test area with the classical integral formulae of Moritz (1980) [Eq. (3)] and Vaníček and Kleusberg (1987) [Eq. (4)], the spherical harmonic formula of Nahavandchi and Sjöberg (1998) [Eq. (5)], the integral formula of Martinec and Vaníček (1994a) [Eq. (11)], and Nahavandchi (2000) combined formula [Eq. (13)]. Table 1 shows the statistics of the results of the computations with the above-mentioned formulae. To give further insight into the differences, the results of the computations of the DTE are

Table 1: Statistics of the direct topographic effect on gravity with different formulae in the test region in mGal.

	Min	Max	Mean	SD
Classical Moritz formula	0.28	6.46	0.97	0.72
Classical Vaníček and Kleusberg formula	-33.61	8.05	0.004	5.11
Spherical harmonic approach of Nahavandchi and Sjöberg	-2.53	3.10	0.01	1.33
Integral formula of Martinec and Vaníček	-45.23	8.03	-0.71	6.96
Combined formula of Nahavandchi	-27.90	7.48	0.13	4.72

plotted. Figures 2-6 depict the DTE obtained with the different formulae mentioned above. Results in Table 1 and Figs. 2-6 show that different procedures for computation of the DTE result in significant differences.

It should be noted that Fig. 5 [integral formula of Martinec and Vaníček (1994a)] and Fig. 6 (combined formula) are similar in shape with minor differences in magnitude. The absolute maximum difference of 5.71 mGal was computed for these two procedures. Figure 3 [classical integral formula of Vaníček and Kleusberg (1987)] is similar in shape with Figs. 5 and 6 but with larger differences in magnitude. The absolute maximum difference of 18.82 mGal was computed for the differences between the combined formula [Nahavandchi (2000)] and the classical integral formula of Vaníček and Kleusberg (1987).

Of course, there are several reasons for these differences. For example, the Moritz (1980) formula is not really comparable to the other expressions in this study as it contains a combination of two different effects. This formula for DTE, however, will be used in the next step of computaions, which is geoid height determination with different methods of handling the topographic corrections. The Vaníček and Kleusberg's (1987) DTE refers to the point on Earth's surface while the Moritz (1980) formula refers to the point on the geoid, which justify the large differences between these two formulae. The spherical harmonic representation of the DTE will include only the long-wavelength information in this study (for M'=360), and most of short-wavelength information, which is included in the other formulae, is missing. This is the main reason for large differences between this method and the other ones. Martinec and Vaníček (1994a) integral formula and Nahavandchi (2000) combined formula for the DTE are in good agreement with each other. These two formulae use the spherical approximation of the geoid, contrary to the classical formulae which use the planar model. There are some minor differences between these two formulae, however, which originate from the exclusion of some parts of the long-wavelength constituents in Martinec and Vaníček (1994a) integral formula, which are included in the combined formula.

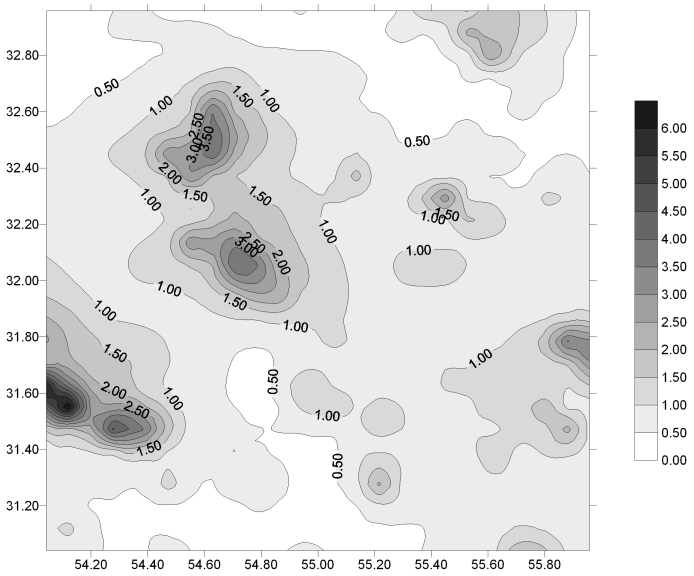

Figure 2: The direct topographic correction computed by the classical integral formula of Moritz (1980). Contour interval = 0.5 mGal

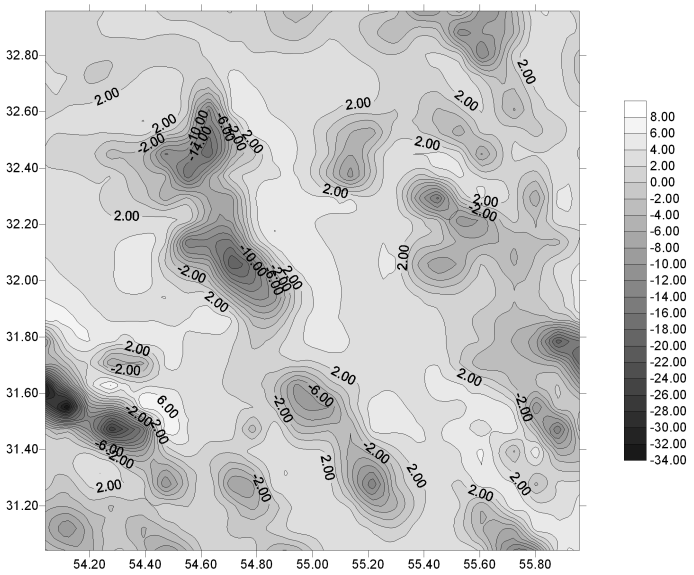

Figure 3: The direct topographic correction computed by the classical integral formula of Vanicek and Kleusberg (1987). Contour interval = 2 mGal

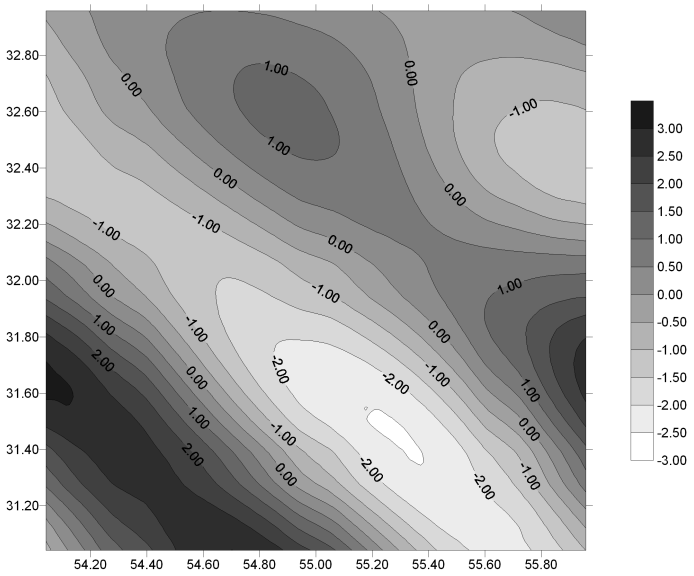

Figure 4: The direct topographic correction computed by the spherical harmonic approach of Nahavandchi and Sjoberg (1998). Contour interval = 0.5 mGal

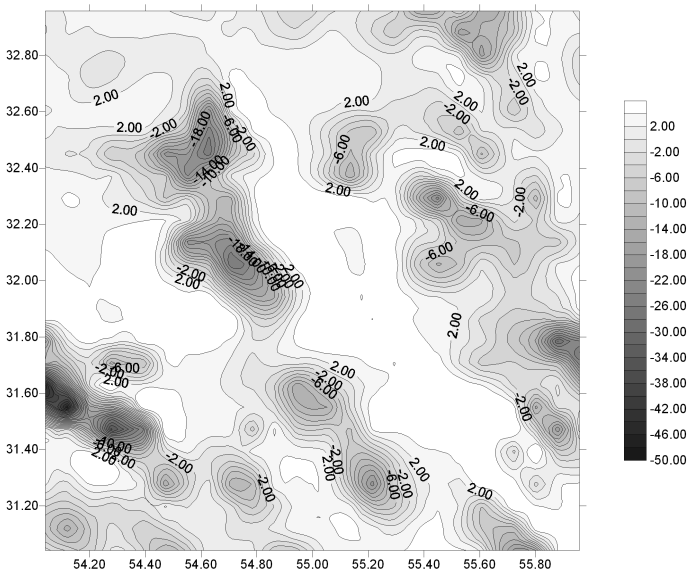

Figure 5: The direct topographic correction computed by the integral l formula of martinec and Vanicek (1994a). Contour interval = 2 mGal

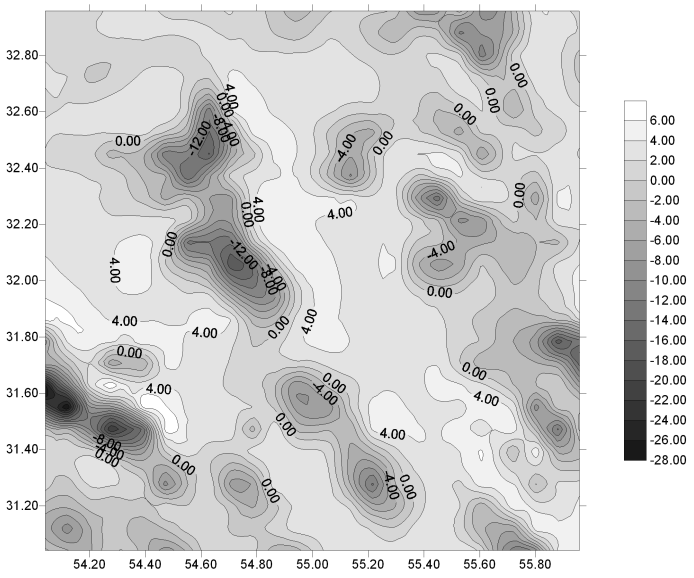

Figure 6: The direct topographic correction computed by the combined formula of Nahavandchi (2000). Contour interval = 2 mGal

Nahavandchi (2000) compared the combined formula [Eq. (13)] with the integral formula of Martinec and Vaníček (1994a) in a test area in Sweden with the maximum elevation of 1147 m. The maximum difference between these two formulae reached 2.31 μGal. In that study, however, Martinec and Vaníček (1994a) formula was integrated up to 20° from computation points using the GETECH $2.5' \times 2.5'$ DTM (GETECH 1995b). Further out the global $30' \times 30'$ DTM (GETECH 1995a) was used. This justifies the belief that some parts of the global information might be missing in the results from the integral formula of Martinec and Vaníček (1994a)(depending to the cap size of integration area).

3.3 Computations of the PITE with different formulae

The PITE is computed in the test area with the classical integral formula [Eq. (14)], the spherical harmonic formula of Nahavandchi and Sjöberg (1998) [Eq. (15)], the integral formula of Martinec and Vaníček (1994b) [Eq. (17)], and Sjöberg and Nahavandchi (1999) combined formula [Eq. (19)]. Table 2 shows the statistics of the results of the computations with the above-mentioned formulae. Again, the results of the computations of the PITE on the geoid height with the different formulae mentioned above are plotted. The results are shown in Figs. 7-10. Table 2 and Figs. 7-10 present the differences between different procedures for computation of the PITE. The same explanations as in case of the direct topographic effect can be repeated here. Figure 9 [integral formula of Martinec and Vaníček (1994b)] and Fig. 10 [combined formula of Sjöberg and Nahavandchi (1999)] are similar in shape but with minor differences in magnitude. The absolute maximum

Table 2: Statistics of the primary indirect topographic effect on the geoidal height with different formulas in the test region in cm.

	Min	Max	Mean	SD
Classical integral formula	-48.69	-3.68	-12.69	7.14
Spherical harmonic approach of Nahavandchi and Sjöberg	-11.48	6.31	-0.04	4.35
Integral formula of Martinec and Vaníček	-34.47	6.23	-0.83	6.29
Combined formula of Sjöberg and Nahavandchi	-36.89	8.08	-0.91	7.11

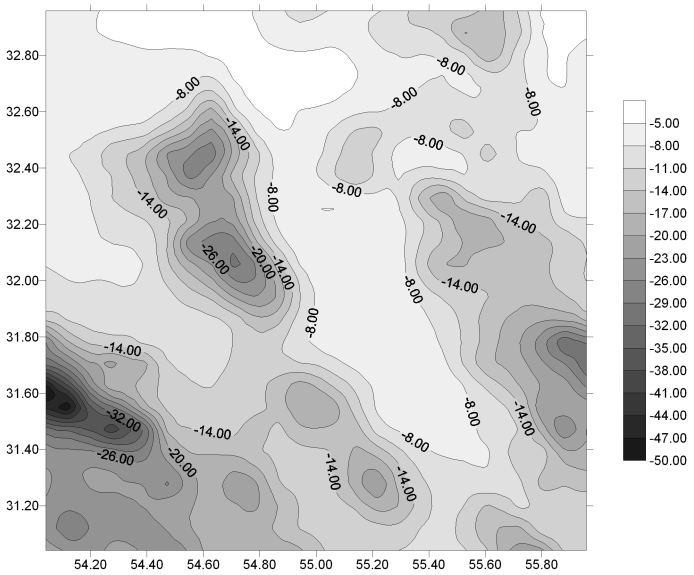

Figure 7: The primary indirect topographic correction computed by the classical integral formula . Contour interval = 3 cm

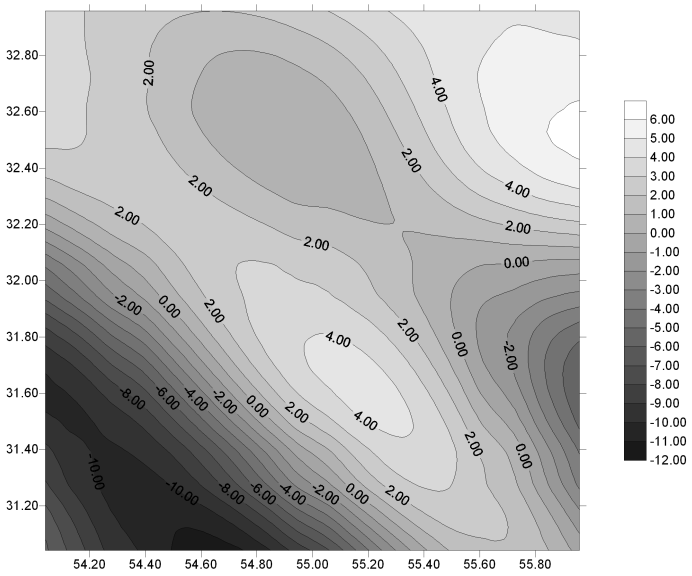

Figure 8: The primary indirect topographic correction computed by the spherical harmonic approach of Nahavandchi and Sjoberg (1998). Contour interval = 1 cm

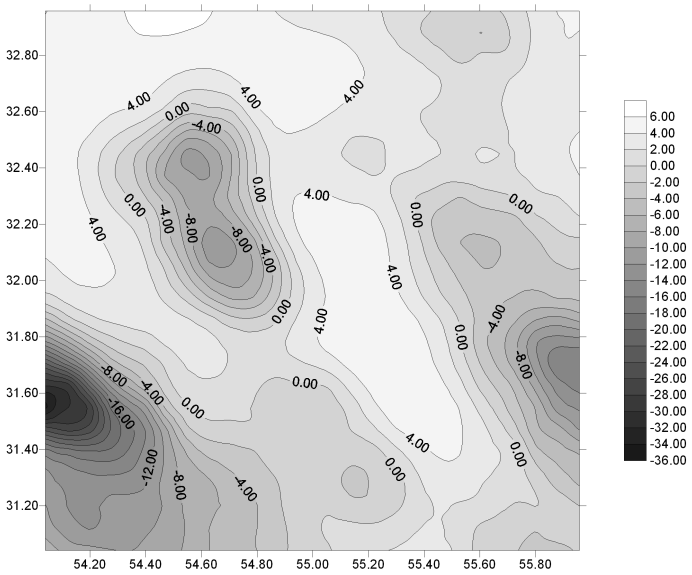

Figure 9: The primary indirect topographic correction computed by the integral formula of Martinec and Vanicek (1994b). Contour interval = 2 cm

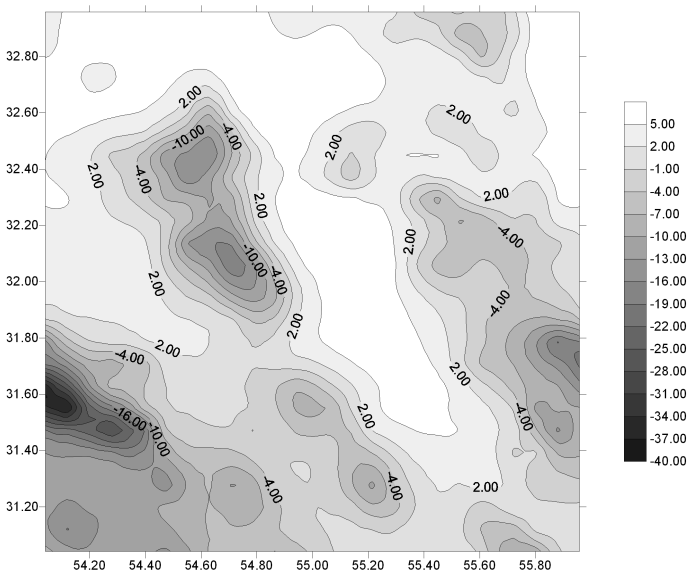

Figure 10: The primary indirect topographic correction computed by the combined formula of Sjoberg and Nahavandchi (1999). Contour interval = 3 cm

difference of 4.94 cm is computed between these two methods. Figure 7 (classical integral formula) is similar in shape with Figs. 9 and 10, but with larger differences. The absolute maximum difference of 11.91 cm was computed between the classical and the combined formulae.

While the classical integral formula suffers from the planar approximation of the geoid, the Martinec and Vaníček (1994b) integral formula and Sjöberg and Nahavandchi (1999) combined formula use the spherical model. The spherical harmonic representation of the PITE only includes the long-wavelength constituents in this study due to the use of M'=360, while the other integral formulae only include the short-wavelength information (due to the use of the integration area). Sjöberg and Nahavandchi (1999) combined formula include both short and long-wavelength information, contrary to Martinec and Vaníček (1994b) integral formula which only include the local contributions. But results from these two formulae are in good agreement with each other in comparison with the other methods. Sjöberg and Nahavandchi (1999) computed the differences between these two formulae in the test area in Sweden with the maximum elevation of 1051 m. They obtained the absolute maximum difference of 0.71 cm between these two formulae. It should be noted, however, that the integral formula of Martinec and Vaníček (1994b) was integrated up to 20° from computation points using the GETECH $2.5' \times 2.5'$ DTM (GETECH 1995b). The global $30' \times 30'$ DTM (GETECH 1995a) was used outside the 20° cap. This again justifies the belief that they might be some parts of the long-wavelength constituents, which are missing in the integral formula of Martinec and Vaníček (1994b) (due to the

choice of integration area).

To see how the different formulae for the DTE and the PITE work in different test areas, a flatter test area in Iran was chosen. The heights in this area vary from 625 to 1537 m. The same computations as above were carried out in this second test area. The results of comparisons between different formulae were the same as in the first test area. The differences were smaller and smoother, however, that shows the expected dependence of the topographical effects on elevations.

3.4 Comparisons

In order to obtain further insight into how the methods differ, and which model is better suited to describe the "height reference surface" of the national height reference system, 7 GPS-leveling stations were used as an external source to obtain the geoid heights. These stations belong to National Cartographic Center of Iran. The elevations of the GPS stations vary from 1431 to 1798 m. The accuracy of the ellipsoidal heights (h) of these stations is of the order of few centimetres. Iran is using the orthometric height system. The GPS-leveling geoidal heights in these 7 stations are computed with the well known formula

$$N \doteq h - H. \tag{21}$$

This formula is, however, only valid if orthometric height refers to the geoid where the "height reference surface" normally does not coincide with the geoid, which is the case in this study too. For the numerical investigation of different methods of handling the effects of topographic masses, the gravimetric geoid heights at these 7 GPS-leveling stations are also computed. Thereafter, the gravimetric results were compared with the GPS-leveling geoid heights. This will help to understand which method of topographic effects computations is better suited to describe the used "height reference surface".

For computing the gravimetric geoid heights, Stokes's formula in Eq. (1) with the least-squares modification of Stokes's kernel is used according to Nahavandchi and Sjöberg (2001a). Short-wavelength part of the geoid height was computed through Stokes's integration up to 6° from computation points and long-to-medium-wavelength part was computed from the global gravity geopotential model EGM96 (Lemoine et al. 1997). It is important to notice, however, that the EGM96 is based on free-air gravity anomalies and the used model here is Helmert's second method of condensation. The differences are normally very small but they might have larger values in mountainous areas. The terrestrial gravity anomalies in Stokes's integral are in $110'' \times 160''$ geographical cells and taken from National Cartographic Center of Iran. The interested readers are referred to Nahavandchi (1998b) and Nahavandchi and Sjöberg (2001a) for the procedures and formulae used in the modification of Stokes's formula.

To compute the gravimetric geoid height with the Stokes-Helmert scheme for geoid determination [see Eq. (1)], Helmert's anomaly at the geoid (Δg^{H^*}) is needed. The Moritz's (1980) DTE formula already includes the effect of the downward continuation to the geoid, while Vaníček and Kleusberg's (1987), Martinec and Vaníček's (1994a), spherical harmonic approach, and Nahavandchi's (2000) DTE formulae refer to a point at the ground level [see Eq. (2)]. Therefore, a downward continuation procedure must be implemented in these methods to reduce the Δg^H from topography to the geoid resulting in Δg^{H^*}. The Poisson integral formula with the same procedure carried out in Vaníček et al. (1996), Nahavandchi (1998c) and Nahavandchi and Sjöberg (2001b) was used.

The modified Poisson formula can be written as (see e.g. Vaníček et al. 1996; Nahavandchi and Sjöberg 2001b)

$$\Delta g^H = \frac{R}{4\pi} \iint_{\sigma_0} \Delta g^{H^*} K^M(r, \psi, R, \psi_0) d\sigma + \delta g_T + \Delta g_M^H \tag{22}$$

where δg_T is the truncation error, Δg_M^H are the low-degree spherical harmonics of the gravity anomaly, $K^M(r, \psi, R, \psi_0)$ is the modified Poisson kernel and σ_0 denotes the integration domain within a spherical cap of radius ψ_0. The truncation error is minimized following the Molodenskij technique to reduce potential errors coming from the employed global gravity model. The minimization is carried out in the sense of minimizing the upper bound of the absolute value of the truncation error by subtracting from Poisson's kernel an appropriately selected linear combination of spherical harmonic functions taken to degree and order M. The interested reader is referred to Vaníček et al. (1996) and Nahavandchi and Sjöberg (2001b) for the complete explanation of the above-mentioned modified Poisson formula to derive unknown Δg^{H^*} from given the Helmert gravity anomaly Δg^H.

Different formulae to determine the topographic effects and downward continuation problem are catagorized in the following 5 procedures. The classical integral formulae of Moritz with the DTE in Eq. (3) (which also includes the downward continuation procedure) and the PITE in Eq. (14) is the first method. Second, the classical integral formulae of Vaníček and Kleusberg with the DTE in Eq. (4) and downward continuation procedure in Eq. (22) and the PITE in Eq. (14) are used. Thereafter, the spherical harmonic approach was employed with the DTE in Eq. (5) and the downward continuation procedure in Eq. (22) and the PITE in Eq. (15). The integral formulae of Martinec and Vaníček with the DTE in Eq. (11) and the downward continuation procedure in Eq. (22) and the PITE in Eq. (17) is the fourth method. Finally, the combined formulae with the DTE in Eq. (13) and the downward continuation procedure of Eq. (22) and the PITE in Eq. (19) are used. Thereafter, the gravimetric geoid heights (with different correction procedures mentioned above) are computed at 7 GPS-leveling stations and the statistics of differences between the gravimetric and the GPS-leveling geoid heights are shown in Table 3. Table 3 shows that the gravimetric geoid heights agree better with the

Table 3: Statistics of the differences between gravimetric and 7 GPS-leveling stations' geoid heights with different procedures of handling the topographic corrections. Units in metres.

	Min	Max	Mean	SD
Classical Moritz formulae	-0.191	1.301	0.560	0.462
Classical Vaníček and Kleusberg formulae	-0.202	1.292	0.583	0.421
Spherical harmonic approaches of Nahavandchi and Sjöberg	-0.238	1.322	0.622	0.518
Integral formulae of Martinec and Vaníček	-0.118	1.221	0.562	0.381
Combined formulae of Nahavandchi and Sjöberg	-0.131	1.118	0.521	0.322

GPS-leveling geoid heights when the integral formulae of Martinec and Vaníček and the combined formulae of Nahavandchi and Sjöberg are used, compared to the other methods, with the latter formula as the best. This justifies the belief that the combined formulae used in this study for handling the effects of topographic masses include all wavelengths and are better suited to describe the height reference surfaces like the geoid.

In addition, a fitting process of the gravimetric and GPS-leveling geoid was conducted. The geoid change ΔN can be written in geographical coordinates as (Heiskanen and Moritz 1967):

$$N_{\mathrm{Grav}} - N_{\mathrm{GPS}} = \Delta N = \cos\phi\cos\lambda\Delta X + \cos\phi\sin\lambda\Delta Y + \sin\phi\Delta Z + kR \qquad (23)$$

where ϕ and λ are the geographical coordinates, ΔX, ΔY, ΔZ are the three translations and k is the scale factor. Equation (23) represents a very useful regression formula, which can be used for fitting a regional gravimetric geoid to the GPS-leveling stations. Table 4 shows the statistics of the differences, after fitting, between gravimetric and GPS-leveling geoid. Results of Table 4 shows that, after regression, the gravimetric geoid heights computed with the topographic effects of the combined formulae of Nahavandchi and Sjöberg still improve the fit of the gravimetric geoid to GPS-leveling stations, significantly. The standard deviation of the fit after regression with this method is computed as $\pm$10.1 cm compared to $\pm$12.3 cm with the integral formulae of Martinec and Vaníček, the second best method among the other methods. It should be mentioned, however, that these computations should be carried out in test areas with more available GPS-leveling stations.

4 Discussion and conclusions

The DTE and the PITE with different methods and different approximations are discussed. Classical integral formulae use the planar approximation of the geoid while the

Table 4: Statistics of the differences between GPS-leveling and gravimetric geoid heights with different procedures of handling the topographic corrections after fitting to 7 GPS stations. Units in metres.

	Min	Max	Mean	SD
Classical Moritz formulae	-0.514	0.435	0.000	0.192
Classical Vaníček and Kleusberg formulae	-0.483	0.466	0.000	0.181
Spherical harmonic approaches of Nahavandchi and Sjöberg	-0.557	0.429	0.000	0.238
Integral formulae of Martinec and Vaníček	-0.361	0.281	0.000	0.123
Combined formulae of Nahavandchi and Sjöberg	-0.252	0.312	0.000	0.101

recent formulae use the spherical approximation of the geoid. The spherical harmonic representation of the topographic effects only include the long-wavelength information with available maximum degree M'=360 used in this study, while pure integral formulae only include the local contributions depending on the integration area. The combined formulae of the PITE and the DTE derived by Sjöberg and Nahavandchi (1999) and Nahavandchi (2000), respectively, include all the significant information. As the important part of the topographic effects are the local contributions, the results of these formulae are in good agreement with the Martinec and Vaníček (1994a, b) integral formulae, which also use the spherical model of the geoid, but do not include the whole long-wavelength contributions. It can be stated that the combined formulae model better the long-wavelength constituents with respect to the procedure described in Martinec and Vaníček (1994a, b). It should be noted that the above-mentioned results should also be tested in other test areas.

The aim of this study was to show the differences between different procedures of handling the effect of topographic masses in precise geoid determination. It is shown that significant differences between different methods exist, which were expected. It is also concluded that the effects of distant topographic masses can not be neglected in precise geoid computations. It means that the long-wavelength contributions of these effects, which are included in the combined formulae, represent better the reality. To justify this belief, geoidal heights were computed applying different topographic effects. The gravimetric geoid heights were then compared with the 7 GPS-leveling geoid heights. The results of these comparisons prove the belief that the gravimetric geoid height computations corrected for topographic effects with the combined formulae work better with GPS-leveling data. The standard deviation of the fit (after the regression procedures) is determined to be equal to $\pm$10.1 cm for the topographic effects of combined formulae, while it is equal to $\pm$19.2 cm for the classical method. Finally, the use of the combined formulae of DTE [Eq. (13)] and PITE [Eq. (19)] are suggested for a precise geoid determination. The results

of gravimetric geoid height comparisons with GPS-leveling height data over Sweden also recommended the use of the combined formulae (Nahavandchi and Sjöberg 2001a, b).

References

[1] GETECH (1995a) Global DTM5. Geophysical Exploration Technology (GETECH), University of Leeds, Leeds

[2] GETECH (1995b) DTM2.5 of Europe. Geophysical Exploration Technology (GETECH), University of Leeds, Leeds

[3] Heck B (1992) A revision of Helmert's second method of condensation in geoid and quasi-geoid determination. In: Montag H, Reigber C (eds) Geodesy and physics of the Earth. International Association of Geodesy Symposia, vol 112. Springer, Berlin Heidelberg New York, pp 246-251

[4] Heiskanen WA, Moritz H (1967) Physical Geodesy. W H Freeman and Company, San Francisco

[5] Lemoine FG, Smith DE, Kunz L, Smith R, Pavlis EC, Pavlis NK, Klosko SM, Chinn DS, Torrence MH, Williamson RG, Cox CM, Rachlin KE, Wang YM, Kenyon SC, Salman R, Trimmer R, Rapp RH, Nerem RS (1997) The development of the NASA GSFC and NIMA Joint Geopotential Model. In: Segawa J, Fujimoto H, Okubo S (eds) Gravity, geoid and marine geodesy. International Association of Geodesy Symposia, vol 117. Springer, Berlin Heidelberg New York, pp 461-469

[6] Martinec Z (1998) Boundary-value problems for gravimetric determination of a precise geoid. Springer-Verlag, Berlin Heidelberg, Germany

[7] Martinec Z, Vaníček P (1994a) Direct topographical effect of Helmert's condensation for a spherical approximation of the geoid. Manuscr Geod 19: 257-268

[8] Martinec Z, Vaníček P (1994b) The indirect effect of topography in the Stokes-Helmert technique for a spherical approximation of the geoid. Manuscr Geod 19: 213-219

[9] Martinec Z, Matyska C, Grafarend EW, and Vaníček P (1993) On the Helmert's 2nd condensation method. Manuscr Geod 18: 417-421

[10] Moritz H (1968) On the use of the terrain correction in solving Molodenskii's problem. Rep 79, Department of Geodetic Science, The Ohio State University, Columbus

[11] Moritz H (1980) Advanced Physical Geodesy. Herbert Wichmann Verlag, Karlsruhe, Germany.

[12] Nahavandchi H (1998a) Terrain correction computations by spherical harmonics and integral formulas. Physics and Chemistry of the Earth. vol 24, 1: 73-78

[13] Nahavandchi H (1998b) Precise gravimetric-GPS geoid determination with improved topographic corrections applied over Sweden. Division of Geodesy, Rep 1051, Royal Institute of Technology, Stockholm

[14] Nahavandchi H (1998c) On some methods of downward continuation of mean free-air gravity anomaly. Int Geoid Ser Bull 8: 1-17

[15] Nahavandchi H (1999) Geoid terrain correction to power H^5 of satellite derived geopotential models. Boll Sci Affini 3: 232-240

[16] Nahavandchi H (2000) The direct topographical correction in gravimetric geoid determination by the Stokes-Helmert method. J Geod 74: 488-496

[17] Nahavandchi H, Sjöberg LE (1998) Terrain correction to power H^3 in gravimetric geoid determination. J Geod 72: 124-135

[18] Nahavandchi H, Sjöberg LE (2001a) Precise geoid determination over Sweden using the Stokes-Helmert method and improved topographic corrections. J Geod 75:74-88.

[19] Nahavandchi H, Sjöberg LE (2001b) Two different views of topographical and downward continuation corrections in the Stokes-Helmert approach to geoid computations. J Geod 74: 816-822

[20] Sjöberg LE (1994) On the total terrain effects in geoid and quasigeoid determinations using Helmert second condensation method. Division of Geodesy, Rep 36, Royal Institute of Technology, Stockholm

[21] Sjöberg LE (1995) On the quasigeoid to geoid separation. Manuscr Geod 20: 182-192

[22] Sjöberg LE (1996) The terrain effect in geoid computation from satellite derived geopotential models. Boll Geod Sci Affini 4: 385-392

[23] Sjöberg LE (2000) The topographic effects by the Stokes-Helmert method of geoid and quasi-geoid determination. J Geod 73: 87-93

[24] Sjöberg LE, Nahavandchi H (1999) On the indirect effect in the Stokes-Helmert method of geoid determination. J Geod 73: 87-93

[25] Sjöberg LE, Nahavandchi H (2000) The atmospheric geoid effects in Stokes's formula. Geophys J Int 140: 95-100

[26] Sun W, Sjöberg LE (2001) Convergence and optimal truncation of binomial expansions used in isostatic compensations and terrain corrections. J Geod 74: 627-636

[27] Vaníček P, Kleusberg A (1987) The Canadian geoid- Stokesian approach. Manuscr Geod 12: 86-98

[28] Vaníček P, Martinec Z (1994) The Stokes-Helmert scheme for the evaluation of a precise geoid. Manuscr Geod 19: 119-128

[29] Vaníček P, Najafi M, Martinec Z, Harrie L, Sjöberg LE (1995) Higher-order reference field in the generalized Stokes-Helmert scheme for geoid computation. J Geod 70: 176-182

[30] Vaníček P, Sun W, Ong P, Martinec Z, Najafi M, Vajda P, Ter Horst B (1996) Downward continuation of Helmert's gravity. J Geod 71: 21-34

[31] Vaníček P, Huand J, Novak P, Veronneau M, Pagiatakis S, Martinec Z, Featherstone WE (1999) Determination of boundary values for the Stokes-Helmert problem. J Geod 73: 180-192

[32] Wang YM, Rapp RH (1990) Terrain effects on geoid undulation computations. Manuscr Geod 15: 23-29

[33] Wichiencharoen C (1982) The indirect effects on the computation of geoid undulations. Rep 336, Department of Geodetic Science, The Ohio State University, Columbus

Quasi-geoid BG03 computation in Belgium

R. Barzaghi (*), A. Borghi (*), B. Ducarme (**), M. Everaerts (**)

(*) DIIAR-Politecnico di Milano, Piazza Leonardo da Vinci 32, 20133 Milano
(**) Royal Observatory of Belgium, Av. Circulaire 3, 1180, Brussels

Introduction

The estimate of a high precision quasi-geoid is nowadays a relevant goal in Geodesy, since from this surface can be derived the geoid. As it is well known, the geoid, i.e. the equipotential surface of the Earth gravity field which is close to the mean ocean surface, can be used in combination with GPS observations to estimate orthometric heights. This is of particular relevance, since this can be done in a faster and cheaper way than using spirit leveling, although with lower precision (which is however sufficient in many practical applications). In 1996, the last estimate of the Belgium quasi-geoid BG96 was computed with the Stokes and the least square collocation methods (Pâquet et al 1997). This quasi-geoid has a precision of 3 to 4 cm in the area well covered by gravity data , which was assessed through comparison with GPS/leveling derived undulations with 36 BEREF points. Since now the gravity coverage of Belgium is completed a higher precision for the geoid could be reached for the south-eastern part and in the northern part of the country.

In this paper, a new estimate of the Belgium quasi-geoid (BG03) is presented. The main improvements with respect to the previous computation are related to gravity data coverage, DTM refinements and new global geopotential models. So, this estimate can be considered a significant step forward in quasi-geoid computation for this area and a basis for a future estimate which will be obtained by merging gravity and GPS/leveling data.

1. Gravity data, DTM and global geopotential models

The gravity date base used in this computation has been sharply improved with respect to the previous one. Furthermore, a new DTM has been prepared including bathymetry. The details related to these new data sets will be discussed in the following together with a description of the geopotential models used to represent the low frequency part of the geopotential field.

1.1 The gravity data set

A first determination of the gravity value in Uccle (ROB) was obtained in 1894 with the help of a pendulum. A first belgian gravity Network with 24 stations was successfully observed in 1928 with an internal error ranging from 1 to 3 mGal. In the years 1947-48 a second gravity survey of the country was performed including 381 stations to cover a territory of 30 000km^2. The precision was everywhere better than 0.7 mGal. Since 1948 The National Geographic Institute (NGI) and the Royal Observatory (ROB) worked in close co-operation to densify the gravity coverage of Belgium. This goal was finally reached in 2002. The density of the coverage is lower in the south-eastern part of the country (1 station per 2.5 km² to 1 per 5 km²) but it reaches 1 station per km² on the rest of the territory. The data base of the ROB holds more than 250 000 gravity measurements for Belgium and the surrounding countries. All these gravity values were include in BG03. The

precision is everywhere better than 0.1 mGal. There are more than 30 000 data on the Belgian territory itself. The rest of the data were provided by the BRGM for France, the BGS for Great Britain, the Rijkswaterstaat for the Netherlands, and Wenzel H.G. (personal communication) for Germany. All those data have been carefully validated. All networks are referenced to the gravity datum of Uccle 1976, (Poitevin 1980).

1.2 The Digital Terrain Model

In the framework of this computation, a new DTM has been set up to properly compute the terrain effect. In Belgium the DTM has been provided by the NGI with a resolution of 3'×6'. For the surrounding territories in the window

$$38° \le \varphi \le 54° \qquad -6° \le \lambda \le 13°$$

an homogeneous 4 km grid was obtained by integrating the land data of the WEEG Project (Fairhead, 1994) with the 5' NOAA bathymetry in the same area.
The DTMs were merged using bilinear interpolation to produce a unique DTM with spacing $\Delta\varphi$=2.5' and $\Delta\lambda$=3' and boundaries

$$47.5° \le \varphi \le 53.5° \qquad 0° \le \lambda \le 8°$$

In this way, the estimated DTM is known over an area that is one degree larger than the one corresponding to the gravity data.
The plot of this DTM is shown in fig.1

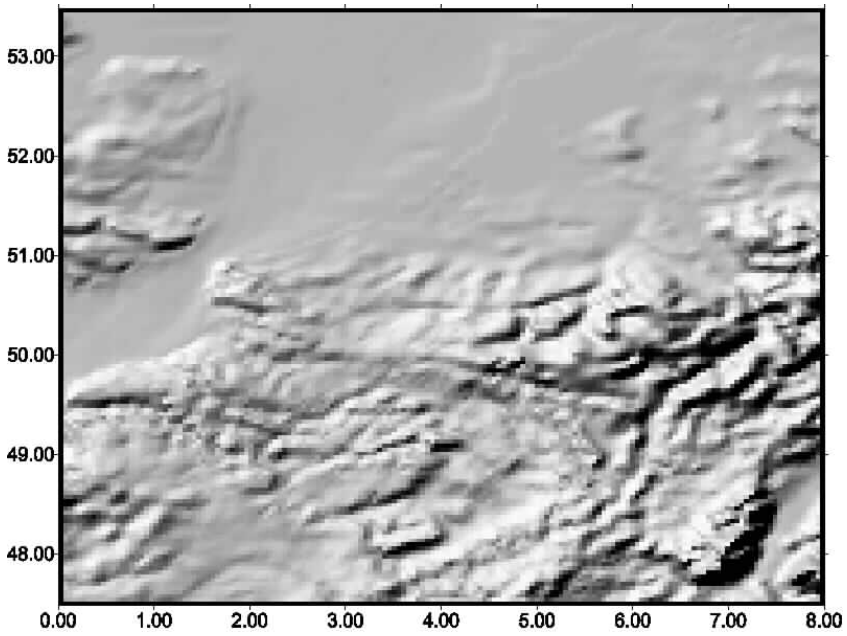

Figure 1 – The DTM in the computation area

1.3 The global geopotential models

Since the previous estimate of the quasi-geoid in Belgium, which was based on OSU91A, two new geopotential models have been made available: EGM96, complete up to degree 360, (Lemoine

et al, 1998; IGeS Bulletin, 1997) and the high resolution model GPM98CR by Wenzel, complete up to degree 720, (Wenzel, 1998). The plots of the gravity anomaly implied by the two more recent models and by OSU91A, bounded to the computation area, are shown in fig 2.

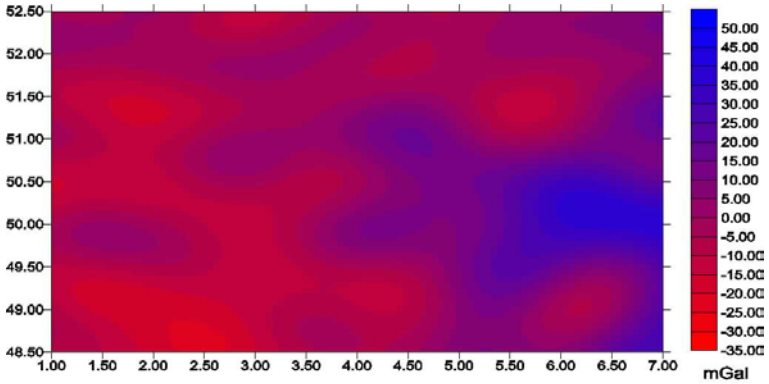

Figure 2a - The OSU91A gravity anomaly

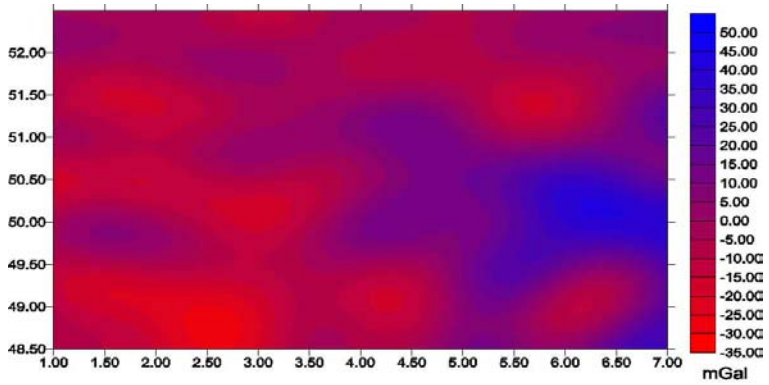

Figure 2b - The EGM96 Gravity anomaly

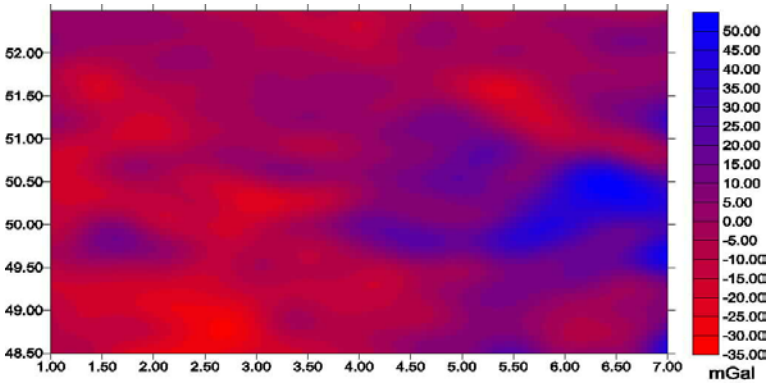

Figure 2c - The GPM98CR gravity anomaly

As one can see, Δg(OSU91A) and Δg(EGM96) are quite similar while Δg(GPM98CR) displays a rougher structure. The same consideration holds for the model undulations which are plotted in fig 3.

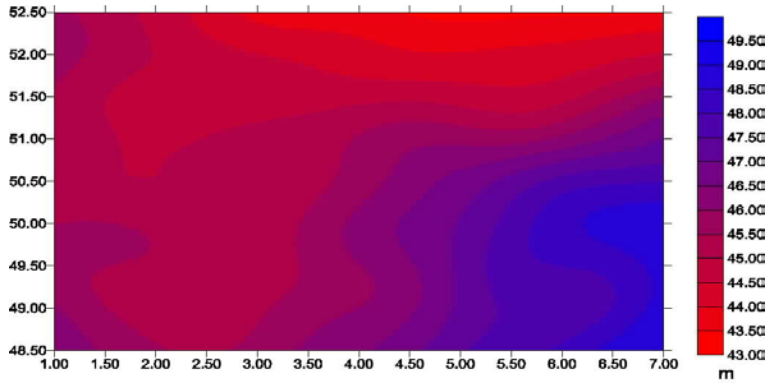

Figure 3a - The OSU91A undulation

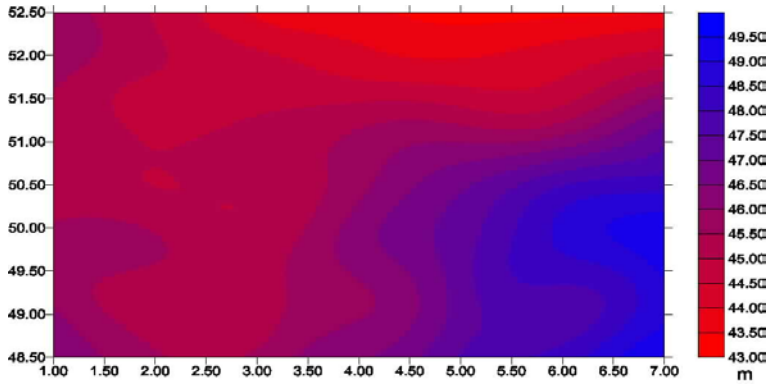

Figure 3b - The EGM96 undulation

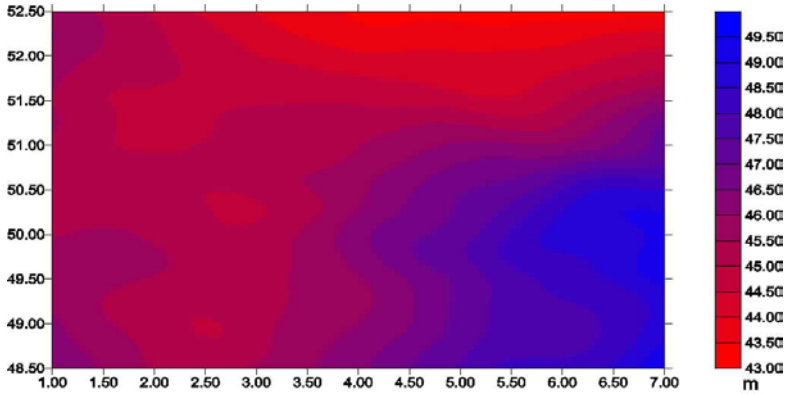

Figure 3c - The GPM98CR undulation

It is quite obvious that OSU91A is close to EGM96 since they have been computed following a similar approach and to the same degree n=360. On the contrary, the Wenzel GPM98CR model is derived following a quite different method and thus differences are expected with respect to OSU91A and EGM96. Furthermore, this model is complete up to degree 720 and it comes from a model which is complete up to degree 1800. Hence, discrepancies in the high frequency content with respect to 360 models are expected too.

Both the geopotential EGM96 model and the GPM98CR model have been used in computing the Belgium quasi-geoid: so, in the end, different estimates will be available to be tested against GPS/leveling data.

2. Estimation procedures and results.

The numerical results related to the estimation procedures are given in the following paragraphs. The classical "remove-restore" (Tscherning, 1994) procedure has been used and the residual quasi-geoid components have been evaluated using the Fast Collocation approach (Bottoni and Barzaghi, 1993) and the FFT technique (Sideris, 1994).

2.1 Quasi-geoid computation and results based on EGM96

The computation of the quasi-geoid named B_EGM96, based on the EGM96 global model, has been carried out on a regular 1' x 1' grid in the area

$$48.5° \le \varphi \le 52.5° \qquad 1° \le \lambda \le 7°$$

With respect to the geopotential model EGM96, the reference DTM for Residual Terrain Correction (RTC) computation has been computed using 25' window size moving average on the detailed DTM. The 25' window size has been tuned on the statistical properties of the residuals with respect to EGM96 model.

RTC has been computed up to 80 km from each computation point both in the gravity and in the quasi-geoid components. Statistics of the "remove" step are listed in tab.1.

Point gravity values have been then gridded on a regular 1' x 1' geographical grid. GEOGRID program of the GRAVSOFT package (Tscherning et al., 1994) was used for such a step: statistics of the residual gridded gravity values Δg_r^G are shown in tab. 1. The empirical covariance of these values and the best fit model, obtained using the COVFIT program (GRAVSOFT), are represented in fig. 4.

As one can see, a satisfactory fit between the empirical values and the model covariance is reached basically up to the first zero. The best fit model, in terms of anomalous potential T(P), has the following general form (Tscherning and Rapp, 1974)

$$COV_{TT}(P,Q) = \sum_{i=2}^{\infty} \sigma_i^2 \left(\frac{R^2}{rr'} \right)^{i+1} P_i(\cos\psi) \qquad (1)$$

where: $\sigma_i^2 = \begin{cases} \text{error degree variances} & i \le 200 \\ \text{degree variances} & \dfrac{A}{(i-1)(i-2)} \left(\dfrac{R_B}{R} \right) \end{cases}$

R = Earth radius R_B = Bjerhammar sphere radius

r, r' = radial distances of points in space P, Q

P_i = Legendre Polynomial of degree i

ψ = spherical distance between P and Q

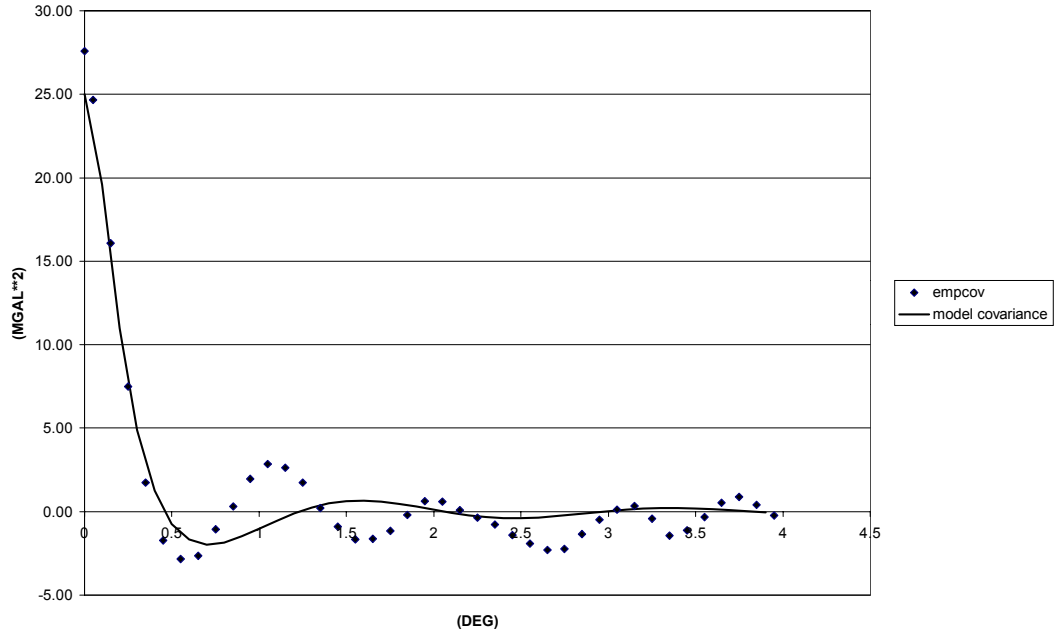

Figure 4 - Empirical and model covariance function of the gridded gravity residuals obtained with the global geopotential model EGM96

	Δg_0 [mGal]	$\Delta g_0 - \Delta g_M$ [mGal]	Δg_r [mGal]	Δg_r^G [mGal]
n	43361	43361	43361	87001
E	-1.21	-1.75	-1.78	-1.54
σ	13.69	7.40	6.31	5.27
min	-39.07	-37.25	-37.78	-25.23
max	64.16	36.88	27.87	22.63

Table 1 - Statistics of the "remove" step using the EGM96 geopotential model.

Δg_0: observed gravity values (free air) Δg_M: gravity geopotential model component
A_{rtc} :gravity terrain correction component $\Delta g_r = \Delta g_0 - \Delta g_M - A_{rtc}$ gravity residuals
Δg_r^G: gridded gravity residuals

The Fast Collocation (FC) solution giving ζ_r has been computed on the same 1'x1' grid used for Δg_r^G.
Furthermore, the FFT estimate of ζ_r was also computed to compare the two estimation methods.
The "restore" step was then accomplished: the ζ_{rtc} and the ζ_M component have been added to ζ_r, thus getting the final quasi-geoid estimate B_EGM96. In tab.2 the statistics of the "restore" step are summarized

	ζ_r (FC) [m]	ζ_r (FFT) [m]	ζ_M (EGM96) [m]	ζ_{RTC} [m]	$\zeta=\zeta_r$ (FC)$+\zeta_M+\zeta_{RTC}$ [m]
n	87001	87001	87001	87001	87001
E	-0.24	-0.37	45.83	0.02	45.61
σ	0.15	0.14	1.35	0.09	1.31
min	-0.58	-0.71	43.28	-0.18	43.16
max	0.08	-0.04	49.33	0.51	49.35

Table 2 - Statistics of the "restore" step using the EGM96 geopotential model

ζ_r : residual quasi-geoid
ζ_M : quasi-geoid geopotential model component
ζ_{rtc} :quasi-geoid terrain correction component
ζ : total quasi-geoid

As one can see, the FC estimate and the FFT solution are practically equivalent but for a bias of 0.13 m. Furthermore, as it is well known, the geopotential model gives nearly the whole quasi-geoid signal, especially in this computation area where no relevant topography and geophysical signals are present.

2.3 Quasi-geoid computation and results based on GPM98CR

In this case, the high resolution geopotential model GPM98CR by Wenzel has been used up to degree 720 to get the B_GPM98CR estimate.

Also in this case, the steps described in the B_EGM96 computation have been performed. The reference DTM in RTC computation was derived by applying a 5' window size moving average on the detailed DTM. As expected, the reference DTM used in this computation differs from the one used in combination with the EGM96 model. Higher frequencies are taken into account when using the GPM98CR geopotential model and so the reference DTM must contain higher frequencies too

Statistics of this "remove" step are given in tab. 3. As done before, residual gravity values have been gridded on a 1'×1' regular geographical grid covering the same area used in the EGM96 based computation (their statistics are listed in tab. 3). The empirical covariance and the best fit model, which belongs to the same kind of function in (1), are shown in fig. 5

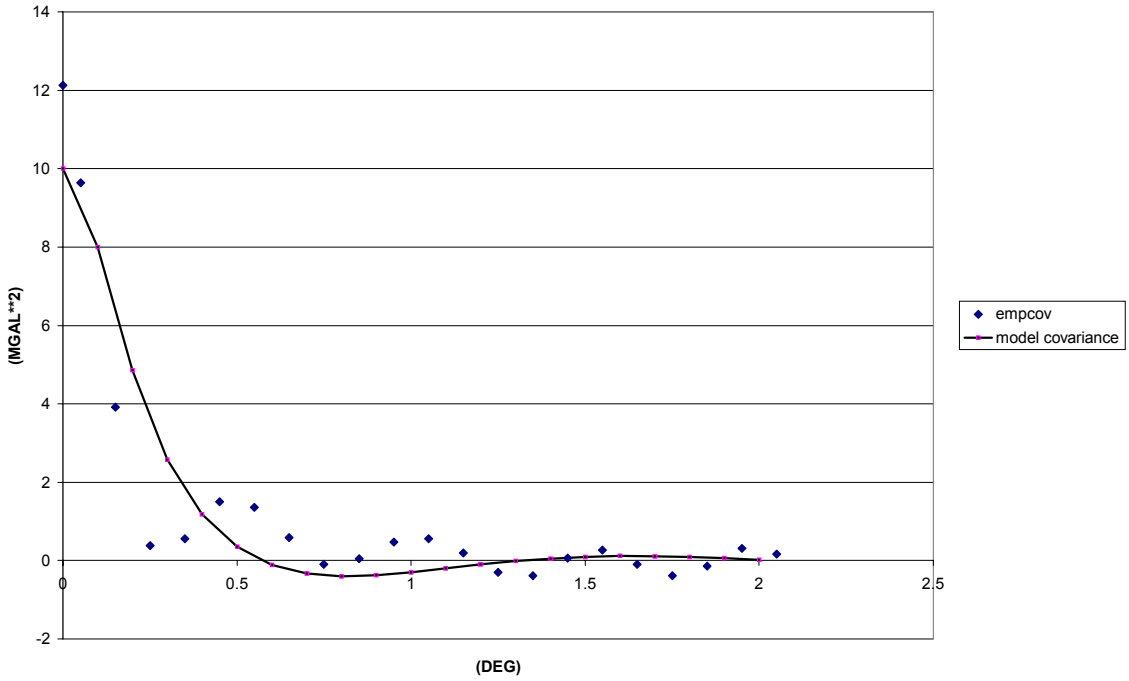

Figure 5 - Empirical and model covariance function of the gridded gravity residuals obtained with the global geopotential model GPM98CR

The empirical covariance is more irregular if compared with the EGM96 empirical covariance but its value in the origin is remarkably smaller that the one obtained for that empirical covariance. This means that the GPM98CR model and the related RTC reduction can give a better representation of the local gravity data than EGM96 (this can be seen also in the statistics of the gravity residuals – compare tab. 1 and tab. 3)

	Δg_0 [mGal]	$\Delta g_0 - \Delta g_M$ [mGal]	Δg_r [mGal]	Δg_r^G [mGal]
N	43361	43361	43361	87001
E	-1.21	-1.62	-1.80	-1.56
σ	13.69	5.00	4.58	3.49
Min	-39.07	-33.93	-32.94	-19.55
Max	64.16	28.08	21.96	12.63

Table 3 - Statistics of the "remove" step using the GPM98CR geopotential model.

Δg_0: observed gravity values (free air)
Δg_M: gravity geopotential model component
A_{rtc} :gravity terrain correction component
$\Delta g_r = \Delta g_0 - \Delta g_M - A_{rtc}$ gravity residuals
Δg_r^G: gridded gravity residuals

As in the previous estimates, Fast Collocation and FFT were applied for computing ζ_r on the 1'x1' regular grid used for Δg_r^G evaluation. The statistics of the "restore" step related to the B_ GPM98CR quasi-geoid are presented in tab. 4.

	ζ_r (FC) [m]	ζ_r (FFT) [m]	ζ_M (GPM98CR) [m]	ζ_{RTC} [m]	$\zeta=\zeta_r$ (FC)$+\zeta_M+\zeta_{RTC}$ [m]
n	87001	87001	87001	87001	87001
E	-0.25	-0.38	45.83	0.02	45.60
σ	0.12	0.11	1.35	0.03	1.31
min	-0.52	-0.64	43.22	-0.80	43.17
max	0.17	-0.03	49.62	0.18	49.43

Table 4 - Statistics of the "restore" step using the GPM98CR geopotential model
ζ_r : residual quasi-geoid
ζ_M : quasi-geoid geopotential model component
ζ_{rtc} :quasi-geoid terrain correction component
ζ : total quasi-geoid

Also for this estimate, the same remarks done for the EGM96 based computation hold.

3. Comparisons with GPS/leveling derived undulations

The two gravimetric quasi-geoid estimates have been compared on 36 points with GPS derived undulations. In these 36 double points, both h (ellipsoidal height) and H (orthometric height) are known so that $N_{GPS/lev}$ = h-H can be computed. Thus, the $N_{GPS/lev}$ values can be compared with the gravimetric estimate to asses its precision. To properly perform the comparison, a datum shift between the gravimetric quasi-geoid estimates and the $N_{GPS/lev}$ must be computed to reduce the data to the same reference system. While $N_{GPS/lev}$ is in the GPS reference system, ζ computed with the "remove-restore" method is in the reference system implied by the global geopotential model.

To this aim, the following formula, which accounts for a translation based datum shift in terms of geoid undulation, has been considered (Heiskanen and Moritz, 1990):

$$\begin{aligned} N_{grav} &= N_{GPS/lev} + \Delta N(\theta,\lambda) = \\ &= N_{GPS/lev} + dx\sin\theta\cos\lambda + dy\sin\theta\sin\lambda + dz\cos\theta \end{aligned} \qquad (2)$$

(dx,dy,dz) = translation between GPS and geoid reference systems
$\theta = 90-\varphi$

(we remark that only translation is considered in this relationship between the two reference systems).

In (2), we also assume that $N_{grav} \sim \zeta$, being ζ the quantity which is effectively estimated: this can induce distorsions and perturbations specially in high mountain areas. However, for a first

rough relative comparison among the different estimates, we decided to do this assumption, leaving the refinements to further computations.

The quantities (dx,dy,dz) were estimated by least squares; outliers rejection, in the hypothesis of normal distributed residuals and with significance level α =1%, was also performed .Due to that, one GPS point, located in Arlon, was skipped from the solution summarized in the following Table.

	B_EGM96(FC) - $N_{GPS/lev}$	B_EGM96(FFT) - $N_{GPS/lev}$	B_GPM98CR(FC) - $N_{GPS/lev}$	B_GPM98CR(FFT) - $N_{GPS/lev}$
#	35	35	35	35
E	0.00	0.00	0.00	0.00
σ	0.03	0.04	0.03	0.03
min	-0.07	-0.07	-0.07	-0.07
max	0.07	0.07	0.07	0.07

Table 5 - Statistics of the residuals between ζ and $N_{GPS/lev}$ after datum shift estimate

As it can be seen, the same results have been obtained for the four estimates which are in a very good agreement with the $N_{GPS/lev}$ values. So, it can be concluded that the different estimates in this area are equivalent in representing the undulations coming from GPS and leveling observations.
The plot of the B_EGM96(FC) geoid, named from now on BG03, is shown in the following figure together with the residuals in the 36 double points. In the discussion of the the BG96 estimate, we thought that only the poor coverage of the Ardennes, in the South East of Belgium, was the cause of its low accuracy. One of the conclusions of this work is that it is mainly the point of Arlon, in red on the figure 6, that was responsible of the problems.

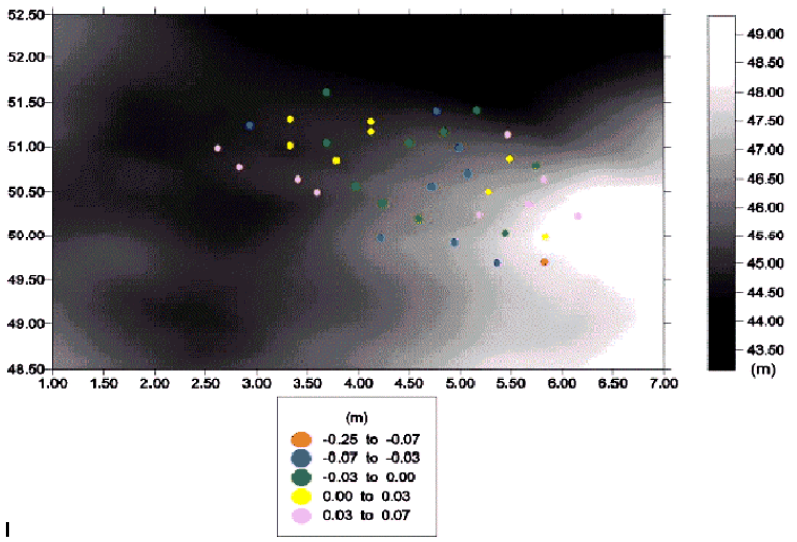

Figure 6 –The estimated quasi-geoid BG03 versus $N_{GPS/lev}$

4. Comparison between BG96 and BG03

The fig 7 shows the comparison between BG96 and BG03. In this figure, there is a clear North-South strong gradient at 4.5° of longitude. This anomaly existing only in BG96 is related to the fact that the gravity coverage East of this line was very poor at that time, so that in BG96 the data to the East and to the West of this line were considered as two different data sets. This figure shows also the area improved by BG03. We see clearly large differences up to 4 cm in eastern part between 4.5° and 5.5° longitude and 50° and 50.5° latitude. It is mainly due to the improved gravity coverage. Surprisingly in the South of Belgium the difference between BG96 and BG03 is rather small although the previous gravity coverage was sparse. It is probably due to the fact that in this area most of the signal comes from the DTM. There is of course a very big difference in the south eastern part in 49.5° latitude and 5.8° longitude which is due to the very bad GPS-leveled point in Arlon. It is only in the new of BG03 computation that we could consider this point as an outlier, as this area is now well covered with gravity data. Large changes in the extreme West of the country are probably due to the use of bathymetry data on sea and a better gravity coverage on land in this area.

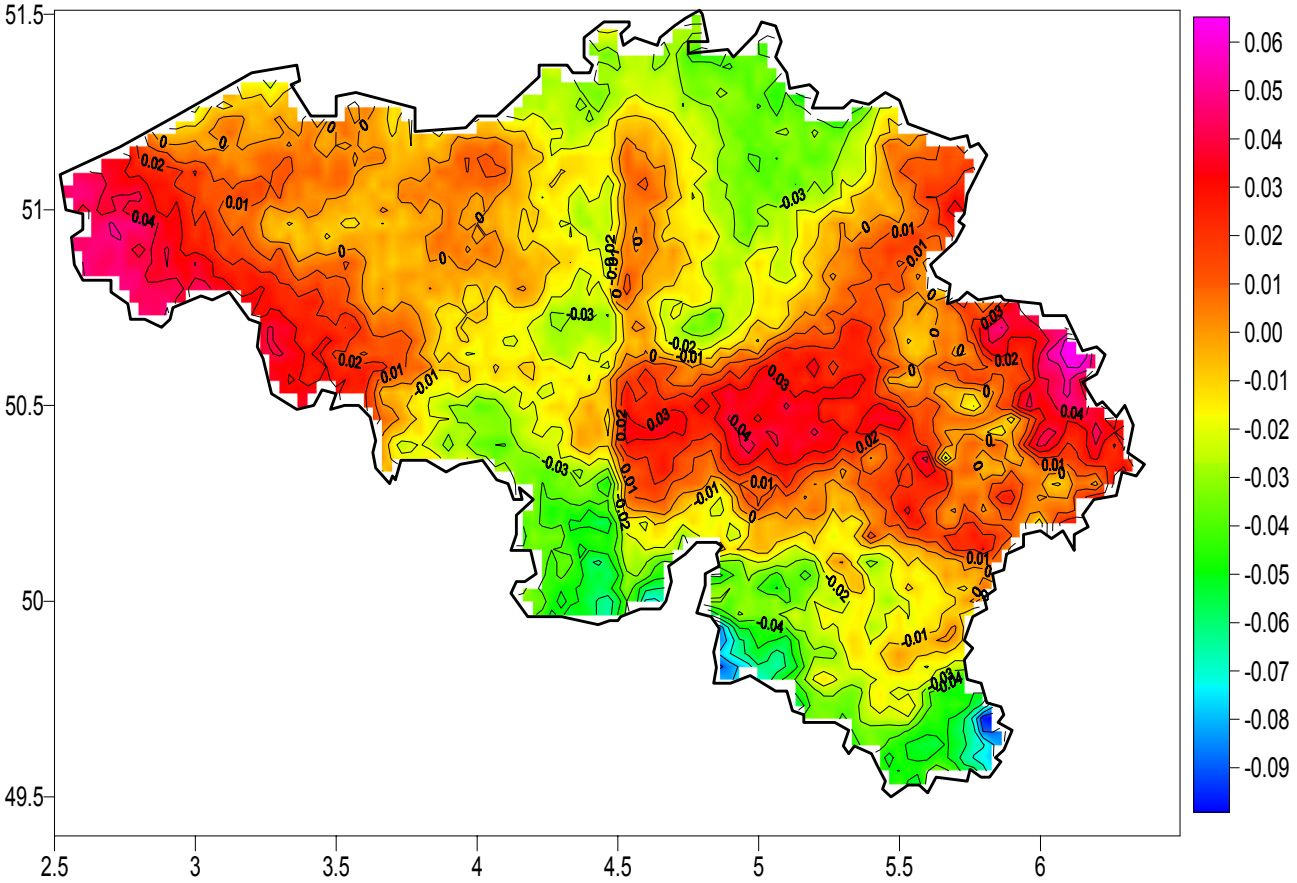

Figure 7 - Comparison between BG96 and BG03 (contour in m)

5. High frequency content of BG03.

Since the gravity coverage is now completed in Belgium, It is interesting to know the areas where the contribution of gravity is more important than the one due to topography. We have thus filtered out from BG03 the low frequency signals. In fig. 8 it can bee seen that, North of 50.5° latitude, where the area is flat, we find back anomalies mainly due to gravity, while South of that line the geoid undulations are mainly due to topography especially in the Eastern part of the country where

the highest altitudes are located. We have clearly found back the two main geological units of Belgium, in the North the eroded lower paleozoic and the typical Bouguer anomalies associated to it and in the South the upper paleozoic not yet eroded, where the topography produces the main part of the signal. Let us point out the Flanders anomalies, the EW gravity gradient at the Southern border of the Brabant massif, the Mons basin, the Famennes depression and the main axis of the Ardennes massif.

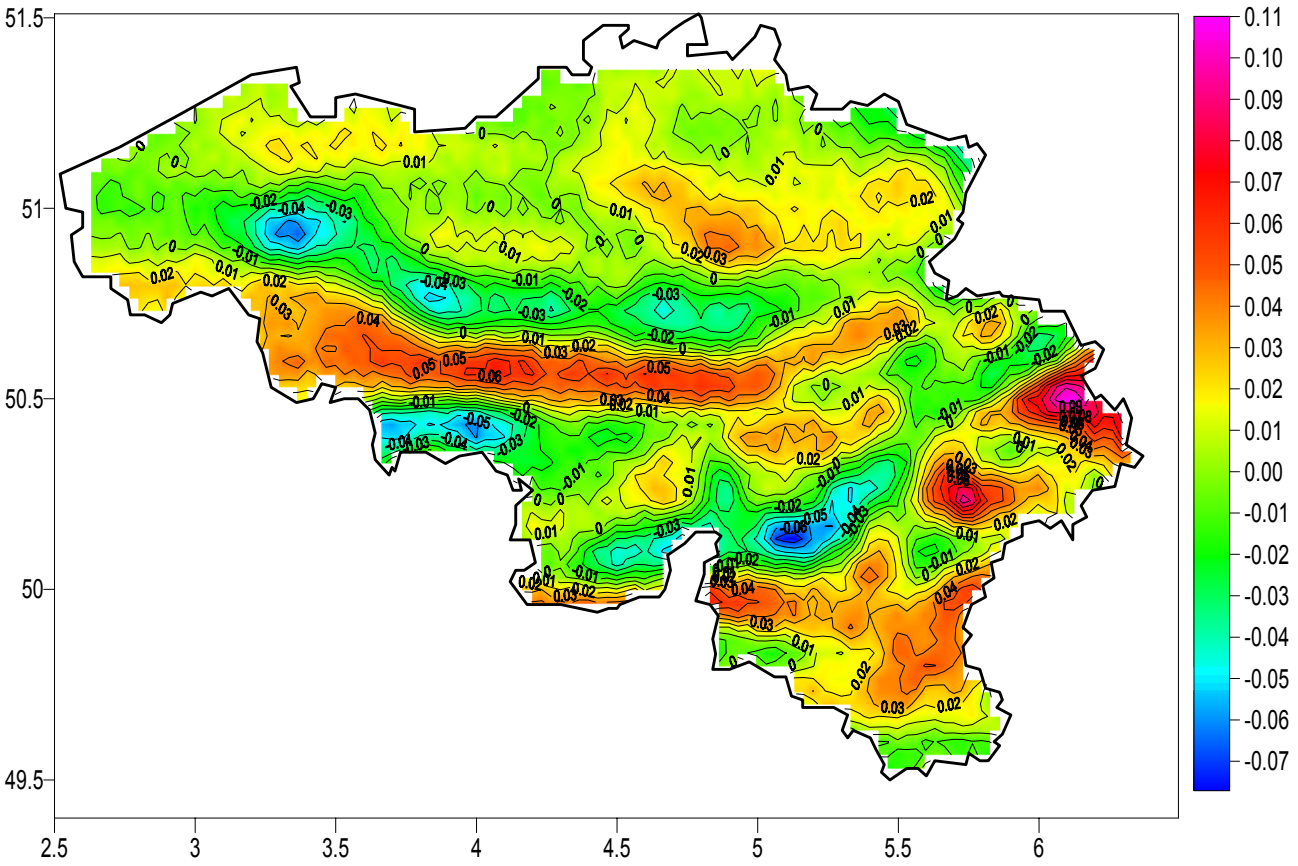

Figure 8 - High frequency content of BG03(contour in m).

6. Conclusions and perspectives

The new quasi-geoid estimate in Belgium is a step forward toward a high precision geoid computation in this area. An improvement has been reached with respect to the previous BG96 solution. This is mainly due to new gravity data, that improved the gravity coverage, more accurate global geopotential models (EGM96 and GPM98CR) and an updated DTM.

Two different techniques, namely FastCollocation and FFT, have been adopted to estimate the residual quasi-geoid component. The obtained results show that, at least for this computation area, the two method are completely equivalent.

The comparisons with $N_{GPS/lev}$ values show that a very good agreement has been reached and prove the obtained refinements in the estimates.

The high frequency content of BG03 is closely connected with the known topographic and geological structures of the Belgian territory.

However, we believe that some efforts must be done to improve the procedure that we adopted to get these solutions.

Particularly, a more detailed DTM should be used to compute a more reliable RTC effect in order to get an homogeneous and isotropic Δg_I field.

Furthermore, the reduction term to transform quasi-geoid into geoid undulations should be also computed to properly compare the gravimetric estimate with $N_{GPS/lev}$ data. Finally, ellipsoidal corrections should be accounted for, although they are more or less constant in the computation window.

It must also be stressed that, in the near future, an integrated quasi-geoid estimate based on gravity and a denser $N_{GPS/lev}$ data set will be computed in the same area.

References

Bottoni, G. and Barzaghi, R. (1993) - *Fast Collocation* - Bulletin Géodésique, Vol. 67, No. 2, pp. 119-126.

Fairhead 1994 confidential report on the West east Gravity project GETECH (Leeds University)

Heisknen, W.A., Moritz, H. (1990) - *Physical Geodesy* - Institute of Physical Geodesy Technical University, Graz, Austria.

Lemoine, F.G., Kenyon, S.C., Factor, J.K., Trimmer, R.G., Pavlis, N.K., Chinn, D.S., Cox, C.M., Klosko, S.M., Luthcke, S.B., Torrence, M.H., Wang, Y.M., Williamson, R.G., Pavlis, E.C., Rapp, R.H., Olson, T.R. (1998) - *The development of the joint NASA GSFC and the National Imaginery and Mapping Agency (NIMA) geopotential model EGM96* - NASA Report TP-1998-206861, Goddard Space Flight Center.

The Earth Gravity Model EGM96: testing procedures at IGeS (1997) - IGeS, Bulletin No. 6, DIIAR, Politecnico di Milano, Italy

Pâquet Z. Jiang and Everaerts M. (1997) A new belgian geoid Determination BG96 International Association of Geodesy vol 117 pp 605- 612

Poitevin (1980) – First order gravity points in Belgium Internal report, Royal Observatory of Belgium

Sideris M.G. (1994) – *Geoid determination by FFT techniques* - Lectures Notes of the International School for the Determination and Use of the Geoid. IGeS, DIIAR, Politecnico di Milano.

Tscherning, C.C., Rapp, R.H. (1974) - *Closed Covariance Expressions for Gravity Anomalies Geoid Undulations, and the Deflections of the Vertical Implied by Anomaly Degree-Variance Models* - Reports of the Department of Geodetic Science, No. 208, The Ohio State University, Columbus, Ohio, 1974.

Tscherning, C.C., P. Knudsen and R. Forsberg (1994) - *Description of the GRAVSOFT package* - Geophysical Institute, University of Copenhagen, Technical Report, 1991, 2. Ed. 1992, 3. Ed. 1993, 4. Ed. 1994.

Tscherning, C.C. (1994) - *Geoid determination by least-squares collocation using GRAVSOFT* - Lectures Notes of the International School for the Determination and Use of the Geoid. IGeS, DIIAR, Politecnico di Milano.

Wenzel, G. (1998) - *Ultra high degree geopotential models GPM98A, B and C to degree 1800* - Submitted to Proceedings Joint Meeting of the International Gravity Commission and International Geoid Commission, September 7 -12, Trieste 1998. Bollettino di Geofisica teorica ed applicata.

II Section: "Communications and News"

Geoid and Ocean Circulation in the North Atlantic (GOCINA)

by

P. Knudsen (1), R. Forsberg (1), O. Andersen (1), D. Solheim (2), R. Hipkin (3), K. Haines (4), J. Johannessen (5), and F. Hernandez (6)

(1) Kort & Matrikelstyrelsen, Denmark, (2) Statens Kartverk, Norway, (3) University of Edinburgh, UK, (4) University of Reading, UK, (5) Nansen Environmental and Remote Sensing Center, Norway, (6) Collecte Localisation Satellites, France. (Contact: P Knudsen pk@kms.dk)

Summary

The overall aim of the GOCINA project is to enhance European capacity in Earth observation technologies. This is done by promoting and developing methods for the joint exploitation of the approved European Space Agency ENVISAT and GOCE missions for ocean circulation studies, associated climate modelling and operational data assimilation.

A major task is to determine an accurate geoid in the region between Greenland and the UK and, thereby, create a platform for validation of future GOCE Level 2 data and higher order scientific products. The new and accurate geoid is used together with an accurate mean sea surface to determine the mean dynamic topography. The mean dynamic topography is used for improved analysis of the ocean circulation and transport through the straits between Greenland and the UK.

GOCINA will develop generic tools to enhance ocean analysis using Earth observation data from ENVISAT and GOCE. The project will examine the mass and heat exchange across the Greenland-Scotland Ridge. This analysis will give invaluable information on the ocean role in climate. The project will in particular support the GOCE mission with a set of specific recommendation for integrating GOCE in ocean circulation studies and an accurate geoid model for validation purposes.

GOCINA is a shared cost project (contract EVG1-CT-2002-00077) co-funded by the Research DG of the European Commission within the RTD activities of a generic nature of the Environment and Sustainable Development sub-programme of the 5th Framework Programme.

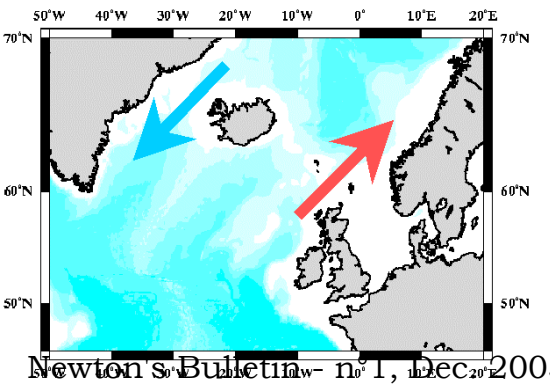

Figure 1. GOCINA study region focusing on the straits between Scotland and Greenland.

Background and motivation

The ocean transport through the straits between Greenland and the UK is known to play an important role in the global circulation as well as on the climate in Northern Europe. Warm Gulf Stream water flows into the Nordic seas and feeds the formation of heavy, cold bottom water that returns back into the Atlantic Ocean.

Increasing temperatures at high latitudes may cause changes in the distribution of ice in glaciers and ice caps. The amount of fresh melt water running into the oceans may change. Furthermore, changes in the distribution of sea ice may cause changes in the formation of heavy, cold bottom water. Both phenomena may have an impact on the ocean circulation.

It is very possible that as global warming takes hold, the climate of Northern Europe will buck the trend and become cooler. A weakening of the warm Gulf Stream would collapse the Northward heat transport between Europe and Greenland by the mean ocean circulation and cooling the Northern Europe. Furthermore, changes in the mean flows and transports in deep waters may change ocean upwelling and transports of larvae, both relevant for fish populations.

The European investment in Earth observing satellites has been significant. It is therefore of great importance that the value and utilization of this extensive provision of space borne data can be properly demonstrated in the context of ocean monitoring.

Scientific Objectives

GOCINA will advance the European capabilities in exploitation of EO data from forthcoming satellite missions, especially ENVISAT RA and GOCE, for ocean analysis of mass and heat transport, through the following specific objectives:

The central quantity bridging the geoid and the ocean circulation is the mean dynamic topography (MDT), which is the difference between the mean sea surface (MSS) and the geoid. The MDT provides the absolute reference surface for the ocean circulation and is, in particular, expected to improve the determination of the mean ocean circulation. The determination of the mean circulation will, in turn, advance the understanding of the role of the ocean mass and heat transport in climate change.

Up to the expected launch of GOCE in 2005 the gravimetric geoid is not known with sufficient accuracy to allow full use of the massive sea surface height information which several satellite altimetry missions have regularly provided since the early 90´ies, in global analysis of the ocean circulation. However, in a few marine regions in the world sufficient in-situ information about the Earths gravity field exists to compute a more accurate geoid. The region covering the Northern North Atlantic and the Nordic seas between Greenland, Iceland, Norway and the UK is one of those regions.

A major goal of this proposal is therefore to determine an accurate geoid in the region between Greenland and the UK and, thereby, create a platform for validation of future GOCE Level 2 data and higher order scientific products.

Another major goal of this proposal is to use the new and accurate geoid for improved analysis of the ocean circulation. The ocean transport through the straits between Greenland and the UK is known to play an important role in the global circulation. Gulf Stream water flows into the Nordic seas and feeds the formation of heavy bottom water that returns back into the Atlantic Ocean. Recent results have shown that changes in this bottom water transport may cause the inflow of Gulf Stream water to slow down or change into another stable circulation mode over a few decades. Such a change of the Gulf Stream with even a possible shut down of the heat transport towards high latitudes would have a huge impact on the North European climate. By analysing the best possible geoid in this region using currently available data we will be able to determine the extent to which GOCE data will improve the measuring and monitoring of ocean transports in this vital region.

GOCINA will advance the European capabilities in exploitation of EO data from forthcoming satellite missions, especially ENVISAT RA and GOCE, for ocean analysis of mass and heat transport, through the following specific objectives.

Objective 1: To determine a regional high accuracy gravimetric geoid.

An air-borne gravity survey will be made in the straits between Greenland, Iceland, the Faeroe Islands, and the UK to complete the coverage of existing gravity data and to establish an additional control of the ship-borne gravity data. Biases in the individual surveys can be detected in the cross-over analysis merging the data from the different sources. The gravimetric geoid and its error characteristics will be computed using state of the art methodology taking both marine and land gravity data into account as well as topographic data. Available data from the new satellite missions CHAMP and GRACE will be considered to enhance the long wavelength parts of the geoid.

Objective 2: To determine a regional high accuracy mean sea surface.

Satellite altimetry from ERS and TOPEX/POSEIDON for the period 1993-2002 will be collected and merged for this task. Furthermore, existing high-resolution global mean sea surfaces (MSS) for the study region will be compared. The quality of the MSS in the study region will also be evaluated through comparison with the altimeter data. Furthermore, the role of the inverted barometer correction will be evaluated. Based on the results of this analysis an optimal high-resolution MSS and its error characteristics will be computed. Later in the project an accurate MSS for 2003 will be computed using data from ENVISAT and JASON-1.

Objective 3: To determine a regional best possible mean dynamic topography using in-situ hydrographic data and ocean modelling.

In-situ climatology, e.g., the Levitus data, will be used in the determination of the mean dynamic topography (MDT). In addition recent hydrographic data will be used for computing an MDT, both in combination with altimetry and involving the use of ocean general circulation models OGCMs. Two different OGCMs and different strategies for assimilation of

hydrographical data will be used for determining several MDT models over particular periods.

Objective 4: To provide detailed assessment of the geoid, the MSS, and the MDT.

To assess the initial models residuals between the models are analysed. Furthermore, the MDT models will be compared with other in-situ data from tide gauges and current meter measurement. Residuals between the computed MSS and the sum of the computed geoid and MDT form the valuable basis for assessment and validation of the derived models. By comparing the residuals with the respective error characteristics, the accuracies of the products will be assessed. The validation will be carried out in different local areas as well as in the spectral domain. The analyses will result in modified error characteristics, which will provide the needed information for the further improvements by iterating on the methods used in WP1, 2, and 3.

Objective 5: To integrate the three techniques for improved (optimal) estimation of the geoid and the MDT.

Integrated techniques that consider all three quantities concurrently, and take their respective error characteristics into account will give optimal estimates of the geoid and the MDT. Especially, in regions with sparse data coverage the integrated techniques will show their strength. The optimal estimation technique based on generalised inversion that allows a full integration of data of different kinds taking the full signal and error covariance relations into account, and the less demanding on computational resources technique that is based on iterative transformation and weighted combination of component data streams will be used. Also new techniques of data assimilation and geoid inversion will be evaluated for calculating the best possible local solution.
The resulting best MDT will be used in the further analysis the ocean circulation. The geoid will be used to compute gravity field components and their errors at the heights of the GOCE satellite. Finally, the error characteristics of GOCE will be used to investigate the integration of GOCE data into the estimation of the geoid and the MDT.

Objective 6: To investigate the impact of the improved MDT on the ocean circulation estimation.

The assimilation methods used in the OGCMs will be modified to allow the assimilation of the best MDT. Sensitivity studies will be performed to assess the impact of assimilation of MDT data on ocean circulation and mass and heat transports. A further exploration of the new and more precise estimates of the MDT will be carried out to examine if they can be used to improve the predictability of seasonal to inter-annual variability of the Northeast Atlantic and Nordic Seas and in particular the variability related to the North Atlantic Oscillation (NAO) Index. The impact on forecasting is investigated by examining the sensitivity of the forecasting anomalies to the new and more accurate mean dynamic topography. This method will therefore also enable the simulation of the precise GOCE derived geoid on forecasting capabilities.

The experiments will examine the mass and heat exchange across the Greenland-Scotland Ridge, considering the Atlantic inflow, the surface outflow in the East Greenland Current, and the overflows. Also the impact on the current running along the continental shelf from the

Bay of Biscay to the northern Norwegian Sea will be analysed. Finally, a best possible ocean circulation experiment will be performed, which will also include sea floor pressure data from GRACE based on methods developed in a separate project. This analysis will give invaluable information on the ocean role in climate.

Objective 7: To provide specific recommendations for quality assessment of GOCE data and for integrating geoid and MDT computations with GOCE.

Many conditions for the success of GOCE lie at the level of the processing of its data, which for a large part is going to be new to everyone. This implies that special and dedicated care of the data processing be taken; to ensure that the best Earth's gravity field model can be delivered to the scientific users. The GOCINA project will in particular support the mission in two distinct cases, namely (1) to educate and prepare the community in using GOCE data for oceanography including sea level and climate research as well as operational prediction; and (2) to develop methods for generating regional gravity fields and to use them to generate a best possible regional gravity field and geoid model for the North Atlantic that can be used in validation of the GOCE products.

Innovation

The GOCINA project will focus on the development of innovative integrated techniques for analyses of the geoid and mean dynamic topography. These methods will rely on new techniques of data assimilation and geoid inversion which have been developed over recent years and will bring these together in order to force the errors down in calculating the best possible solutions based on all the currently available data.

More information

More information on the GOCINA project may be found on the Internet at http://www.gocina.dk

The New 'International Centre for Global Gravity Field Models (ICGG)' at GFZ Potsdam

Peter Schwintzer, Franz Barthelmes, Wolfgang Köhler, Hartmut Pflug
GeoForschungsZentrum Potsdam, Germany,
Dept. 1 'Geodesy and Remote Sensing'

Within the framework of the **IAG International Gravity Field Service (IGFS)** GFZ Potsdam has committed himself to establish the new **International Centre for Global Gravity Field Models (ICGG)**. ICGG is one of five centres under the roof of IGFS. The other centres are the three traditional ones: Bureau Gravimetrique International (BGI) in Toulouse, France, International Geoid Service (IGeS) in Milan, Italy, and International Centre for Earth Tides (ICET) in Brussels, Belgium. These centres shall be completed by the new 2nd International Geoid Service (IGeS) at NIMA, Saint-Louis, USA. The kick-off for the new IAG IGFS Service with its five centres shall be during the IUGG 2003 General Assembly in Sapparo, Japan.

According to the IGFS 'Terms of Reference' it is the purpose of the new **International Centre for Global Gravity Field Models** to collect all existing global gravity models, to validate and to distribute them. Moreover, it shall provide the geodetic community with software for global gravity models' manipulation and applications and shall contribute to the IGeS schools.

The ICGG scientific staff at GFZ Potsdam is composed of Peter Schwintzer (head), Franz Barthelmes and Wolfgang Köhler with technical support by Hartmut Pflug.

A web-based portal for global gravity models' data and product retrieval and download, and user interaction with the centre is presently under preparation. The status of the functionality as implemented at the tentative ICGG web site at GFZ Potsdam is described in the following. The functions and contents are subject for continuous updating and upgrading according to the actual scientific state-of-the-art. In particular the service has also to be designed to accept and handle time series of spherical harmonic coefficients that are going to be derived from the CHAMP and GRACE gravity satellite missions. The public access to the site shall be made available as soon as the establishment of the new IAG Service is officially decided.

The functions and the preparation status of the Data Base and Information System of the **'International Centre for Global Gravity Field Models (ICGG)'** are as follows:

Collecting and long-term archiving of all existing global gravity field models

The models, including all necessary background information, will be available as data sets in a uniform self-explanatory format that is open for possible future requirements as e.g. time series of coefficients.
Currently available models in spherical harmonic coefficients (based on a compilation by H. G. Wenzel, transformed into the ICGG-format):
SE1, RAPP67, SE2, GEM1, GEM2, GEM3, GEM4, SEIII, RAPP73, GEM5, GEM6, KOCH74, GRIM1, HARMOGRAV, GEM7, GEM8, GRIM2, GEM9, GEM10, GEM10A, GEM10B, GEM10C, RAPP78, RAPP81, GRIM3, GEML2, GRIM3B, GPM1, HAJELA84, GRIM3L1, GPM2, OSU86C, OSU86D, OSU86E, OSU86F, GEMT1, OSU89A, OSU89B,

TEG1, GEMT2S, GEMT2, GRIM4S1, GRIM4C1, TEG2, TEG2B, GEMT3S, GEMT3, GRIM4S2, GRIM4C2, OSU91A, GRIM4S3, GRIM4C3, OGE12, JGM1S, JGM1, GFZ93A, GFZ93B, JGM2S, JGM2, JGM3, GRIM4S4, GRIM4C4, GFZ95A, EGM96S, TEG3, GFZ96, EGM96, GFZ97, GRIM5S1, GRIM5C1, TEG4, PGM2000A, EIGEN1S, EIGEN2

Validation of global gravity field models by standardized procedures

To enable a standardized evaluation of a global model, an on-line procedure will be installed that compares it in the spatial and spectral domain with other models and data sets for various resolutions. The results will be provided as tables containing the statistics as well as maps and graphs showing the spatial and spectral distribution of differences.
The currently available validation process contains the following calculations using the model to be evaluated:

- geoid and gravity anomaly differences to the best known reference models (presently EIGEN, EGM96, TEG4) after adequate filtering with various filter lengths
- differences to ocean geoids from altimetry after adequate filtering with various filter lengths
- differences to a global set of gravity anomalies from NIMA (continents only) after adequate filtering with various filter lengths
- degree variances of geoid and standard deviations and of differences with respect to selected models
- differences to GPS/levelling-derived geoid point values from U.S.A., Canada, Europe

Calculation of various products derived from the global models

Currently the following input parameters can be chosen to generate gridded data from the spherical harmonic coefficients of a selected model and from differences in spherical harmonic coefficients between two models, respectively:

- name of the model
- name of the difference model
- reference system
- functional (geoidal height, gravity anomaly, gravity disturbance)
- grid (resolution, height) or set of coordinates (lat., long, height)
- in case of grid: point or block mean value
- degree and order window (lmin => lmax, mmin => mmax)

Collecting and long-term archiving of software for global gravity field models' manipulation and transformation

Currently available:

- calculation of geoid, gravity anomalies and gravity disturbances on grids or given coordinates from spherical harmonic coefficients for 'windows' of degree or order (lmin => lmax, mmin => mmax)
- differences of grids (including some statistics)
- degree variances from spherical harmonic coefficients, standard deviations and differences of spherical harmonic models
- filtering of grids in the spatial domain

Web site for access to global gravity field models and derived products, user interaction with the service, animation and on-line software application

Currently available:
ICGG home page with the following features:

- table of available models including information about year of generation, maximal degree, used data, reference, download-link
- table of global gravity field modelling related publications
- interactive online visualization of the models in form of coloured, illuminated geoid relief, projected on a sphere; implemented interactions are:
  - animation of a rotating geoid (cf. Figure 1)
  - interactive control of view on rotating geoid
  - zoom in/out
  - difference of two models
  - arbitrary degree windows
  - visualization of selected spherical harmonics for tutorial purposes
    (cf. Figure 2 for examples of zonal, sectorial and tesseral spherical harmonics)

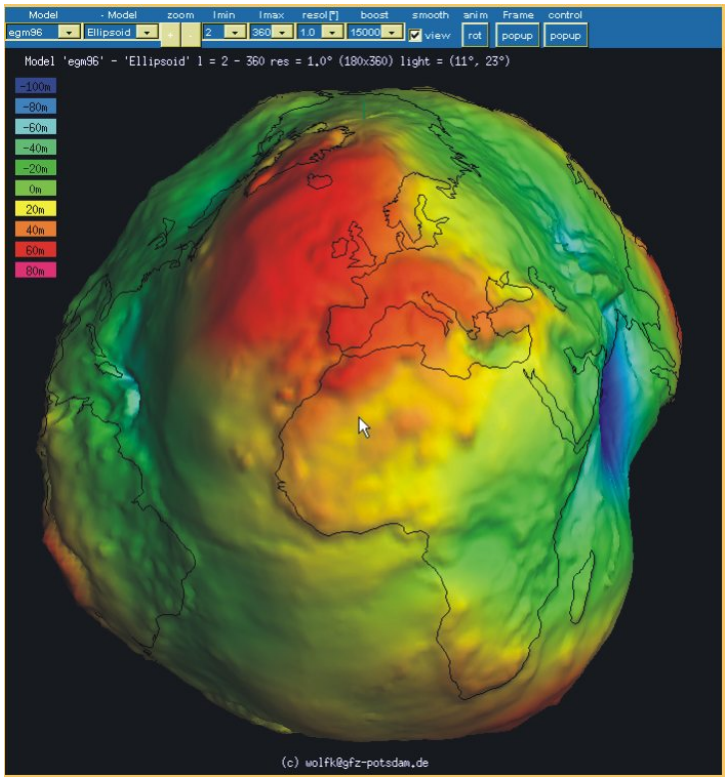

Fig. 1: Visualisation (Geoid) of a global gravity field model.

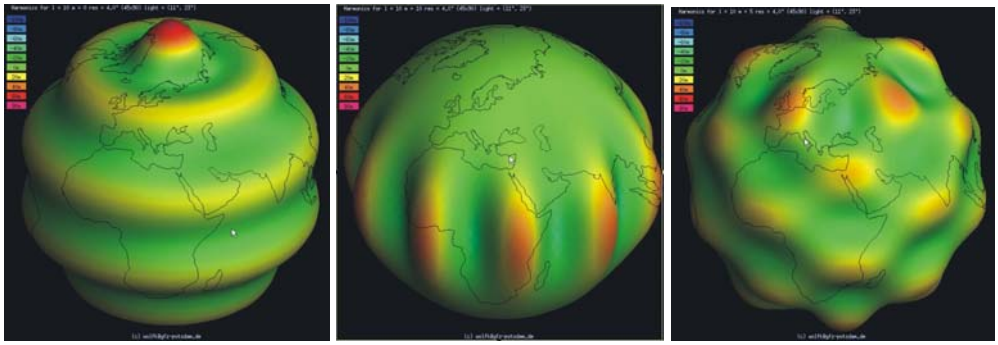

Fig. 2: Visualisation of selected spherical harmonics: zonal, sectorial and tesseral

Planned:

- user interface for model validation and download of results
- user interface for product generation (e.g. gridded data) and product download
- user interface for getting the manipulation software

Contribution to IGeS schools

Concise tutorials on global gravity field models and its application shall be prepared, collected and made available here.

Yearly activity report

List of reports for download

Data policy

The access to the global gravity field models, its derived products, software and tutorials, once offered by the centre, shall be unrestricted for any external user.